

Design and development of a lathe spindle

Asım Kutlu



Master of Science Thesis MMK 2016:02 MKN 064
KTH Industrial Engineering and Management
Machine Design
SE-100 44 STOCKHOLM



KTH Industriell teknik
och management

Examensarbete MMK 2016:02 MKN 064

Konstruktion och utveckling av svarvmaskinsspindel

Asım Kutlu

Godkänt 2016-01-14	Examinator Ulf Sellgren	Handledare Mario Sosa
	Uppdragsgivare	Kontaktperson

Sammanfattning

Verktygsmaskiner möjliggör tillverkning av materiekroppar med olika form. Svarvar är de vanligaste maskinerna för att bearbeta runda detaljer. Man kan säga att en svarvspindeln möjliggör hela skärprocessen och att den därfor är den viktigaste komponenten i en svarv. En svarvaxel, eller en spindel, bearbetar det roterande ämnet med ett stationärt skärverktyg, och materialet tas bort vid skärverktygets kontakt med ämnet.

Det här arbetet syftar till att konstruera en spindel som uppfyller en given kravspecifikation. Specifikationen innehåller prestandakrav, som rotationshastighet och kraft, geometri och dimensionskrav, som storlek och håldiameter, samt vilka komponenttyper som ska användas, som t.ex. motorn.

I enlighet medprestandakravet definieras maximalt lastscenario. Med givna svarvningsparametrar beräknas skärkraften på materialet vid dess kontakt med skärverktyget. En inbyggd motor som är tillräckligt kraftfull och uppfyller hastighets- och effektkraven väljs och en preliminär konstruktion skapas med valda lager, lagerordningar och axelmateriel.

Beteendet av den preliminära spindelkonstruktionen, under påverkan av skärkrafter och rotation analyseras statiskt och dynamiskt med hjälp av FEM och analytiska modeller. Inom ett givet område optimeras avståndet mellan lagren, vilka utgör spindelns stöd.

Genom verifikation och optimering av den preliminära konstruktionen skapas den slutliga detaljkonstruktionen. Slutkonstruktionen innefattar alla nödvändiga detaljer och viktiga krav beaktas och balanseras, som att vara tillverningsbar och monterbar, tätningssystem, ett system för hastighetsmätning och lägesmätning, kabelvägar och andra nödvändiga punkter. I slutänden konstrueras en spindel som uppfyller den definierade kravspecifikationen.

Nyckelord: Svarvmaskin, spindel konstruktion, statisk analys, dynamisk analys



KTH Industrial Engineering
and Management

Design and development of a lathe spindle

Asım Kutlu

Approved 2016-01-14	Examiner Ulf Sellgren	Supervisor Mario Sosa
	Commissioner	Contact person

Abstract

Machine tools enable the industry to shape almost any material by a variety of methods. Lathes are one of the most common machines to cut circular parts with precision and accuracy. And the spindle of a lathe can be entitled as the most critical mechanical component which makes the cutting process possible. A lathe spindle rotates the workpiece to be cut against a stationary rigid cutting tool, therefore removing material through the contact edge. In this thesis, a spindle is aimed to be designed which complies with a set of specifications defined. These specifications consists of performance requirements such as speed and power, dimensional constraints for space and bore diameter, and component types which must be used, such as for the motor.

Based on the performance requirements, a maximum loading case with cutting parameters is defined. With these cutting parameters, cutting forces acting to the material from at the contact point with the cutting tool are calculated. A built-in motor with sufficient power and speed specifications is selected based on the maximum cutting forces and speed requirements. A preliminary design is made up by selecting bearings, bearing arrangements and shaft material.

With static and dynamic analysis conducted on the preliminary design through analytical models and FEM, the behavior of the spindle is investigated separately under the cutting forces and during the rotation. Within an allowable range, optimization is made on the bearing span distances which are the support locations for the spindle.

Following the verification and optimization of the preliminary design, the final detail design of the spindle is made. The final design includes the design of all the necessary parts, by taking the manufacturability, assemblability, sealing design, a system for speed and position measurements, cable paths and more necessary points into account. Ultimately, a spindle which meets the requirements and specifications successfully is designed as the expected outcome of this thesis.

Keywords: *lathe, spindle design, static analysis, dynamic analysis*

FOREWORD

“Be grateful for whoever comes, because each has been sent as a guide from beyond.”

- Rumi

I am greatly indebted to all those who lent me a hand, backed me and guided me in various ways on my very long journey of writing this thesis.

Ahmet Oral, for poisoning my life with machine tools, broadening my mind and being a great manager, a great mentor and an exceptional engineer.

Ali Avcı, for making my master studies happen.

Mario Sosa, for his wisdom, understanding, guidance and supervision. Without him it would have been impossible to walk this path.

Görkem and Murat, for the desk, chair, teapot and their precious friendship they shared for months.

Ulf Sellgren our dear teacher, for always being very patient with me, his continuous support and help during my thesis, his guidance and counsel during my studies.

Special thanks to Ertan, Minoo, Nagore, Athul and all my dear friends from KTH for making my life awesome during my studies.

Finally, I am deeply grateful to my parents, my sisters Kevser and Sumeyye, Naci, my beloved nephew Ömer for being there with their unconditional love and support whenever I need.

Asım Kutlu

Istanbul, January 2016

NOMENCLATURE

Here are the Notations and Abbreviations that are used in this Master thesis.

Notations

Symbol	Description
α	Rake angle of the tool
α_T	Thermal expansion coefficient
β	Friction angle
$\delta_1, \delta_2, \delta_3$	Deflection of the bearings on the spindle for rigid shaft-elastic support case (mm)
δ'_1, δ'_2	Deflection of the bearings in test model for rigid shaft-elastic support case (mm)
δ_S, δ_B	Deflection of the spindle for different superposition cases (mm)
$\delta_{S\text{Test}}, \delta_{B\text{Test}}$	Deflection of the test model for different superposition cases (mm)
$\delta_{spindle}$	Total deflection of the spindle tip (mm)
δ_{Test}	Total deflection of the test model tip (mm)
$\delta_{Thermal}$	Thermal expansion (mm)
ΔT	Temperature difference
μ	Friction coefficient
τ_s	Shear strength (GPa)
ϕ	Cutting angle
a	Overhung distance on the spindle (mm)
A_s	Area of the shearing zone (mm^2)
a_{Test}	Overhung distance of the test model (mm)
b	Extension distance on the spindle (mm)
b_c	Width of cut (mm)
c_1, c_2	Test model deflection function coefficients
C_1, C_2	Spindle deflection function coefficients
D	Inner diameter of the bearing (mm)
D_i	Inner diameter of the spindle shaft (mm)
D_m	Pitch diameter of the bearing (mm)
D_{max}	Maximum diameter of the spindle (mm)

D_o	Outer diameter of the spindle shaft (mm)
D_S	Workpiece diameter (mm)
D_{Test}	Diameter of the shaft in the test model (mm)
e	Machine tool efficiency
E	Modulus of elasticity of Ck45 (GPa)
E_{Test}	Young's Modulus of the test model (GPa)
F	Friction force (N)
F_f	Cutting feed force (N)
F_s	Shearing force (N)
F_t	Tangential cutting force (N)
F_{Test}	Test load in the test model (N)
I	Moment area of inertia of the spindle (mm^4)
I_{Test}	Area moment of inertia of the test model (mm^4)
k_α	Chip angle factor
k_λ	Slope angle factor
k_a	Tool wear factor
k_B	Stiffness of the angular contact ball bearings (N/mm)
k_C	Stiffness of the double-row cylindrical roller bearing (N/mm)
K_f	Specific feed force factor
k_{ft}	Chip thickness dependent specific tangential force factor
k_T	Cutting tool material and cutting method factor
K_t	Specific tangential force factor
k_{Test}	Bearing stiffness of the test model (N/mm)
k_{tt}	Chip thickness dependent specific cutting force factor
L_i	Initial length (mm)
L_S	Workpiece length (mm)
L_{Test}	Length of the shaft in the test model (mm)
M_s	Moment function of the spindle (N.mm)
M_t	Coupled moment generated by the cutting force (N.mm)
M'	Moment function of the test model (N.mm)
n	Maximum spindle speed (rpm)
N	Normal force generating the friction force F (N)
n_{motor}	Maximum speed of the motor (rpm)
n_S	Rotational speed of the workpiece (rpm)
P_f	Friction power (W)
P_M	Motor power (W)

P_{motor}	Total power needed at the motor (kW)
P_s	Shearing power (W)
P_t	Total cutting power drawn at the tool (W)
R	Resultant cutting force (N)
R_1, R_2	Reaction forces on the test model (N)
R_A, R_B, R_C	Reaction forces on the spindle in elastic shaft-rigid support case (N)
R'_A, R'_B, R'_C	Reaction forces on the spindle in rigid shaft-elastic support case (N)
s_1, s_2	Span distance between bearings on the spindle (mm)
s_{Test}	Span distance in the test model (mm)
t	Uncut chip thickness (mm)
V	Cutting speed (m/min)
V_c	Chip velocity (m/sec)
v_s	Deflection function of the spindle (mm)
V_s	Shear function of the spindle (N)
V_{sh}	Shearing velocity (m/min)
V'	Shear function of the test model (N)
v'	Deflection function of the test model (mm)
w_s	Loading function of the spindle (N)
w'	Loading function of the test model (N)
x	position on the shaft (mm)

Abbreviations

<i>BOM</i>	Bill of Material
<i>CAD</i>	Computer Aided Design
<i>CNC</i>	Computer Numerically Controlled
<i>EL</i>	Extra Light
<i>FE</i>	Finite Element
<i>FEM</i>	Finite Element Method

TABLE OF CONTENTS

SAMMANFATTNING (SWEDISH)	1
ABSTRACT	3
FOREWORD	5
NOMENCLATURE.....	7
TABLE OF CONTENTS	11
1 INTRODUCTION.....	13
1.1 Background	13
1.2 Purpose	15
1.3 Delimitations	16
1.3.1 Dimensional limitations.....	16
1.3.2 Power and torque limitations	16
1.3.3 Limitations regarding the spindle calculations	17
1.4 Method	17
1.4.1 Calculation of Cutting Forces and Power Requirements	17
1.4.2 Selection of the components and preliminary design	17
1.4.3 Verification of preliminary design.....	18
1.4.4 Detail design and finalization	18
2 FRAME OF REFERENCE	19
2.1 Basic Spindle Structure	19
2.1.1 Spindle housing	20
2.1.2 Spindle bearings	20
2.1.3 Spindle motor	20
2.1.4 Spindle shaft	21
2.1.5 Other parts	22
2.2 Spindle Design and Optimization	22
3 ANALYSIS AND PRELIMINARY DESIGN	25
3.1 Calculations and Preliminary Design	25
3.1.1 Force and power calculations	25
3.1.2 Selection of the motor.....	29
3.1.3 Selection of the bearings.....	31
3.1.4 Preliminary design.....	37

3.2 Analysis and Optimization	38
3.2.1 Static analysis	39
3.2.1.1 <i>Test model</i>	39
3.2.1.2 <i>Analysis of the spindle</i>	47
3.2.2 Dynamic analysis.....	58
4 FINAL DESIGN	63
4.1 Assembly Design.....	63
4.1.1 Overcoming the thermal expansion.....	65
4.1.2 Sealing design.....	65
4.1.3 Encoder.....	67
4.2 Assembly to the machine	67
4.3 Spindle BOM.....	68
5 DISCUSSION AND CONCLUSIONS	71
5.1 Discussion	71
5.2 Conclusions	72
6 RECOMMENDATIONS AND FUTURE WORK.....	75
6.1 Recommendations	75
6.2 Future work	75
7 REFERENCES	77
APPENDIX A: SPECS OF SIMILAR SPINDLES ON THE MARKET.....	80
APPENDIX B: SIEMENS 1FE1093 MOTOR SPECS	84
APPENDIX C: MACALUAY AND SINGULARITY FUNCTIONS	88
APPENDIX D: MATLAB SOLUTION FOR TEST MODEL.....	90
APPENDIX E: MATLAB SOLUTION FOR SPINDLE	92

1 INTRODUCTION

In this chapter, spindle as a critical component of the machine tools is introduced. The background of the thesis is explained extensively and the purpose, the limitations and the methods used are expressed.

1.1 Background

Even though many new manufacturing processes are introduced over the last decades, the main heart of manufacturing, metal cutting –or chip removal- processes have remained dominant in the metal working industry. In consistence with the industrialization, machine tool industry has always been in continuous development and many technological advancements have made the metal cutting processes faster and more reliable with lower costs, which eventually led to less expensive products with less delivery times.

Over the decades, the basic principles of metal cutting and the main mechanical components of the machine tools remained same. Same as 30 years ago, a machine tool is still composed of the basic components: spindle, moving axes and a cutting tool. Among these components, spindle is almost the most critical one due to its vital duty in the metal cutting process. Even though the spindles differ in structure and design for different machine tools (milling, lathe, etc.) they all serve to the same basic purpose: rotating either the workpiece or the cutter with enough torque and speed against the other which is fixed to enable the cutting happen.

The spindle, as mentioned above, which constraints the workpiece or the cutting tool to rotate around a fixed axis can be powered from a variety of sources. In the ancient times they were run manually through human or animal power, until the development of steam engines in the 18th century (Wikipedia, 2015). Later, technological advancements led also hydraulic and pneumatic power to be used in factories as well as steam power until the wide use of electric in the industry. Today most machine tools are powered by electric motors, however in some process related specific cases hydraulic and pneumatic power are also used.

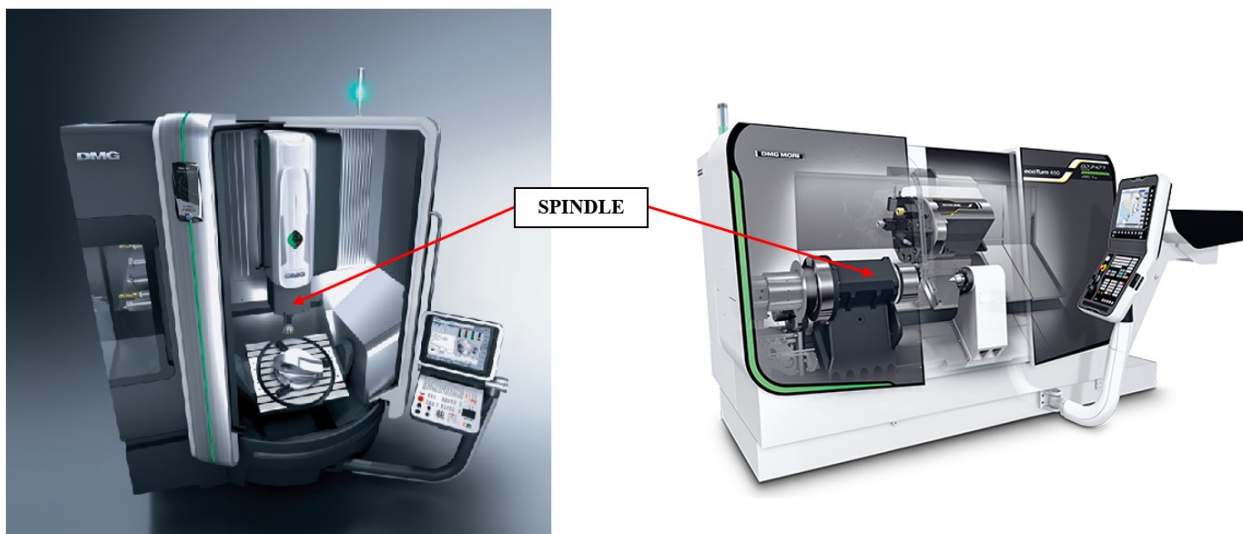


Figure 1. Milling machine and lathe spindles (DMG Mori, 2015)

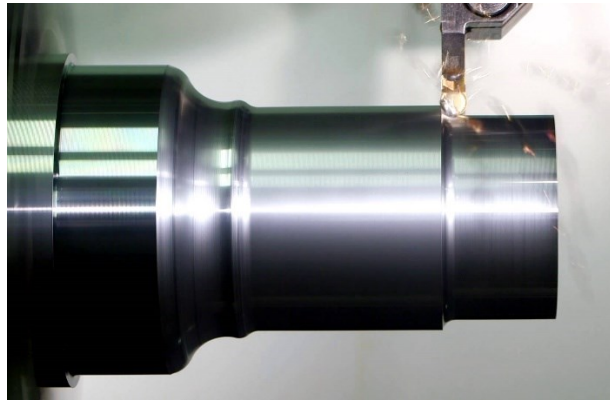


Figure 2. Lathe spindle constraints and rotates the workpiece against the cutting tool to remove material. (Seco Tools, 2015)

There are different ways of driving a spindle with an electric motor. Nowadays, machine tool spindles are categorized as external or internal (built-in) driven based on the connection and assembly method of the electric motor to spindle. Externally driven spindles have their motor outside the spindle housing and the power is transmitted through belt, gear or chain systems. On the other hand, internal driven spindles have built-in electric motors inside the housing coupled with the spindle shaft.

There are many factors affecting the choice of spindle drive system, i.e. process, cost, space and performance. Today many low end machine lathe builders prefer less expensive solutions for their spindles, such as external drive with a belt transmission. And in contrast, high end lathe builders prefer integral motor spindles due to their superior performance and space advantages in small to medium size spindles -spindles with bore diameter lower than $\varnothing 100$ mm or spindles for machining metals over $\varnothing 400$ mm. Although internal motors provide better performance than external motors, their dimensions can make it a difficult task to integrate into the spindles design, especially for the big size spindles. Still today, most lathes spindles with high torque/low speed output are run with external motors and belt transmission.

Internal spindle motors can be either asynchronous or synchronous, depending on the building materials of their rotor and the synchronization of the magnetic field in the motor and the rotation of the rotor. In asynchronous motors, rotors are made of electrical steel and conductive bars of aluminum or copper. The magnetic field generated in the stator creates a voltage and current flow through these laminations and makes the rotor rotate in the magnetic field. However there is always a phase difference between the rotations of the magnetic field and the rotor, which makes asynchronous motors less precise and less efficient. On the other hand synchronous motors with their permanent magnet rotors which prevents slip effect and phase differences provide better power and thermal characteristics. Asynchronous motors had significant price advantages and ease of production in the last decade. However synchronous motors are getting more competitive in price and increasingly preferred due to their significant performance benefits. Many machine tool builders are now switching to synchronous motors in their spindles to increase the performance and competitiveness of their machines.

Since synchronous motors have usually smaller dimensions than asynchronous motors with similar power and speed specifications, they can help to design smaller spindles with better performance specs, which will eventually increase the competitiveness of the machines of the producer.

1.2 Purpose

The main purpose of this MSc degree project is to design and develop a lathe spindle that will meet the design requirements listed and explained below. These requirements are defined based on the market trends and other technological developments.

The design requirements are:

1. *The spindle should run with an internal synchronous motor.* Currently, many integrated motor spindles are equipped with asynchronous motors, but latest technological developments led spindle designers to prefer using synchronous motors more and more due to their significant advantages. In this thesis, the spindle should be designed with a suitable synchronous motor. Synchronous motor to be used can be selected from any spindle motor producer company.
2. *The spindle should have 52mm bar capacity.* CNC lathes provide customers faster machining and production. To automate the production further, customers can couple the machine with a bar feeder from behind the spindle. Hence the lathe can produce and cut the parts from steel bars continuously fed by the feeder inside the working area through the spindle. One of the capacity specs for the spindles used in the market is the maximum bar diameter that can be fed through the spindle. In this thesis the spindle to be designed should have 52mm bar capacity. In Figure 3, bar feeding process is depicted simply.

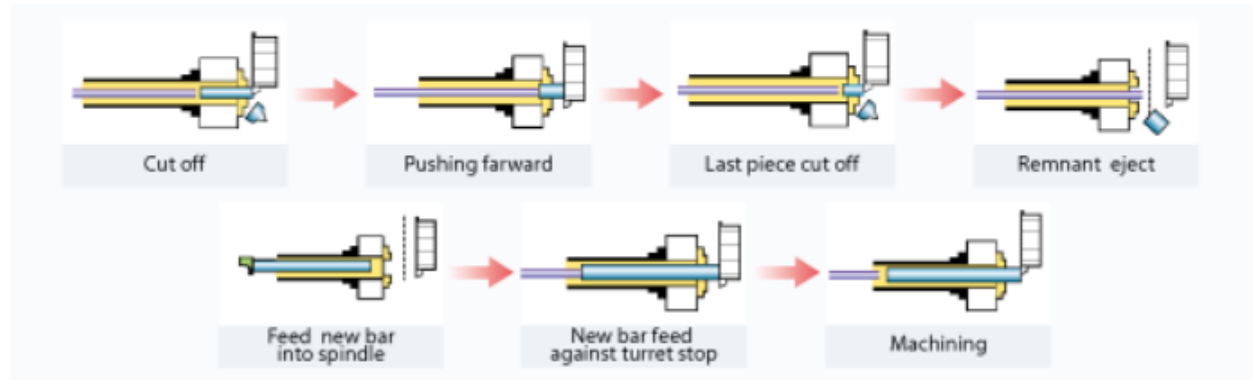


Figure 3. Bar feeding process (Goodway, 2015)

3. *The spindle should have at least 15 kW maximum power and 6,000 rpm maximum speed.* The approach for defining the specifications for the spindle cutting performance should be done through the customer and market surveys. However in this thesis the minimum performance requirements are selected through benchmarking of the lathes of well-known producers and their spindles with similar bar capacity on the market. DMG MORI, Mazak and Doosan lathes are examined and it is seen that these spindles have different motor power varying between 11-18 kW, while the maximum speed is 6,000 rpm for all (see Appendix A). Therefore competitive specs are aimed to be selected for the design.
4. *The spindle should have the maximum dimensions of 650 mm in length and Ø250 mm in outer diameter.* Many machine tool builders try to produce space efficient machines and spindle is one of the main factors defining the machine sizes. Especially for the machines with subspindle (2nd spindle in the working area), the space that the subspindle covers affects the machine axes motions and limits directly. Hence designers should always limit their design in terms of dimensions.
5. *The spindle tip should not deform more than 0.03 mm under the cutting loads.* Spindle tip deformation under the cutting forces affects the surface finish and the precision of the workpiece cut. Although, for finish cuts or light cuts, the deformations have lesser effects

on the precision, the maximum allowable deformation of the spindle should be limited to guarantee the precision of the machine even for the challenging rough cuts.

6. *The spindle should be cartridge type.* Cartridge spindles are lately a trend in the market due to their assembly method. Spindles usually assembled into a big housing which is then connected to machine body. However, cartridge type spindles are complete spindle units separate than the big spindle housing and it consists of a shell housing in which all the necessary parts are assembled as shown in Figure 4. It allows easy maintenance and fast replacement of the spindles for both the customer and the producer. Also many spindle producers (spindle suppliers for machine producers) design and sell their spindles as cartridge type to make it easier for the lathe builders to adapt them on their machines.



Figure 4. Cartridge spindle is a complete assembly unit which contains all the necessary parts. (Ima Tecno, 2015)

7. *The spindle should have A6 nose connection.* Almost all the lathe spindles on the market are produced with certain spindle nose designs such as A5, A6, A8, etc. for standardizing the chuck (workpiece holder) interface. The German standard DIN 55026 Type A should be used for the design of the spindle nose, and A6 is a convenient size for this spindle which has 52mm bar capacity.

1.3 Delimitations

1.3.1 Dimensional limitations

Dimensional specifications set in this thesis require a spindle design with 52mm bore diameter that will at the same time fit in a defined space; a maximum Ø250 mm x 600 mm volume. Spindle size limitations are usually set according to the machine it is designed for, however in this thesis no such machine is of question. Spindle size itself is one of the main factors for defining both the inner workspace and outer dimensions of a lathe. Therefore, it is always preferred the spindles to be as compact as possible with a sufficient performance. In this thesis, the requirements for dimensions will affect the assembly design and more importantly selection of the components such as the motor and bearings. The components that will meet both the size and performance requirements at the same time should be selected. Hence, the dimensional limitations appears to be essential factors affecting the design.

1.3.2 Power and torque limitations

Power and speed requirements for the spindle are mostly defined through benchmarking and based on similar spindles specs on the market as shown previously. There are no regulations or basic rule about deciding on the power and torque specifications of the spindle to be designed. Therefore, in this area of no boundaries, limits are usually set with the help of market reviews together with the benchmarking and observations on the use of similar sized machines. In this project, the target machining conditions for power calculations are selected based on a sample case which seems to be challenging in terms of power and torque for a 52mm sized spindle. This

specific cutting case will be treated as the worst case scenario and its parameters will be used to calculate the necessary power, and to check if the 15 kW specification set is sufficient for target worst case.

The spindle power of a machine tool defines the cutting limits of that machine. Even though most of the time the machining operations do not push the spindle to its limits, the spindle must be designed based on the estimated challenging cutting parameters, which is the so-called worst case scenario. However, estimated cutting parameters and calculated spindle performance might be different than in the real case.

1.3.3 Limitations regarding the spindle calculations

Spindle consists of many critical elements and different components such as bearings, electric motor and sealing elements for water tightness. Including all the properties and effects of these parts in this complex system will make the calculations and design complicated and harder. Therefore, during calculations many simplifications must be made and many effects are to be estimated due to adversity of obtaining real data about these effects.

Bearings play a crucial role on the performance of the spindle. Their specifications define the speed, load carrying capacity and life span of the spindle. Also to be able to analyse the static and dynamic performance of the spindle, damping and spring coefficients of the bearings should be known. However, since these values best obtained by experimental methods and due to limited opportunities for such work, these coefficients will be defined by assumptions and estimations with the help of bearing data given by suppliers.

1.4 Method

1.4.1 Calculation of Cutting Forces and Power Requirements

Machining power and torque specs of a lathe or a spindle given in the machine builders' product catalogues actually refer to the spindle motor properties. In most cases spindle motor defines the maximum power and torque specs of the spindle, unless there is a transmission system (belt, gear drive, etc.) without 1:1 ratio. Hence the calculations of the cutting forces and required motor power for the spindle will help to select the integral motor with correct specifications.

Power and force calculations will be made for a possible worst case scenario, which is a sample case challenging enough to push the spindle. The machining case, where a specific material with specified dimensions is to be machined with certain cutting conditions of speed, feed rate, cutting depth, etc., is studied.

The demanded machining capability from the lathe and spindle should also correlate and compete with the competitor machines in the market. Thus the sample case parameters will be estimated and improvised through a benchmarking activity that investigates the cutting performances and sample cases tested on similar spindles. The sample case will also allow us to check if the power requirements set are sufficient to perform similar cutting operations.

1.4.2 Selection of the components and preliminary design

Following the calculations of spindle power requirement, first preliminary design can be made by choosing the appropriate motor and bearings based on the speed, power and size limitations.

The motor will be selected from the product ranges of motor supplier companies. Companies such as Siemens, Fanuc, and etc. produces synchronous spindle motor. A suitable motor that meets size and performance criteria will be used.

The bearings can be chosen from a variety of options with different specifications and configurations. An optimum selection approach considering performance, space and cost should

be applied. Similar to the motor, bearings will be selected from spindle bearing producing companies such as NSK, SKF, FAG, etc.

Both for the motor and bearings, there is almost no difference and significant superiority between the products of different companies. Usually cost is the decisive factor when selecting the supplier for the same kind of standard products.

1.4.3 Verification of preliminary design

Before designing the spindle assembly further, preliminary mechanical design should be checked and verified through static and dynamic analyses. An analytical model will be created to understand the spindle static behavior under cutting forces. The analytical model results will be compared with FEM results to validate the models and the method. The spindle will be optimized in bearing span distances within the size limits through these model.

The dynamic stiffness of the spindle is important to prevent vibration and any related problems which will eventually affect the spindle life and machining process quality. Therefore, the dynamic behavior of the spindle will be analyzed with FEM through its Eigen frequencies and harmonic response.

1.4.4 Detail design and finalization

Spindle design now can be finalized following the verification of the preliminary design and optimization of the bearing positions. There are more factors to consider for the further steps of spindle design.

- design of other components in the arrangement
- appropriate fits and mounting methods
- design for manufacturing
- sealing of the system
- measurement system adaptation
- mounting and dismounting methods
- coolant circulation system design

Design of the components and the overall system for assembly and manufacturing is important for mass production and serviceability in the future. Sealing and water tightness of the system will also be designed together with the other minor points (coolant circulation system for motor, position and speed measurement system, etc.) at this stage. The finalized design will be the basis for prototype production and testing.

2 FRAME OF REFERENCE

In this chapter, the basic structure of a spindle and its major components are explained extensively. Additionally a literature review conducted on the spindle design and optimization is also presented.

Machine tools have been an important part of various industries and technologies for over centuries. In the ancient Roman times simple lathes were used to machine big stone pillars of the wonderful buildings and artifacts. Almost 200 years old lathes to machine woods and metal can be found in the Deutsche Museum. Accordingly, the spindle unit of a lathe always existed but with different drive technologies behind it.

The main functions of spindles for metal cutting machine tools can be listed as:

1. Rotating the cutting tool or the workpiece with a certain precision
2. Providing necessary power and speed to the tool or the work piece for cutting operation
3. Resisting against the cutting forces generated during cutting operation

A spindle, regardless of the machine (milling, turning or grinding) it will be used on, consists of some basic components. As for the integral motor spindles, they might need some extra units different than the traditional spindles due to their different driving technology.

2.1 Basic Spindle Structure

Today, the majority of machine tools spindles sold are internal driven type and unlike the external driven spindles they do not require a mechanical transmission unit such as gears, belt, etc. Their performance and efficiency make them preferred over external driven spindles. Spindles with bearing inner diameter bigger than Ø150 mm are usually external driven, due to cost and dimensional reasons.

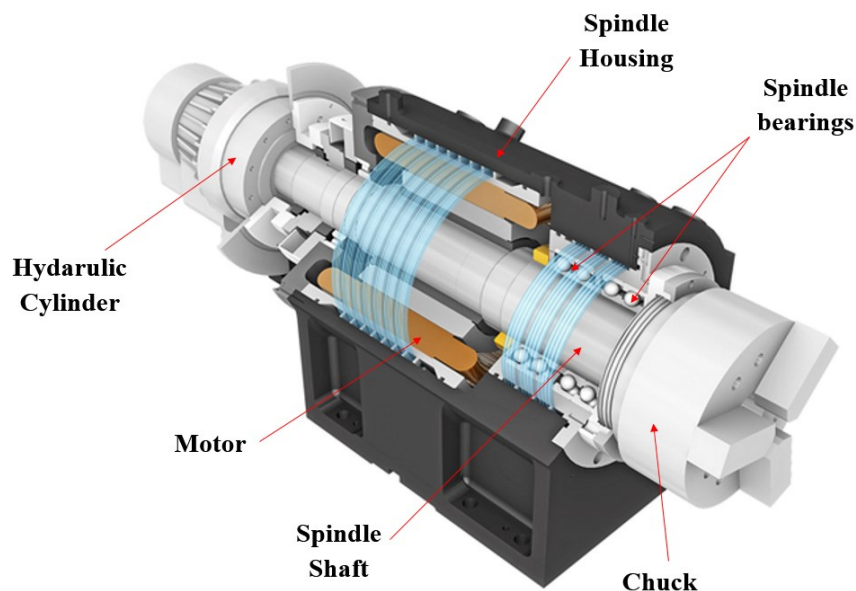


Figure 5. Basic lathe spindle structure and major components (Hyundai WIA, 2015)

As shown in Figure 5, a lathe spindle basically consists of the following major components:

- Spindle housing
- Spindle bearings
- Spindle motor
- Spindle shaft

2.1.1 Spindle housing

Housing is the unit holding the spindle structure and basic components together, i.e. the spindle shaft, bearings and other functional parts are ultimately assembled inside the housing, as shown in Figure 5.

The housing may be an integrated part of the machine tool body, or a separate stock, or a flange mount cartridge housing. Cartridge type spindles need an additional housing for the complete cartridge unit to be mounted on. Cartridge type spindles utilize the maintenance and replacement of broken spindles both for the machine builders and the customers, therefore they are being adopted widely in the market lately.

The primary function of the spindle housing is to locate the spindle bearings and support them. It must be robust and stiff enough, as all the forces generated on the spindle during machining are transferred to machine body through the housing. (Dynomax, 2011)

2.1.2 Spindle bearings

Depending on the design and metal cutting process, a spindle consists of at least two sets of bearing sets to hold the spindle and carry the necessary loads, one in the front and one at the back. The bearings are the transition elements between the spindle and its housing which acts as the support elements to withstand against the reaction forces generated by both the motor and the machining operation itself. Therefore bearings are the components with the greatest influence on the lifetime of a spindle due to the heat and stresses generated due to friction and loading during cutting operation. The internal motor is assembled onto the spindle shaft and positioned between the two bearing sets.

2.1.3 Spindle motor

Vast majority of the machine tool spindles are driven by an electric motor, except some very few specific cases. However, as mentioned before, the transmission of the power from the motor to the spindle can be achieved with different methods and these methods can be divided into two categories depending on the type of the motor used to drive.

- **External motor:** in this case, the spindle is run by an external drive motor and the motor is completely independent from the spindle system. The transmission between the motor and spindle is attained by either a direct coupling system or a belt, chain or gear system as depicted in Figure 6.

Spindles with external drive motors have been in use widely until the last decade due to their reasonable costs and flexible structure which allows different power/torque outputs for different manufacturing processes. However, low permissible speeds, extra loads on spindle bearings due to gear/belt/chain systems and low efficiency create limitations for this type of spindles.

- **Internal (built-in) motor:** Technological advancements have led the development of internal motors specific for machine tool spindles for the last two decades. Internal motors are assembled into the spindle housing and on the spindle shaft as in Figure 5. This type of spindles became more widely used due to their some significant advantages over the

external motor type. Compact design and smaller installation area for smaller spindles help builders to make smaller machines, which is an important demand especially by the Japanese and European customers. Also no extra load on the bearings and no physical contact with the spindle as an integral part of the spindle allows higher rotational speeds to be achieved. No physical contact in contrast to the belt/chain/gear systems also eliminates transmission related vibrations. The necessity of cooling the internal motor due to heat generated, more complex assembly structure and procedures, higher costs compared to external motors are also the limitations of these spindles. Due to the high ratio of “power to volume” ratio of the internal motors active cooling is often required, which is generally implemented through liquid based cooling. The cooling liquid flows through a cooling sleeve around the stator of the motor and often the outer bearing rings.

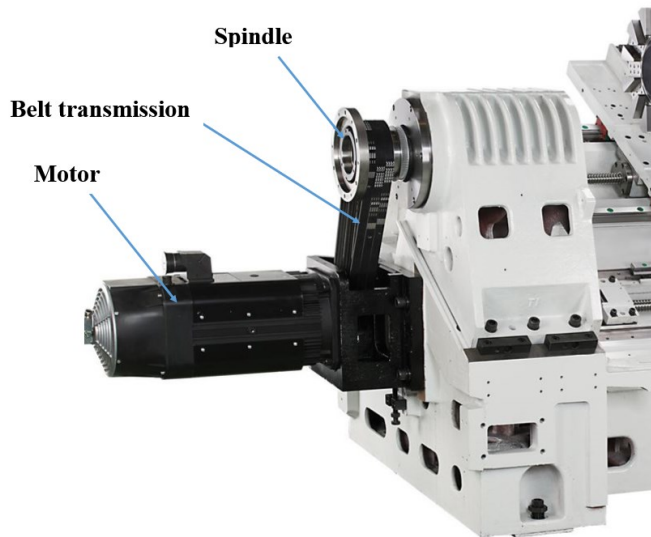


Figure 6. Spindle with an external motor and belt transmission (Hurco, 2014)

Integral motors can be divided into two categories depending on their rotor type. *Asynchronous motors* are produced mostly as squirrel cage type and consist of a stator and rotor made of metal laminations. The magnetic field created through the stator induces a magnetic flux in the rotor and enables rotation of the shaft. However by the nature of the induction process, the speed of the rotor is different than the rotating magnetic field, which is why these motors called asynchronous.

Synchronous motors have their rotor made of permanent magnets. Therefore synchronous motors does not experience the phase difference in its rotation. These type of motors provide less heat generation and thermal drift in the spindle due to less magnetic friction, higher efficiency and smaller dimensions with similar power/torque characteristics compared to the asynchronous motors. However the relatively higher costs of synchronous motors than the asynchronous ones made them less common for machine tools until the last decade. Currently the price differences are significantly lower that the advantages of synchronous motors make them widely preferred.

2.1.4 Spindle shaft

A spindle shaft, similar to the housing, holds the components together and locates the spindle bearings as shown in Figure 5. Because spindle shaft is the main rotating component of the system and one of the first component to withstand the loads during cutting, its stiffness and robustness greatly affect both static and dynamic behavior of the spindle system, ultimately the performance of the machine tool.

2.1.5 Other parts

Spindle bearings are sensitive against water based liquids which shortens their life and causes them to fail. Therefore a water-proof design for spindles must be achieved to prevent unexpected failures. Sealing elements (o-rings, seals, protection flanges, etc.) are very important components of the spindle.

CNC machines require tracking of the rotational speed and angular position measurement of the spindle continuously and precisely for machining quality. Encoders (optic, magnetic, etc.) are usually used on spindles for this task.

A spindle, depending on the application, might include a tool retention drawbar and tooling system as well as clamping and unclamping systems assembled onto it. A clamping system is used either to lock the tool holders to the spindle in case of a milling spindle through a tool interface (such as HSK, SK, etc.), or to clamp/unclamp the workpiece onto the chuck in case of a turning/grinding machine.

Also today, latest technologies and demands in the industry drives almost every spindle to be equipped with sensors for monitoring motor temperature and the position of the clamping system. Additional sensors for monitoring the bearings, the drive and the process stability can be attached. (Abele, Altintas and Brecher, 2010)

2.2 Spindle Design and Optimization

A precision spindle design is essentially made based on the below listed predefined requirements and constraints.

- Desired spindle power
- Maximum spindle loads, in other words the forces generated during cutting operation
- Maximum spindle speed
- Spindle type (externally or internally driven)
- Tooling style, size and capacities
- Dimensional constraints regarding the machine outer and inner space.
- Availability of the components to be purchased in the market
- Cost

Depending on the machine tool application area, spindles are subjected to different requirements. For example in high speed cutting applications with aluminum, high speeds with low stiffness spindles are performing better, whereas heavy duty machining of titanium or nickel based alloys require spindles that can endure to high cutting forces at low speeds. (Abele, Altintas and Brecher, 2010)

In this manner the selection of the drive motor, bearings and relative components as well as the design of the bearing configuration play a vital role on the performance, reliability and service life of the spindle. Additionally there are other factors to be considered during the design, which are lubrication of the bearings, clamping/unclamping mechanism, tool interfaces (for milling) and cooling of necessary units (bearings, motor, etc).

Spindle running life is dominantly decided by the spindle bearings but the overall performance of a spindle is affected by a set of factors which are the dimensions of the spindle shaft, stiffness, preload and spacing of the bearings, centrifugal forces from all rotating parts and work material properties. The static and dynamic stiffness of the spindle system directly affect the machining productivity and finish quality. Altintas and Cao (2005) developed a general finite element

model to simulate and optimize the spindle dimension to achieve maximum dynamic stiffness and increased material removal rate. The model can predict the stiffness of the bearings, contact forces on the bearing balls, natural frequencies and mode shapes, frequency response functions and time history response under cutting loads. The model includes the bearing preload, rotation effects from both bearings and the spindle shaft.

The configuration of the spindle essentially decided from the specifications of the workpiece material, desired cutting conditions and most common tools used on the machine tool. The spindle drive mechanism, drive motor, bearing types and spindle shaft dimensions are selected based on the target applications. Maeda, Cao and Altintas (2004), focusing on this issue, developed an expert spindle design system strategy which provides an interactive and automatic design of spindle drive configurations through a set of fuzzy design rules.

The speeds a spindle can reach and the loads it can carry are limited by its bearings. Friction and its thermal effects are the main factors affecting the speed limits, while the load capacity is determined by ball dimensions, ball material and bearing design. Sawamoto and Konishi (1982) showed $D_m n$ (spindle speed factor: D_m , pitch diameter of the bearing; n , maximum spindle speed) value of a spindle can be improved just by changing the bearing type, bearing design and lubrication method without any further changes on other parts.

Soshi, Yu, Ishii and Yamazaki (2011) concluded in their study that synchronous motors improve the performance of a spindle especially in heavy duty operations. Therefore a better performance spindle design can be achieved by using synchronous motor.

Static and dynamic properties of a spindle affect the quality and the efficiency of the machining operation. Better static and dynamic properties of a spindle allow to increase MRR (material removal rate) while providing good surface finish and precise dimensions. Hence the design of a spindle should be definitely analyzed to investigate its static and dynamic behavior during machining. Zhang, Wang, Zan and Hu (2011) conducted static and dynamic analyses on the high speed electric spindles with ANSYS, commercial FEM software. Lin (2014) used FEM to analyze the spindle and developed an approach to optimize the bearing span on the spindle shaft based on the first mode natural frequency of the spindle. Zhu, Zhu, Yu, Shi and Wang (2007) analyzed a turn-milling center spindle by FE simulation and presented that independent increases in bearing stiffness and bearing span lead to natural frequency increase hence improving the dynamic behavior of the spindle.

Altintas and Budak (1995) investigated the spindle performance further by taking the tool holder and tool into account and derive a stability diagram of the spindle as a function of speed which helps to predict the chatter zones and how to avoid them. Gagnol, Bouzgarrou, Ray and Barra (2006) suggested an approach to optimize the spindle design based on the stability lobes.

3 ANALYSIS AND PRELIMINARY DESIGN

In this chapter, necessary calculations and component selection process are studied to generate a preliminary spindle design. The analysis of the preliminary design is also presented to understand the static and dynamic behavior of the spindle.

3.1 Calculations and Preliminary Design

3.1.1 Force and power calculations

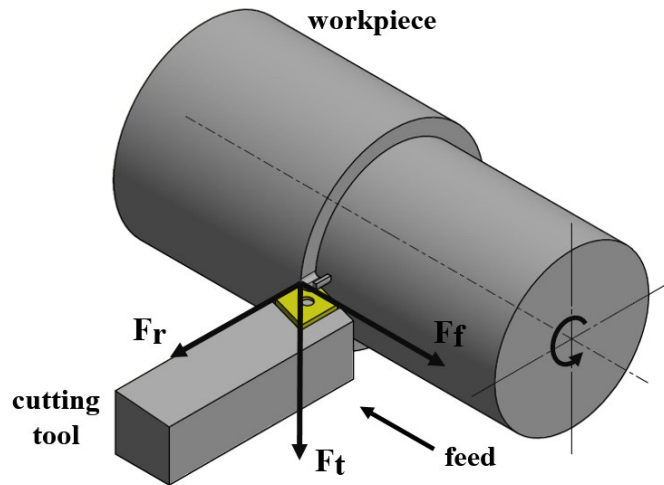


Figure 7. Cutting forces generated during turning operation

To remove material from the workpiece during the machining process, a chip removal force is applied through the cutting tool against the reaction forces generated in the cutting plane. Cutting plane is a theoretical plane where the material broken away from the workpiece by the tool turns into chip. The forces on the cutting plane consist of cutting force, friction forces between the chip and the tool, and the workpiece and the tool. The components of a cutting force in a turning operation is shown in Figure 7. In reality, it is a difficult task to analyze the cutting forces and mechanics in cutting operations due to complex workpiece and cutting tool geometries. To simplify the process and make easier estimations for the force and power calculations, the turning operation in our case will be assumed to be orthogonal cutting. In orthogonal cutting, the cutting edge of the tool is perpendicular to the feed direction. Hence no cutting force in the radial direction is generated on the tool, which makes the operation a two dimensional cutting process.

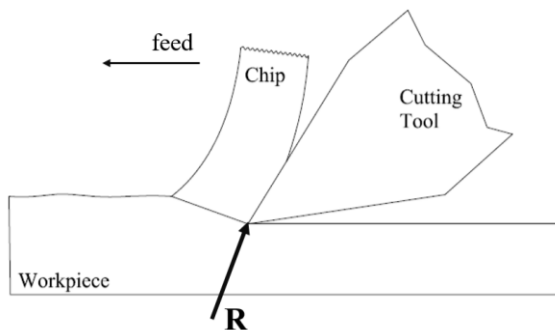


Figure 8. Cutting force, R

In the calculations, orthogonal cutting basics will be used to find the cutting force (see Figure 8) and its components. Although the cutting forces are actually distributed over the plane in orthogonal cutting, they can be shown as point forces applied to the tip of the cutting tool, according to Merchant (Akkurt, 2000). Therefore, all the forces acting at the tool tip can be shown in a Merchant circle as in Figure 9.

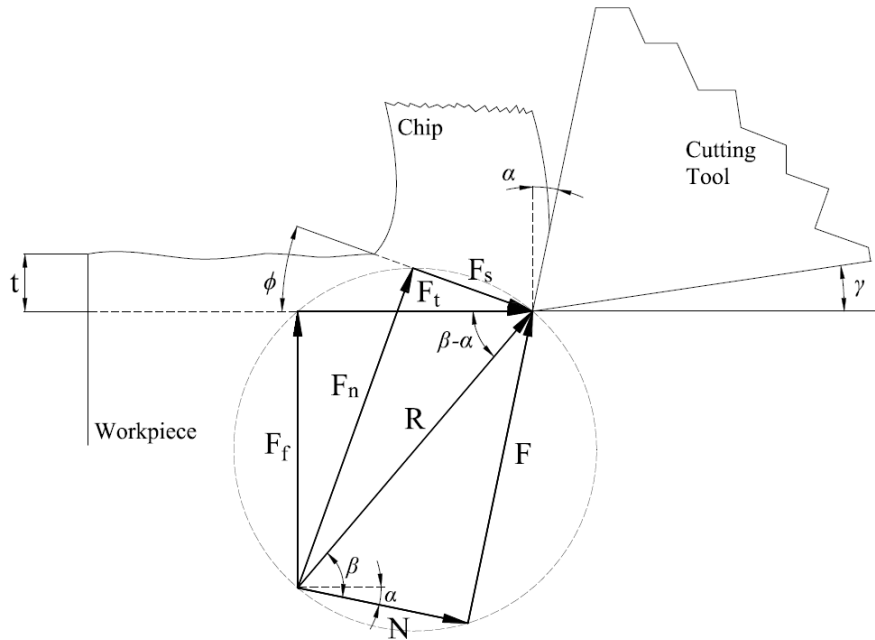


Figure 9. Cutting force diagram and Merchant circle

The forces in this diagram and their descriptions are listed below in Table 1.

Table 1. Forces in cutting zone and their descriptions

R	resultant cutting force [N]
F_f	cutting (feed) force component perpendicular to cutting direction [N]
F_t	tangential force on the cutting plane [N]
F_s	shearing force between the workpiece and chip that is shearing over [N]
F	friction force [N]
N	normal force generating the friction force F [N]

β angle can be defined as the friction angle between cutting force R and normal force N , and this angle can be defined in terms of μ , the friction coefficient.

$$\mu = F/N = \tan \beta \quad (1)$$

Then,

$$\beta = \tan^{-1} \mu \quad (2)$$

The shear force F_s and cutting section A_s of the shearing zone where the shear force occurs, can be defined through τ_s , the shear strength of the material.

$$F_s = A_s \tau_s \quad (3)$$

where,

$$A_s = t b_c / \sin \phi \quad (4)$$

b_c is the width of the cut in radial direction and ϕ angle is defined as the cutting angle, which is the angle between the cutting plane and the cutting direction.

Hence from the geometry in the Merchant circle, the components of R can be obtained as,

$$F_t = t b_c \tau_s \frac{\cos(\beta - \alpha)}{\sin \phi \cos(\phi + \beta - \alpha)} \quad (5)$$

$$F_f = t b_c \tau_s \frac{\sin(\beta - \alpha)}{\sin \phi \cos(\phi + \beta - \alpha)} \quad (6)$$

From above equations, minimization of total cutting energy, applying $d\tau_s/d\phi = 0$ gives;

$$\phi = \frac{\pi}{4} - \frac{\beta}{2} + \frac{\alpha}{2} \quad (7)$$

As given in equations (5) and (6), cutting forces can be obtained through the process parameters in the formulas. However, predicting and obtaining these operation specific parameters, especially friction angle, is difficult, therefore these formulas are used differently in practical applications. New K_t and K_f parameters, called as specific cutting and tangential force factors, are introduced as;

$$K_t = \tau_s \frac{\cos(\beta - \alpha)}{\sin \phi \cos(\phi + \beta - \alpha)} \quad (8)$$

$$K_f = \tau_s \frac{\sin(\beta - \alpha)}{\sin \phi \cos(\phi + \beta - \alpha)} \quad (9)$$

Using these new coefficients in equations (8) and (9), the cutting force and tangential force can be rewritten as,

$$F_t = t b_c K_t \quad (10)$$

$$F_f = t b_c K_f \quad (11)$$

K_t and K_f factors dependent on both the material (shear strength τ_s) and process specific (chip thickness t , chip angle α , cutting angle ϕ , slope angle λ , tool wear) parameters (Akkurt, 2000). Hence K_t and K_f are formulated as,

$$K_t = k_{tt} k_\alpha k_\lambda k_T k_a \quad (12)$$

$$K_f = k_{ft} k_\alpha k_\lambda k_T k_a \quad (13)$$

Table 2. Parameters affecting K_t and K_f

k_{tt}	chip thickness dependent specific cutting force factor
k_{ft}	chip thickness dependent specific tangential force factor
k_α	chip angle factor
k_λ	slope angle factor
k_T	cutting tool material and cutting method factor
k_a	tool wear factor

Among the above factors, chip thickness is the most decisive factor affecting K_t and K_f values as it is shown in the plot on Figure 10Figure 10. Chip thickness vs K_t and K_f plot (Akkurt, 2000). K_t and K_f are obtained through experimental methods for specific material, tool geometry and specific cutting conditions.

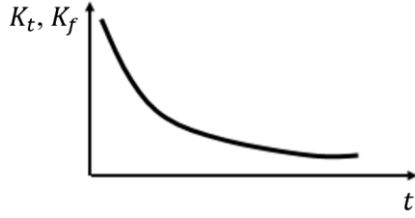


Figure 10. Chip thickness vs K_t and K_f plot (Akkurt, 2000)

To estimate the cutting forces and necessary power for the spindle, a possible worst case scenario is needed to be generated. The cutting process parameters are selected and made up according to the market survey. The cutting operations tested and succeeded on similar 52 mm spindles in the market are taken as reference to select our own parameters.

Hence, the sample case is: 200HB AISI 4340 part with a diameter of $D_S = \emptyset 110$ mm, length $L_S = 50$ mm is to be turned with a feed rate of $f = 0.35$ mm/rev, depth of cut $b_c = 6$ mm and spindle speed of $n_S = 600$ rpm. The machine tool efficiency is accepted as $e = 0.95$ (95%).

In this case, the cutting speed V ,

$$V = \pi D_S n = 207.3 \text{ m/min} \quad (14)$$

For AISI 4340 with 200HB hardness, the parameter formulas necessary to find the material specific K_t and K_f values are given in Table 3. These parameters are obtained experimentally specifically for AISI 4340 steel (Altintas, 2012).

Table 3. Orthogonal Cutting Parameters for AISI 4340 (Budak and Ozlu, 2014)

Friction Angle	$\beta = 20.6 + 0.12\alpha$
Shear Angle	$\phi = \tan^{-1} \left(\frac{r_c \cos(\alpha)}{1 - r_c \sin(\alpha)} \right)$ $r_c = C_0 t^{C_1}$ $C_0 = 0.8477 - 0.0048\alpha$ $C_1 = 0.2775 - 0.0047\alpha$
Shear Stress	$\tau_s = 650 \text{ MPa}$

Then, if we assume $\alpha = 5^\circ$ as the cutting tool rake angle, which is a common value for the cutting tools, we obtain;

$$\beta = 20.6 + 0.12\alpha = 21.2^\circ \quad (15)$$

$$C_0 = 0.8477 - 0.0048\alpha = 0.8237 \quad (16)$$

$$C_1 = 0.2775 - 0.0047\alpha = 0.254 \quad (17)$$

$$r_c = C_0 t^{C_1} = 0.631 \quad (18)$$

$$\phi = \tan^{-1} \left(\frac{r_c \cos \alpha}{1 - r_c \sin \alpha} \right) = 33.63^\circ \quad (19)$$

Then K_t and K_f factors can be calculated as,

$$K_t = \tau_s \frac{\cos(\beta - \alpha)}{\sin \phi \cos(\phi + \beta - \alpha)} = 1,742.2 \text{ N/mm}^2 \quad (20)$$

$$K_f = \tau_s \frac{\sin(\beta - \alpha)}{\sin \phi \cos(\phi + \beta - \alpha)} = 507.6 \text{ N/mm}^2 \quad (21)$$

F_t and F_f forces are,

$$F_t = t b_c K_t = 3,662 \text{ N} \quad (22)$$

$$F_f = t b_c K_f = 1,066 \text{ N} \quad (23)$$

Resultant cutting force R ,

$$R = \sqrt{F_f^2 + F_t^2} = 3,821 \text{ N} \quad (24)$$

The power required to rotate the spindle and the workpiece at a constant speed is often neglected in motor power calculations, because it is relatively low compared to the machining power needed during the cutting process. Even the power necessary to accelerate the spindle and workpiece from stationary condition until they reach the constant rotational speed, is still much smaller than the maximum machining power needed in this case. Additionally, since the cutting process starts after the spindle reaches constant rotational speed, the power needed for this initial speeding stage is ignored.

The shearing force F_s , between the workpiece and the material shearing over during cutting can be calculated from Merchant circle as,

$$F_s = F \cos(\phi + \beta - \alpha) = 2,465 \text{ N} \quad (25)$$

Shearing velocity V_{sh} and shearing power P_s ,

$$V_{sh} = V \frac{\cos \alpha}{\cos(\phi - \alpha)} = 235.3 \text{ m/min} = 3.922 \text{ m/sec} \quad (26)$$

$$P_s = F_s V_{sh} = 9,667.3 \text{ W} \quad (27)$$

Friction force generated by the chip flowing over the tool,

$$F = R \sin \beta = 1,382 \text{ N} \quad (28)$$

Chip velocity,

$$V_c = r_c V = 130.8 \text{ m/min} = 2.18 \text{ m/sec} \quad (29)$$

Friction power,

$$P_f = F V_c = 3,012.5 \text{ W} \quad (30)$$

Total cutting power needed at the tool tip,

$$P_t = P_f + P_s = 12,680 \text{ W} = 12.7 \text{ kW} \quad (31)$$

Total cutting power drawn from the motor,

$$P_{Motor} = \frac{P_t}{e} = 13.3 \text{ kW} \quad (32)$$

Therefore, the necessary motor power should be 13.3 kW minimum. Selection of the motor will be based on this power value.

3.1.2 Selection of the motor

The machining power required for turning operations is directly supplied by the internal motor in the spindle system. Therefore the motor to be selected must be sufficient to meet the power and speed requirements, besides of fitting into the size limitations.

Due to cost issues, it is always desired to use standard commercial components in the designs rather than custom made ones. Therefore, the motor is preferred to be selected from standard catalogue products of well-known motor suppliers. As it was explained in the previous sections briefly, the motor is required to be a synchronous permanent magnet internal motor. In this

thesis, since Siemens spindle motors have a widest range and use in the machine tool area, their products are examined for selection.

Based on the requirements of $n_{motor} = 6,000$ rpm, $P_{motor} = 13.3$ kW and a spindle outer diameter of less than $D_{max} = \emptyset 250$ mm, the available motors in the product range of Siemens with possible matching specs are listed in Table 4.

Table 4. Siemens synchronous built-in motors for the design (Siemens, 2010)

Motor	Rated Torque [Nm]			Rated Speed [rpm] 380V	Max Speed [rpm]	Power [kW] 380V	Outer Ø [mm]	Inner Ø [mm]	Length [mm]
	S1	S6-%40	S6-%25						
1FE1084-6WR*1	130	175	200	2,000	9,000	27.2	190	74.2	295
1FE1084-6WU*1	130	175	200	1,450	7,000	19.7	190	74.2	295
1FE1093-6WN*0	100	128	147	3,130	7,000	32.8	205	80.2	250
1FE1093-6WV*1	100	128	149	1,600	7,000	16.8	205	80.2	250
1FE1113-6WU*1	150	190	220	1,880	6,500	29.5	250	80.2	260
1FE1114-6WR*1	200	256	292	1,790	6,500	37.5	250	82.2	310
1FE1114-6WT*1	200	256	292	1,250	6,500	26.2	250	82.2	310

In Table 4, the red marked motor is the one selected for the spindle design. It has the specifications which meet the requirements better than any other.

1. It has 16.8kW power which is more than the necessary motor power $P_{motor} = 13.3$ kW calculated for the reference machining operation.
2. It has the maximum speed of 7,000 rpm which is above the requirements, $n_{motor} = 6,000$ rpm.



Figure 11. Components of Siemens synchronous built-in motors (Siemens, 2010)

3. Outer diameter of $\emptyset 205$ mm and inner diameter of $\emptyset 80.2$ mm of the motor seem to be sufficient to achieve the cartridge spindle design with $\emptyset 250$ mm outer diameter and $\emptyset 52$ mm bore diameter. Although our spindle outer diameter limit is $D_{max} = \emptyset 250$ mm, the motor should be much smaller when the stator housing that the motor is installed into is considered. Therefore, the other motors would obviously cause many problems in terms of dimensions since they have either too big outer diameter or too small inner diameter. Hence selected motor almost comes out as the only option in terms of size. Please see Appendix B for the detailed performance data and dimension drawings of the motor.

3.1.3 Selection of the bearings

A spindle system consists of many parts other including bearings and every part has its own duty and importance in the overall system. Even the lubricant and sealing elements have crucial roles in the performance and life of the spindle. Therefore, while selecting bearings, the overall system requirements and limitations must also be taken into account.

Several factors must be taken into account and their importance differs when selecting a bearing, therefore no universal rules exists for bearing selection. Even the total cost of a shaft system and inventory considerations can influence bearing selection. The critical factors that matters in the bearing selection process can be listed as:

- loads on the bearing
- desired speed
- available space
- precision and stiffness required
- operating temperature
- vibration
- contamination levels
- lubrication type and method

Bearings used on spindles are specialized products and they mostly have specific use only in spindles or similar shafts. Spindle bearings vary in structure, design, material, accuracy and dimensions to meet different spindle specifications and needs. Therefore the differentiation can provide different load carrying capacities, permissible speeds and precision levels for spindles. Below in Figure 12, a comparison chart for the performance requirements of the spindles for different applications is given.

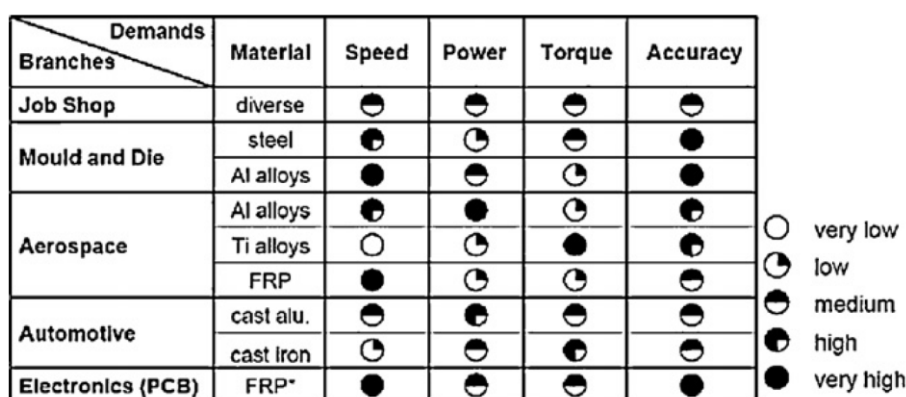


Figure 12. Comparison of spindle performance requirements for different applications (Abele, Altintas and Brecher, 2010)

There are many different types of bearings used in spindles depending on the application requirements. Some of the most common bearing types are:

- rolling bearings (angular contact ball bearings, roller bearings, etc.)
- hydrodynamic bearings
- hydrostatic bearings
- electromagnetic bearings
- aerostatic bearings

The dimensional accuracy and surface finish of the work being machined, as well as the rate of metal removal of a machine, are among the factors directly governed by the static, dynamic and thermal behavior of the spindle bearings. Different bearing types and designs have their own advantages and disadvantages. Different type of bearings are compared by their effects on different spindle properties as shown in Figure 13.

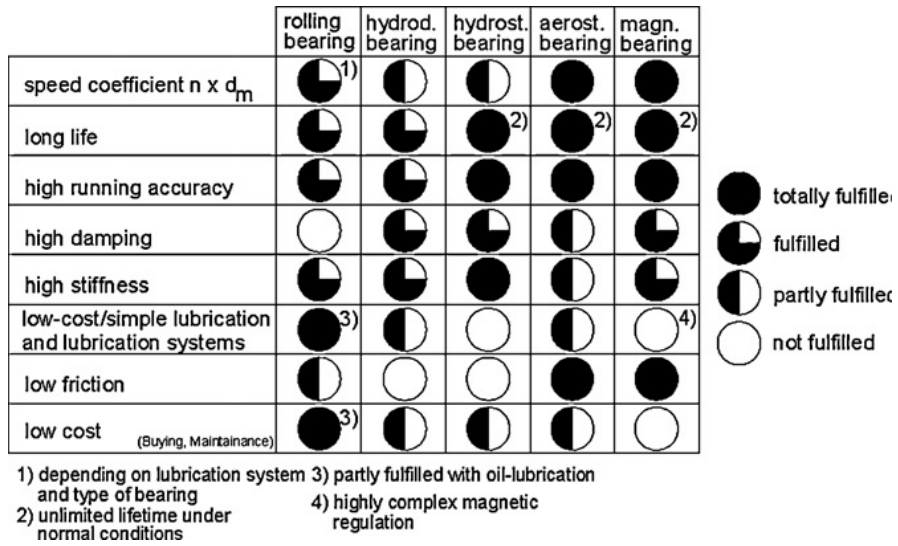


Figure 13. Comparison of bearing system properties (Weck, 1984)

The design requirements in this thesis state that the design should provide a medium speed spindle (spindle speed factor $Dn < 800,000$: D , inner diameter of the bearing; n , maximum spindle speed, Stephenson and Agapiou, 1997) and be capable of reasonable loading, stiffness and life together. Therefore, the bearing type used must be consistent with these demands, hence rolling bearings are found sufficient to meet the requirements. However, the selection criteria of which rolling bearing type to use depends upon the spindle specifications, as each will have an impact or impact upon the bearing selection as it is shown in Table 5.

Table 5. Rolling bearing selection criteria (Dynomax, 2011)

Requirement	Best Bearing Type	Design Impact
High Speed	Small Contact Angle	Small Shaft, Low Power
High Stiffness	Large Roller	Low Speed, Large Shaft
Axial Loading	High Contact Angle	Lower Speed
Radial Loading	Low Contact Angle	Higher Speed
High Accuracy	ISO P2 type High Preload	Expensive, Lower Speed

Clearly seen from Table 5, the spindle with the highest speed will not have the maximum stiffness possible, and the spindle with the highest stiffness cannot run at high speed without sacrificing bearing life. So, compromises must be made in order to arrive at the most efficient design possible.

In our case, since demanded speeds are not in the high speed zone and required load carrying capacity is relatively lower than in the heavy duty turning operations, a medium performance bearing type will be sufficient. Angular contact ball bearings are selected for the design in this thesis. Angular contact ball bearings are today most commonly used in medium and high speed spindle designs, since with a wide range they can provide the precision, load carrying capacity, and speed necessary for different metal cutting spindles.

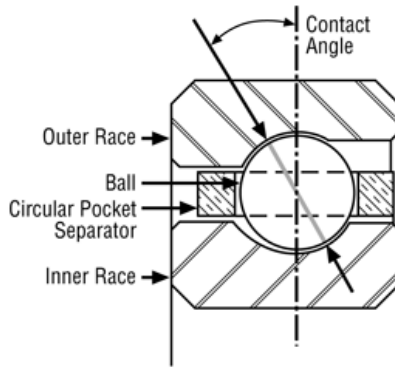


Figure 14. Cross section of an angular contact ball bearing (Kaydon Bearings, 2015)

An angular contact ball bearing, as the name indicates, features a contact angle between its balls and the raceways on the rings as shown in Figure 14. The contact angle defines the load carrying capacity of the bearing in axial and radial directions. Bearings with smaller angles can take more radial loads than the same size bearings with higher angles, while higher angles helps to carry more axial loads. The standard angles for angular contact ball bearings in the market are 15° , 18° and 25° .

In spindles which utilizes internal motor for medium and high speed applications, the internal heat generation can be much higher than in the belt/gear driven spindles. Heat generation leads thermal expansion in the components and especially can reduce the bearing internal clearance, sometimes causing failures at top speeds. For these applications it is more beneficial to use bearings with 25° contact angle. These bearings have greater radial internal clearances compared to one with smaller contact angles and can more easily accommodate a reduction in internal clearance due to thermal expansion (NSK, 2009). Also bearings with 25° contact angle are better for combined loadings, since they have a more balanced axial and radial load ratings, which is better for turning operations.

Regarding the rigidity of machine tool spindles, it is possible to think of the bearings as springs with certain stiffness and damping values. Axial displacement, when an axial load is applied to the spindle, is determined by the axial rigidity of the bearings which constraints the shaft axially. Axial loads are usually sustained by three or four angular contact ball bearings. The bigger the contact angle of the angular contact ball bearings, the higher the axial rigidity. When high radial rigidity is required, cylindrical roller bearings are generally used. In our case angular contact ball bearings are sufficient to withstand the axial and radial loads during machining.

Normally preload is applied to the bearings in order to increase the rigidity of machine tool spindles. A larger preload results in higher rigidity. However, if preload is larger than necessary, abnormal heat is generated, which reduces fatigue life and maximum permissible speeds. In extreme cases, it may result in excessive wear or even seizure. Hence, the correct preload should be selected and applied on the bearings to get the best performance. The main purposes of preloaded bearings in a machine tool spindle are as follows;

- To improve and maintain the running accuracy of the shaft
- To increase bearing rigidity
- To minimize noise due to axial vibration and resonance
- To prevent false brinelling
- To prevent sliding between the rolling elements and raceways due to gyroscopic moments
- To maintain the rolling elements in their proper position (NSK, 2011)

An angular contact ball bearing cannot be used by itself and withstand the loads due to its unique design which creates the angular contact and allows preloading. Therefore, they must be used at least as a pair supporting each other. There are many possibilities for the number of the bearings and their layouts that may be chosen, as shown in Figure 15. The number of the bearings and their layout directly affect the load carrying capacity and permissible maximum speed of the spindle.

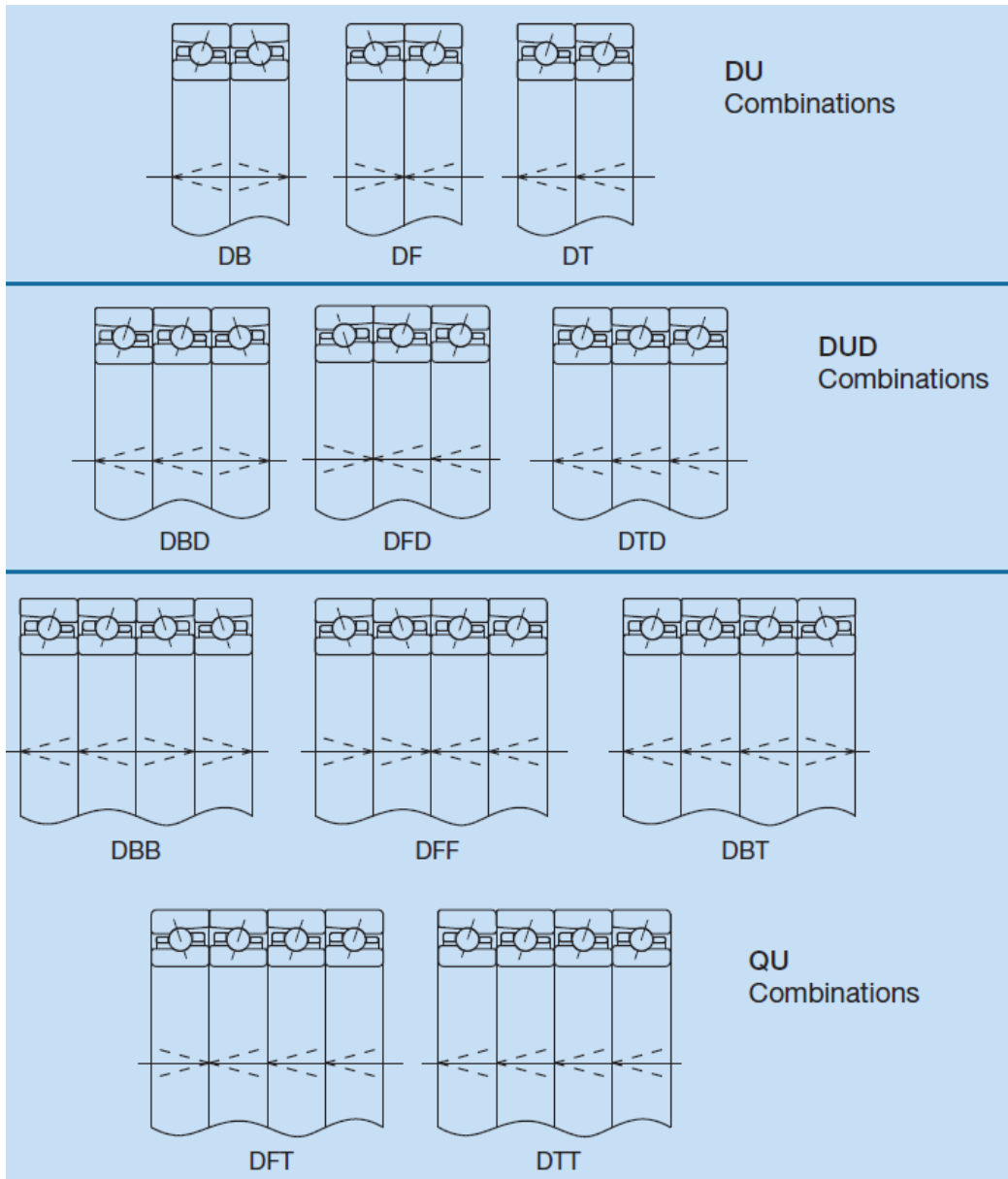


Figure 15. Different angular contact ball bearing layouts (NSK, 2009)

Different layouts and their performance comparison based on the application is given in Table 6. Since different applications have different needs, particular designs are usually preferred for each. The marked design layout is selected for the spindle design in thesis due to its speed, rigidity and load carrying capacity properties. Although grinding spindles are the typical application for this layout, it can be used in a lathe spindle as well. Also this layout has superior performance properties compared to the other lathe spindle configurations in the table. The selected layout consists of four angular contact ball bearings in the front with DBB arrangement and a double row cylindrical roller bearing at the rear.

Table 6. Comparison of the different bearing layouts based on applications and performance data (FAG, 2010)

Bearing arrangement		Typical application	Speed suitability %	System rigidity %		Load carrying capacity %		Temperature behaviour	
front	rear			axial	radial	axial	radial	Load	Sensitivity
==≤	==	Universal	50	100	100	60	100	+	+
<<>>	==	Grinding	72	65	100	75	50	++	++
<<>	==	Turning	65	44	86	75	47	+	++
<<>	<>	Turning, grinding	65	44	84	75	44	++	+
<>	=	Wood, motor	75	32	79	35	42	+++	+++
<>	<>	Drilling, motor	75	32	77	35	40	+++	+++
<	>	Milling, drilling	85	30	62	35	22	+++++	++++++
<<	>>	Milling, drilling, universal	80	61	95	75	44	****	*****
<<>	>>	Milling, drilling, universal	75	76	98	100	46	***	****
<	≈>	Motor	100	23	60	30	27	++++++	++++++
<<	≈>>	Motor	100	46	92	60	52	+++++	+++++
<≈>	≈>	Motor	100	25	89	25	60	+++++	++++++
<≈>	=	Motor	80	23	82	30	46	+++++	+++
<<≈>	≈>	Motor	100	46	93	50	65	+++++	++++
<<≈>>	≈>>	Motor	100	48	98	48	65	+++	++++

100 Optimum
 + Very unfavourable
 +++++++ Very good
 < Spindle bearing
 = Single row cylindrical roller bearing
 == Double row cylindrical roller bearing
 ≈≤ Double direction axial angular contact ball bearing
 ≈ Spring

The DBB layout used in this design has the advantage of providing a good end restraint for the shaft due to the line of action for the force transmission of the balls, and is, therefore, particularly well-suited for the absorption of cantilever loads. Furthermore, this arrangement is able to deal with axial loads in both directions. Also, when angular contact ball bearings are mounted in pairs and with opposite directions of the axes of the rolling elements, then the radial load is evenly distributed between them (Weck, 1984).

For the angular contact ball bearings in the front, **NSK 7020A5-TRS-DB-EL-P3** spindle bearings are selected. The specifications of these angular contact ball bearings are given in Table 7. The bearings are selected EL (Extra Light) preload level due to its advantage in limiting speeds as it will be discussed below and shown in Table 9. The preload level of the bearings can be increased if the rigidity of the spindle is found insufficient in the analyses.

Table 7. Properties of NSK 7020A5-TRS-DB-EL-P3 bearings (NSK, 2011)

Bearing Code	Dimensions [mm]			Load Ratings [kN]		Permissible Axial Load [kN]	Mass [kg]	Limiting Speeds [rpm]	
	Inner dia.	Outer dia.	Width	Dynamic	Static			Grease	Oil
7020A5	100	150	24	71.0	73.5	57.5	1.45	8,000	12,000

For the rear bearings, there are more factors to consider. Heat is the vital enemy of the machine tools and spindle is one of the prime sources of heat generation in the machine. Before the

introduction of internal spindles, most machine tool spindles were driven with belts or gearboxes attached externally to the drive motor. Therefore less heat was generated in the working area.

However, integrating the electric motor into the spindle creates a heat source that in precision machining applications must be controlled. The cutting tool is always in direct contact with the spindle and as the spindle dimensions change due to thermal expansion, the cutting tool's position on the workpiece is affected as well. Figure 16 shows how the temperature influences the dimensions of certain parts of the spindle.

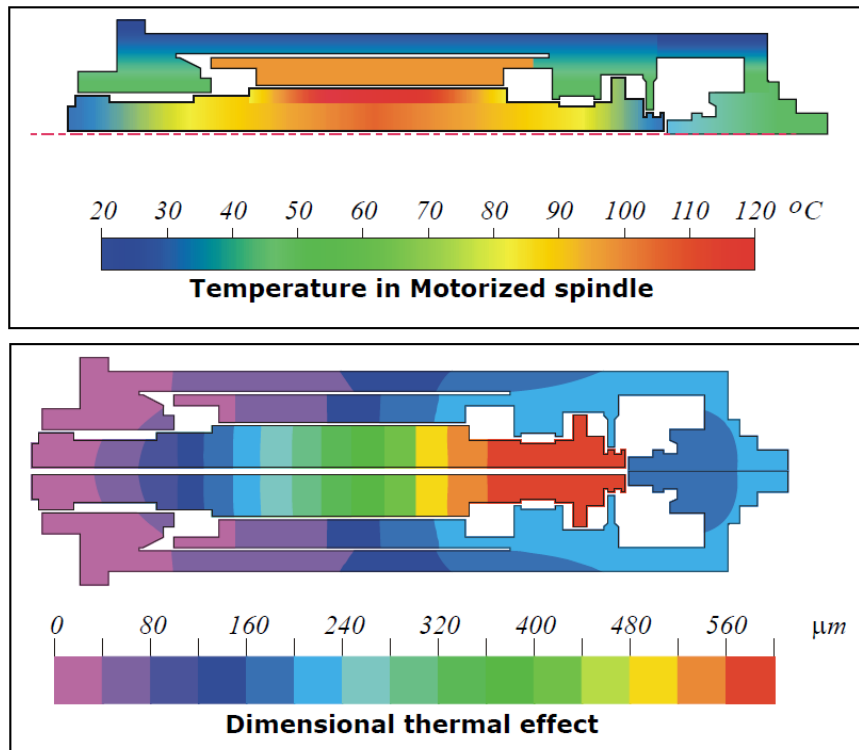


Figure 16. Heat generation in a milling spindle due to built-in motor and its dimensional effects (Dynomax, 2011)

Many machine builders use an active system to stabilize the temperature of the spindle. Most integral spindles use a cooling jacket around the outside of the motor stator housing with water or coolant as the cooling medium. The water jacket that surrounds the motor indirectly removes heat created by the rotating rotor and internal winding that has then transferred to the stator. The cooling water is pumped and circulated through a separate heat exchanger.

Despite the active cooling system on the stator, the core of the motor and rotor is still affected by the heat generated, and they cause the spindle shaft to thermally expand. The shaft will elongate in both radial and longitudinal directions due to temperature rise, but the expansion in the latter one will be more significant due to the thermal expansion:

$$\delta_{Thermal} = \alpha_T \Delta T L_i \quad (33)$$

where $\delta_{Thermal}$ is the change in length due to temperature increase, α_T is the thermal expansion coefficient, ΔT is the temperature increase and L_i is the initial length in the direction of expansion. Since the initial length of the shaft is greater than the shaft diameter, the longitudinal expansion will be much more than the radial one. Thermal expansion greatly affects the overall system and especially the bearings, finally increasing the preload and friction in them. Increased friction will cause temperature rise on the balls, less grease/oil effectiveness, therefore less bearing life and performance. To overcome this expansion problem, the spindle is designed to let the shaft elongate freely on the rear end to let the bearings only experience the preload increase in radial direction which is less significant.

The bearings layout are selected in Table 6 also aims to have a fixed-free support design, which is fixed at front and free at rear. Front bearings are secured in their place by preloading and other associated parts to have fixed support. Front bearings support the system both in axial and radial direction, carry most of the radial and all of the axial loads in the system, and provide the axial rigidity of the spindle. On the other hand, rear bearings support the spindle only in radial direction and they let the spindle to expand axially towards the rear end, therefore the front bearings are affected less from the thermal expansion and the spindle nose stays almost at the same position, providing accuracy and repeatability.

To overcome the expansion problem, **NSK NN3020-TB-KR-CC1-P3** double-row cylindrical roller bearing with tapered bore is selected for the rear (free end) support of the spindle shaft. The specifications of these bearings are given in Table 8. These bearings feature an outer ring which does not constrain the rollers in axial direction, hence allows them to slide in the raceway axially. Tapered bore of the bearing helps to get zero clearance in radial direction, hence reducing vibrations and increasing precision, though it requires special gauges for assembly.

Table 8. Properties of NSK NN3020-TB-KR-CC1-P3 bearing (NSK, 2011)

Bearing Code	Dimensions [mm]			Load Ratings [kN]		Mass [kg]	Limiting Speeds [rpm]	
	Inner dia.	Outer dia.	Width	Dynamic	Static		Grease	Oil
NN3020-TB-KR	100	150	37	149	247	2.12	6,800	8,000

The permissible speed should be checked for the layout selected to ensure the design requirements are met with the selected bearings. Table 9 shows the limiting speed factors for different layouts. For DBB layout with EL preloaded bearings the speed factor is 0.80. Hence, when 7020A5-TRS-DB-EL-P3 bearings are used, the limiting speed will be $8,000 \text{ rpm} \times 0.80 = 6,400 \text{ rpm}$ with grease lubrication. For the rear bearing, NN3020-TB-KR-CC1-P3, the limiting speed is 6,800 rpm. Therefore both for the front and rear bearings the limiting speeds are above 6,000 rpm, selected bearings meet the speed requirements.

Table 9. Limiting speed factors for different arrangements and preloads (NSK, 2011)

	Arrangement	EL	L	M	H
DB		0.85	0.80	0.65	0.55
DBB		0.80	0.75	0.60	0.45
DBD		0.75	0.70	0.55	0.40

The sufficiency of the load ratings and life of the bearings selected could be investigated for the cutting operations. However, since the basic load ratings given in Table 7 and Table 8 are far above the calculated cutting forces, they are assumed to be enough to carry the necessary loads. Hence, no further verification is needed for the bearing load ratings.

3.1.4 Preliminary design

The preliminary design of the spindle is shown in Figure 17. Angular contact ball bearings are mounted on the shaft with DBB configuration. The span between the pairs in the front are granted with spacers. When a DBB arrangement is used, the span distance between the pairs is advised be at least 1.25x of the width of a single bearing (NSK, 2009). The double row

cylindrical roller bearing is mounted on a bearing seat which has interference fit with the shaft. The rotor also mounted on the shaft as shown with an interference fit. The spindle has A6 interface design for the workpiece holder.

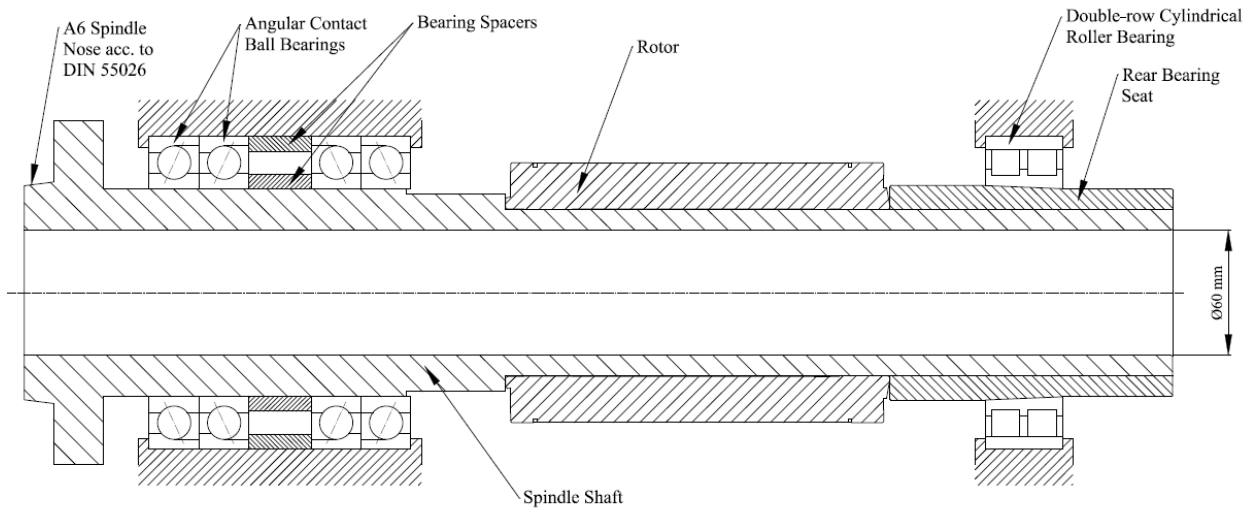


Figure 17. Preliminary design of the spindle

Ck45 (AISI 1045) steel is selected as the material of the spindle shaft. Ck45 is a common spindle shaft material with its sufficient mechanical properties, good machinability, good response to heat treatment and moderate cost. The properties of Ck45 are given in Table 10. The shaft material can be changed with another steel which has higher yield strength, if the analyses show that the preliminary design deforms plastically under maximum loading.

Table 10. Properties of Ck45 (AISI 1045) steel, as cold drawn (Matweb, 2015)

Density	7.87 g/cm ³
Hardness, Brinell	170 HB
Ultimate tensile strength	515 MPa
Yield strength	485 MPa
Modulus of Elasticity	206 GPa
Poissons Ratio	0.29
Shear Modulus	80 GPa

3.2 Analysis and Optimization

During machining, spindle experiences various loads due to cutting, centrifugal effects, etc. These loads may invoke self-excited vibrations and a spindle failure due to high deformation and high stresses generated. Therefore, the spindle design should be analyzed and verified statically and dynamically.

The static analysis of the spindle basically deals with the spindle stiffness which is closely related to the load capacity and vibration resistance of the spindle. It also helps to analyze the accuracy loss during limit pushing cutting operations.

Every spindle experiences vibration due to the nature of cutting operation, but the severity of the vibration greatly influences the machining accuracy, the life of cutting tool and spindle, cutting power necessary for the operation. Compared to milling spindles, lathe spindles experience less vibration related problems due to lower rotational speeds and higher spindle stiffness. But still, the dynamic analysis is important to investigate and understand the spindle modal behavior.

Then the design should be modified if there is any possible vibration problem within the working speed range of the spindle.

In this thesis, the preliminary spindle design is analyzed both statically and dynamically. The static analysis mainly focuses on the spindle deflection and stiffness in the loaded case, which is the worst case machining scenario examined in the Section 3.1.1. The distances between the bearings, or the support locations on the spindle shaft, directly affect the spindle static stiffness, therefore in the static analyses, investigation and selection of optimum bearing spans within an applicable range is calculated analytically. These optimum values are used in the further analyses and the final design. And finally in the dynamic analysis, the modes, natural frequencies and the critical speeds of the design are investigated.

3.2.1 Static analysis

During machining, both in axial and lateral directions, cutting forces are generated on the spindle. However, in most cases, lateral loads are greater than the axial loads, and similarly the axial stiffness of the spindle is greater than the bending stiffness. Therefore, especially for lathe spindles, it is more important to investigate the lateral loading of the spindle in the static analysis. In this thesis only the lateral deflection and bending stiffness are studied and calculated.

The resulting lateral deflection of a spindle due to loading is determined by the elastic behaviors of both the shaft and the bearings, or stiffness in this case. Therefore, a superposition method is applied to calculate the total spindle deflection analytically, then to verify the FEM solution in ANSYS. Superposition method examines spindle in two separate cases and calculates the deflection for each case, and then adding them up algebraically to obtain the total deflection in the original case. The spindle superposition is composed of the two cases:

1. Elastic spindle shaft supported with completely rigid bearings (no spring behavior by the bearings)
2. Completely rigid spindle shaft, with flexible elastic bearings

Preliminary spindle design is actually a statically indeterminate structure with three bearing supports on it. To validate our superposition method first, a simpler test model is created and analyzed with both analytical method and FEM.

3.2.1.1 Test model

To be able to validate that the superposition method is correct and FEM results correlate with the analytical Matlab model, a simple test model is created and studied.

Similar to the spindle, the test model is a simplified straight steel shaft with a diameter of Ø50 mm. The shaft is supported and fixed at two points by two ball bearings with stiffness, k_{Test} . A test load of F_{Test} is applied at the end of the shaft as shown in Figure 18. The test model data is given in Table 11.

Table 11. Test model data

Length of shaft, L_{Test}	600 mm
Span distance, s_{Test}	360 mm
Overhung distance, a_{Test}	240 mm
Diameter of shaft, D_{Test}	Ø50 mm
Young's Modulus, E_{Test}	200 GPa (generic steel)
Load, F_{Test}	1000 N
Bearing stiffness, k_{Test}	5×10^5 N/mm

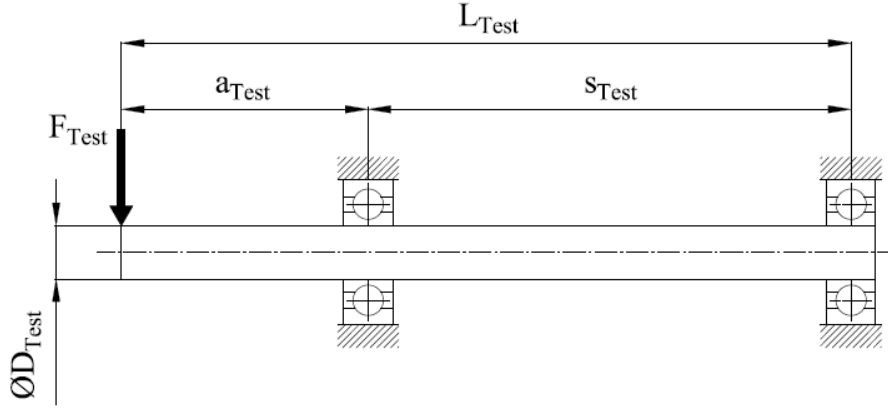


Figure 18. Test model

a. Analytic analysis of the test model

The test model can be represented as shown in the Figure 19 where the shaft is a beam with an area moment of inertia I_{Test} , and the bearings are longitudinal springs with k_{Test} stiffness.

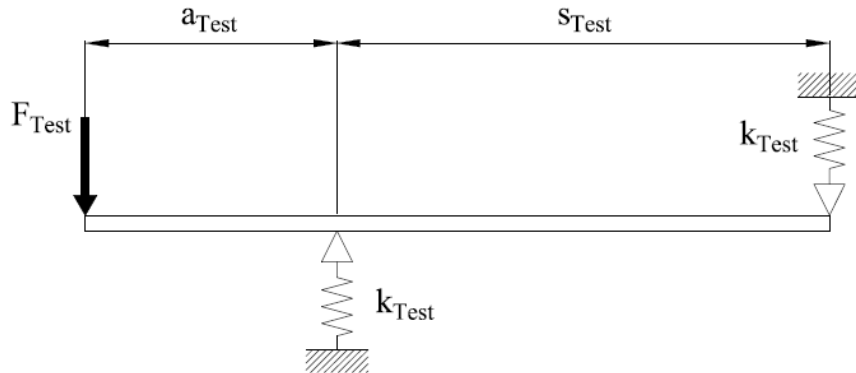


Figure 19. Test model representation

The Matlab model and analytical solution of the deflection for the test model are made with the superposition method explained before. The deflections for separate cases, elastic beam-rigid supports and rigid beam-elastic supports, are superposed as shown below Figure 20 to get the total shaft deflection at the end.

The total deflection at the shaft end of the test model, δ_{Test} , will be the algebraic sum of the deflections for each superposition case. Therefore the resulting deflection will be as,

$$\delta_{Test} = \delta_{S_{Test}} + \delta_{B_{Test}} \quad (34)$$

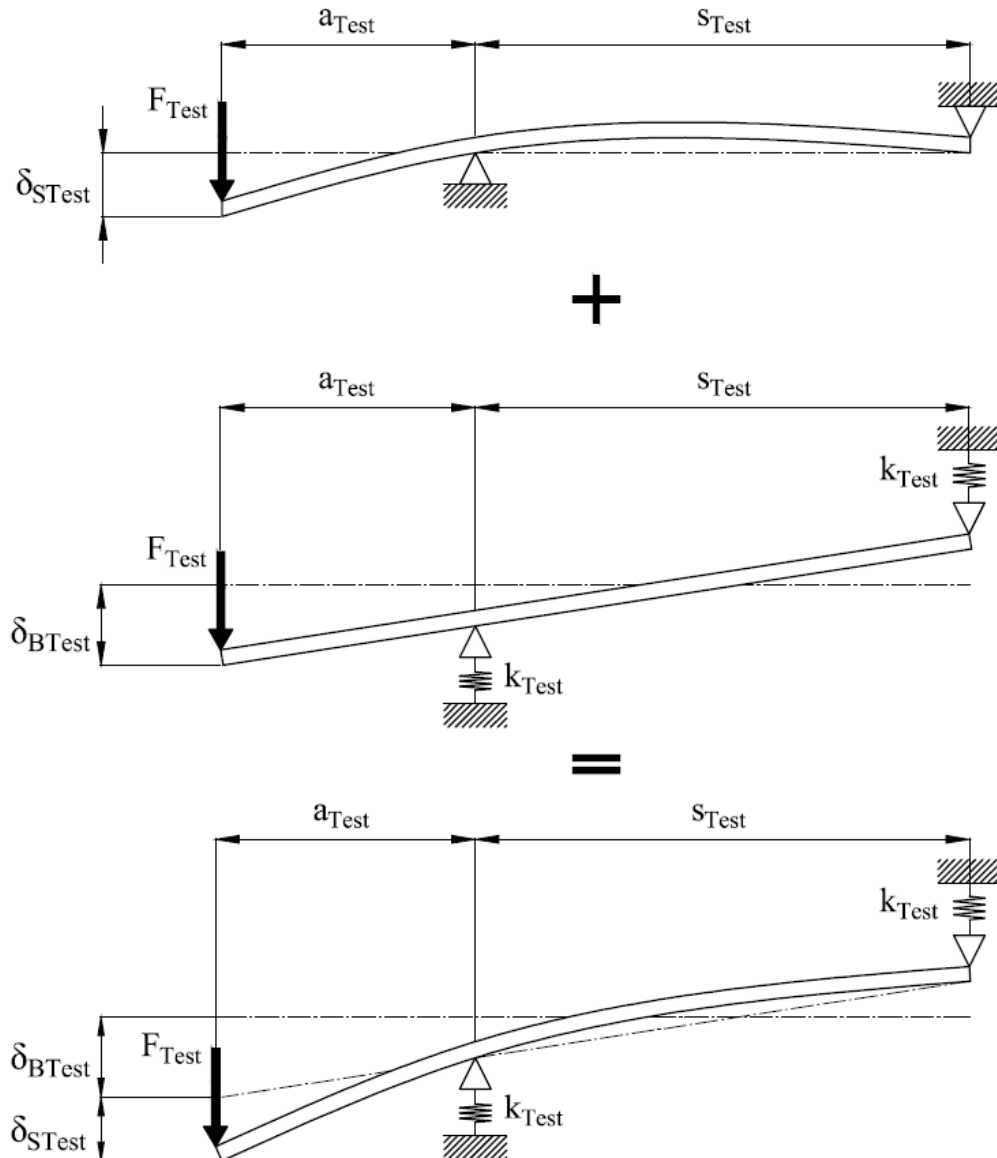


Figure 20. Superposition of the test model

The basic assumptions of the superposition method and analytical analysis for the test model can be listed as;

1. The test model shaft is assumed to be an Euler-Bernoulli beam.
2. Both the beam and the bearings act according to the Hooke's Law.
3. Any torsional and axial deflections of the shaft are neglected.
4. Deflections and slopes are small.
5. The bearing housings are assumed to have infinite stiffness.
6. The contribution of transverse shear deformation to the overall lateral deflection is assumed to be negligible.
7. Deflections do not change the behavior of the loads or reactions.

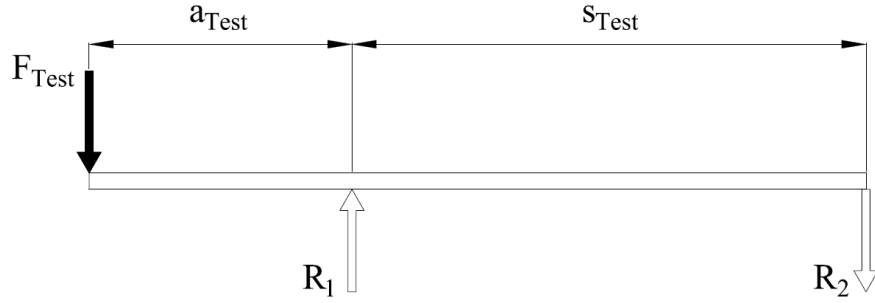


Figure 21. Free body diagram of the test model

To be able to get the deflection equations, the reaction forces are needed at the support locations. Free body diagrams for both *superposition I* and *superposition II* will be identical as shown in Figure 21, therefore reaction forces R_1 and R_2 generated in the bearings can be expressed as,

$$R_1 = \frac{F_{Test} L_{Test}}{s_{Test}} \quad (35)$$

$$R_2 = \frac{F_{Test} a_{Test}}{s_{Test}} \quad (36)$$

Test model superposition I

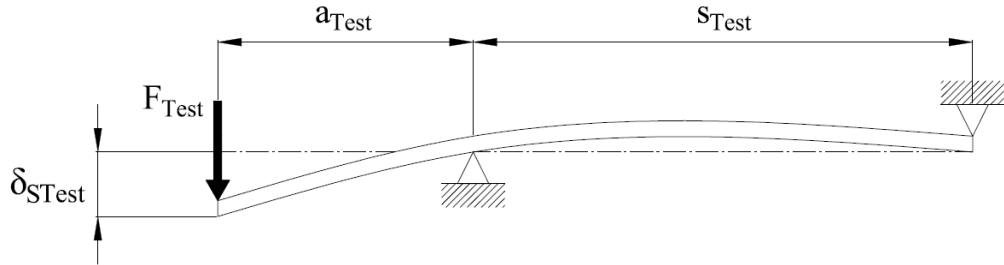


Figure 22. Superposition I of the test model

The load on the shaft in elastic beam-rigid supports case can be expressed as a loading function, which will eventually help us to obtain deflection equation of the shaft. Macaulay functions and singularity functions will be used to define the loading as a single function on the shaft (see Appendix C).

Hence, the loading function of the test model can be expressed as,

$$w' = F_{Test} \langle x - 0 \rangle^{-1} - R_1 \langle x - a_{Test} \rangle^{-1} \quad (37)$$

Then integrating the loading function will yield to the shear function, where $dV'/dx = -w'(x)$;

$$V' = -F_{Test} \langle x - 0 \rangle^0 + R_1 \langle x - a_{Test} \rangle^0 \quad (38)$$

$dM'/dx = V'(x)$, therefore integrating again will give the moment function of the shaft;

$$M' = -F_{Test} \langle x - 0 \rangle^1 + R_1 \langle x - a_{Test} \rangle^1 \quad (39)$$

$$M' = -F_{Test} x + R_1 \langle x - a_{Test} \rangle^1 \quad (40)$$

Using the moment and deflection relationship,

$$E_{Test} I_{Test} \frac{d^2 v'}{dx^2} = M'(x) \quad (41)$$

$$E_{Test} I_{Test} \frac{d^2 v'}{dx^2} = -F_{Test} x + R_1 \langle x - a_{Test} \rangle^1 \quad (42)$$

Then the slope function of the shaft will be as,

$$E_{Test} I_{Test} \frac{dv'}{dx} = -\frac{F_{Test} x^2}{2} + \frac{R_1}{2} (x - a_{Test})^2 + c_1 \quad (43)$$

Integrating above equation once more will provide the deflection function of the shaft.

$$E_{Test} I_{Test} v' = -\frac{F_{Test} x^3}{6} + \frac{R_1}{6} (x - a_{Test})^3 + c_1 x + c_2 \quad (44)$$

From equation (44), the boundary conditions of the model, which are $v' = 0$ at $x = a_{Test}$ and $v' = 0$ at $x = L_{Test}$ give us,

$$0 = -\frac{F_{Test} a_{Test}^3}{6} + c_1 a_{Test} + c_2 \quad (45)$$

$$0 = -\frac{F_{Test} L_{Test}^3}{6} + \frac{R_1}{6} (L_{Test} - a_{Test})^3 + c_1 L_{Test} + c_2 \quad (46)$$

Solving these equations simultaneously in Matlab (see Appendix D), we obtain $c_1 = 57.6 \times 10^6$ and $c_2 = -1.15 \times 10^{10}$. Thus the deflection function of the test model for elastic beam-rigid bearings case will be as,

$$v' = -\frac{1}{E_{Test} I_{Test}} \left(\frac{F_{Test} x^3}{6} + \frac{R_1}{6} (x - a_{Test})^3 + 57.6 \times 10^6 x - 1.15 \times 10^{10} \right) \quad (47)$$

where $I_{Test} = \pi D_{Test}^4 / 64 = 3.068 \times 10^5 \text{ mm}^4$.

Therefore from equation (47) the deflection at the shaft end of the test model for *superposition I* will be as calculated in equation (48). Note that the negative sign of the deflection shows the direction, which is downwards in this case.

$$\delta_{S_{Test}} = v'(x = 0) = -0.18775 \text{ mm} \quad (48)$$

Test model superposition II

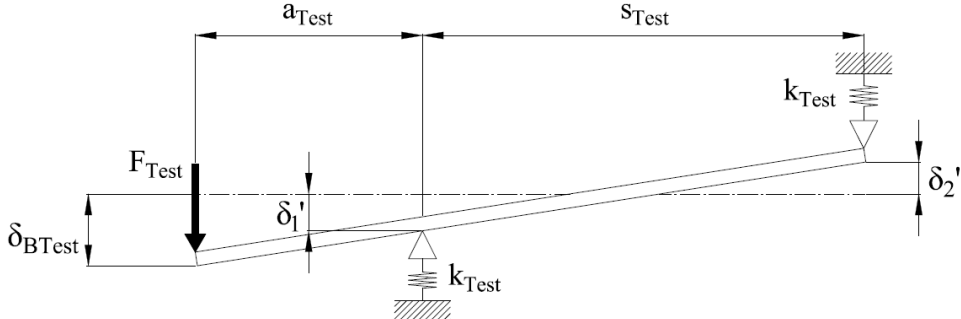


Figure 23. Superposition II of the test model

In *superposition II*, rigid beam-elastic supports, the deflections at the bearing locations can be expressed in terms of reaction forces at the location as,

$$\delta'_1 = -\frac{R_1}{k_{Test}} \quad (49)$$

$$\delta'_2 = -\frac{R_2}{k_{Test}} \quad (50)$$

The signs of the deflections show the direction with respect to the reaction forces. In this case since the deflections are both in reverse direction of reaction forces, they are expressed as negative. From simple geometry in Figure 23,

$$\frac{\delta_1' + \delta_2'}{\delta_{B_{Test}} + \delta_2'} = \frac{s_{Test}}{L_{Test}} \quad (51)$$

Using equations (49) and (50), the deflection at the test model tip for the *superposition II* will be,

$$\delta_{B_{Test}} = \frac{R_1 L_{Test} + R_2 s_{Test}}{s_{Test} k_{Test}} = -0.00644 \text{ mm} \quad (52)$$

Combining the findings from equations (48) and (52), the resulting total deflection for the test model can be found as,

$$\delta_{Test} = \delta_{s_{Test}} + \delta_{B_{Test}} = (-0.18775) + (-0.00644) = -0.19419 \text{ mm} \quad (53)$$

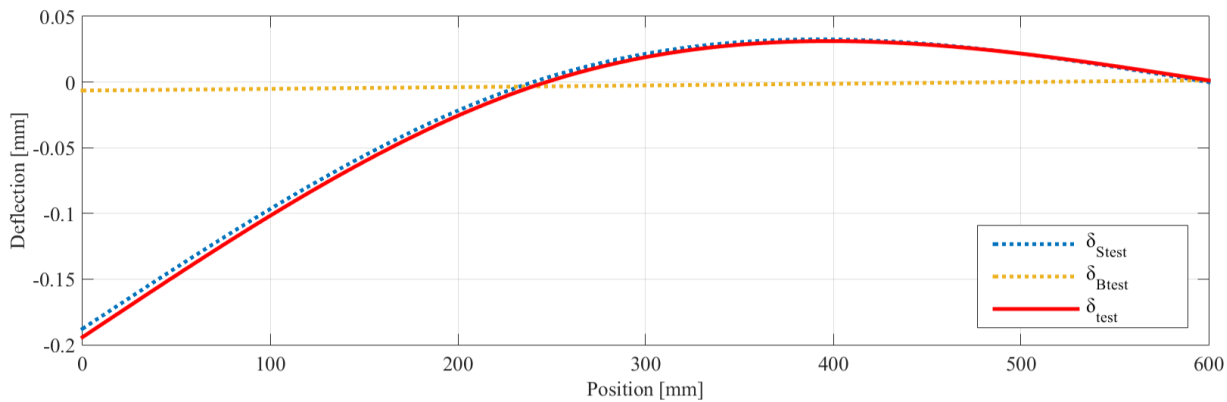


Figure 24. Deflection plot of the test model for superposition and combined cases

b. FE analysis of the test model

FEM model and analysis of the test model are made in ANSYS Workbench 15.0. The simple geometry of the test model is created in ANSYS Design Modeler. The shaft is represented with a line which has an inertia of I' and consists of 121 nodes and 60 elements as shown in Figure 25. A very large value is given for the shaft area, so that the beam can act as an Euler-Bernoulli beam. The shaft is built with BEAM188 elements.

Mesh

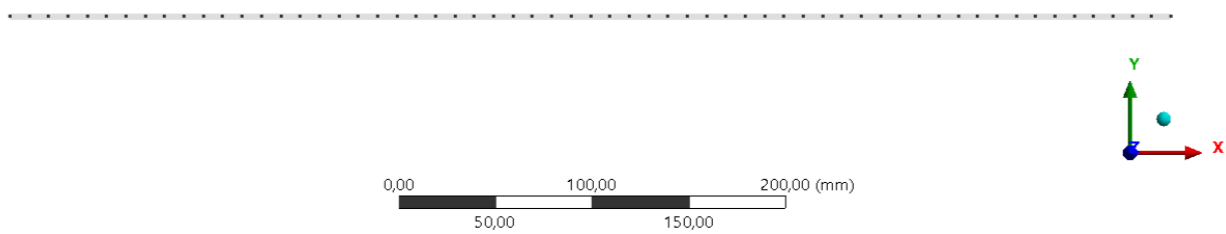


Figure 25. FE Mesh model of the test model in ANSYS

Both bearings on the shaft are modeled with ground-to-body type bearing connection. The bearing connection uses COMBI214 elements which has longitudinal and cross-coupling properties for 2D applications. In other words, as shown in Figure 26, it creates spring-damper elements between the shaft node and the ground, on the rotational plane, in the directions of plane axes. K_{11} and K_{22} representing the stiffness of the bearing in these planar directions (Y and Z), which are equal to $k_{Test} = 5 \times 10^5 \text{ N/mm}$.

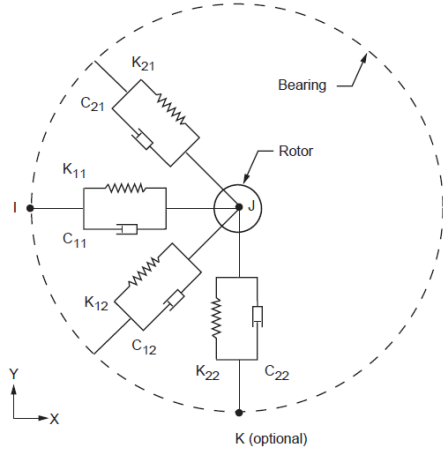


Figure 26. COMBI214 element geometry (ANSYS, 2013)

Since damping behavior of the bearings has very little effect on both the static and dynamic behavior of the structure, C_{11} and C_{22} are neglected in all analyses. Additionally, it is assumed that the bearings show no cross-coupling behavior, therefore cross-coupling stiffness and damping properties (K_{12}, K_{21} and C_{12}, C_{21}) are ignored as well. A vertical load of 1,000 N is applied to the shaft.

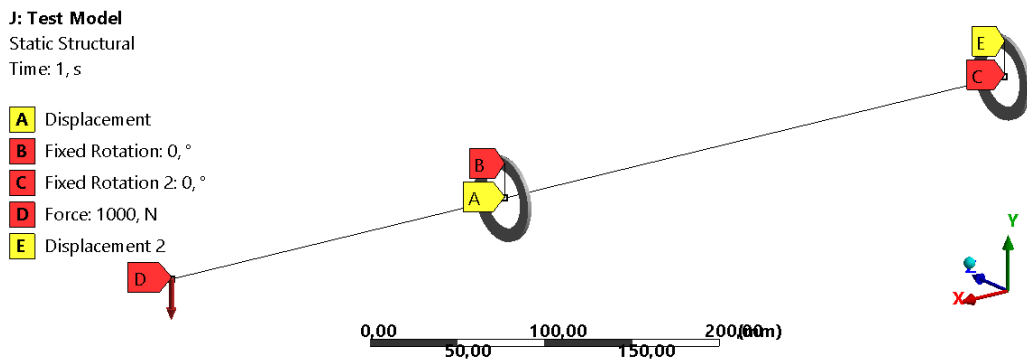


Figure 27. Test model in ANSYS

The model shown in Figure 27 is solved for 3 different cases to validate the superposition method and results obtained in the analytical model. These models are;

1. Elastic beam with rigid supports: In this case it is assumed that the bearings in the model have very high stiffness ($k_{Test} = 1 \times 10^{12}$ N/mm), therefore the bearings deform at negligible amounts and act as rigid supports; only shaft deformation is calculated.
2. Rigid beam with elastic supports: In this case, it is assumed that the shaft material has a very high modulus of elasticity ($E_{Test} = 1 \times 10^{12}$ MPa), therefore the shaft deforms at a negligible amount and act as rigid beam; only bearing deformations are calculated.
3. Combined case: The original case where both the shaft and the bearings act elastically and deform. According to the superposition method, this case is assumed to be the combination of case 1 and case 2.

Figure 28, Figure 29 and Figure 30 shows the FEM results of the test model obtained with ANSYS for each of the three cases respectively.

J: Test Model - Elastic beam with rigid bearings

Directional Deformation

Type: Directional Deformation(Y Axis)

Unit: mm

Global Coordinate System

Time: 1

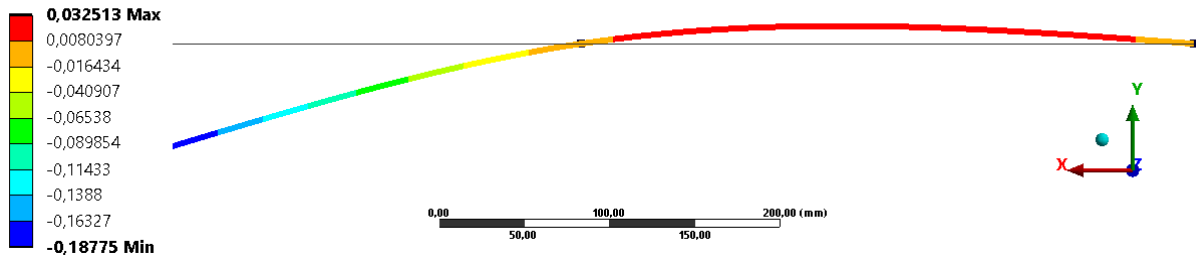


Figure 28. Deflection of the test model for elastic shaft-rigid bearings case

J: Test Model - Rigid beam with elastic bearings

Directional Deformation

Type: Directional Deformation(Y Axis)

Unit: mm

Global Coordinate System

Time: 1

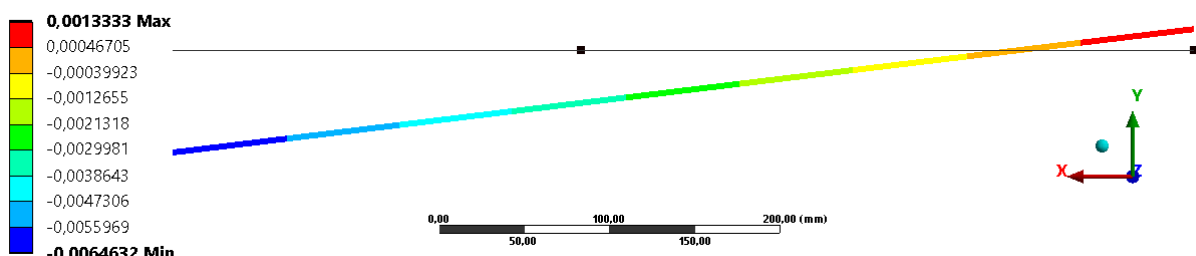


Figure 29. Deflection of the test model for rigid shaft-elastic bearings case

J: Test Model

Directional Deformation

Type: Directional Deformation(Y Axis)

Unit: mm

Global Coordinate System

Time: 1

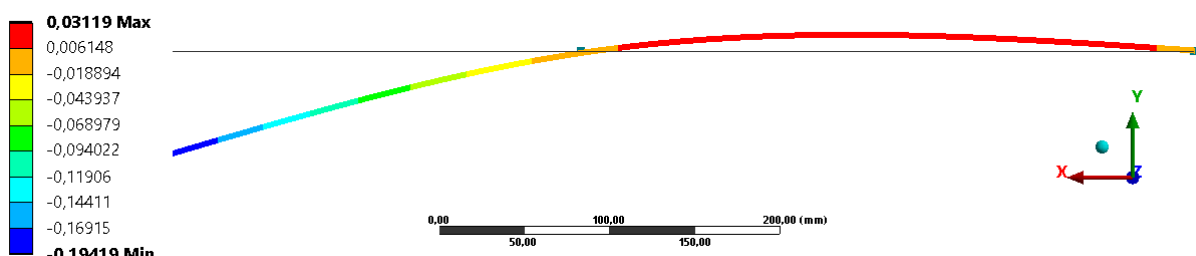


Figure 30. Deflection of the test model for the combined (original) case

A comparison between the results for analytical model in Matlab and FEM model in ANSYS is given in the Table 12. The results of the two model correlate perfectly, therefore the solution method applied to the test model is correct. The same superposition method will be used to find the tip deflection in the actual spindle design.

Table 12. Comparison of the results of the analytic and FE models for the test model

	Analytic Results	FEM Results
Reaction force at first bearing, R_1	1,666.7 N ↑	1,666.7 N ↑
Reaction force at second bearing, R_2	666.7 N ↓	666.7 N ↓
Elastic shaft, rigid bearings deflection, $\delta_{S_{Test}}$	0.18775 mm	0.18775 mm
Rigid shaft, elastic bearings deflection, $\delta_{B_{Test}}$	0.00644 mm	0.00644 mm
Combined case deflection, δ_{Test}	0.19419 mm	0.19419 mm

3.2.1.2 Analysis of the spindle

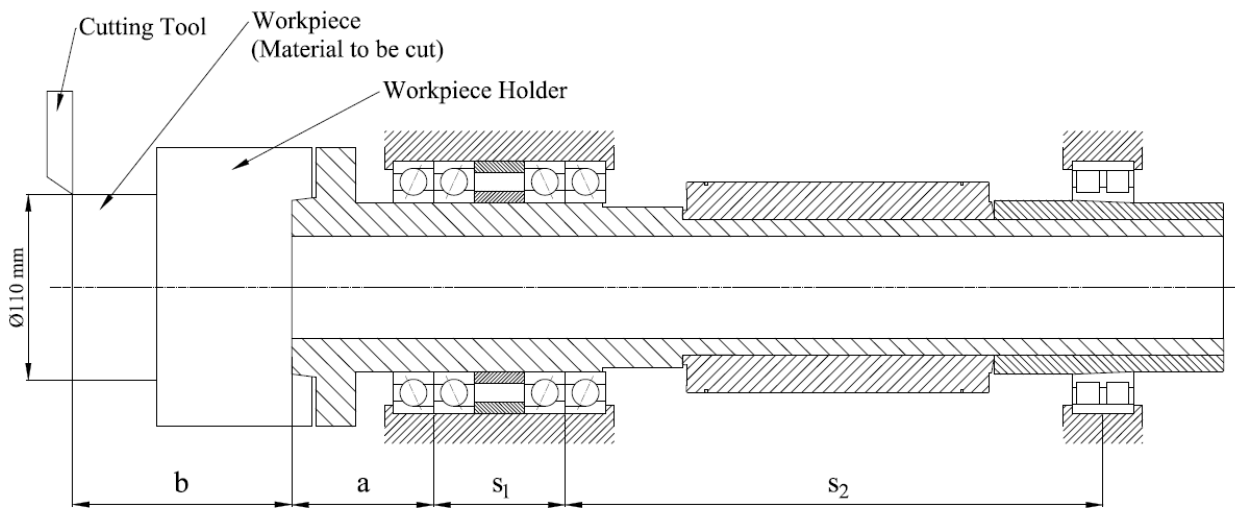


Figure 31. Preliminary spindle design during machining

Spindle as a complete system consists of many different parts and subassemblies. But, as can be seen in Figure 32, the preliminary design is reduced to a simpler structure which only consists of spindle shaft, bearings, rotor and rear bearing seat. It also shows the tool cutting point with respect to the spindle in the machining case analyzed. This point is also the location where the cutting force to be used in the analyses acts on the shaft.

Although the spindle shaft has sections with different diameters and certain lengths, preliminary spindle design is simplified further to facilitate the analyses. It is assumed that the spindle is a straight hallow shaft with an outer diameter of $D_o = \emptyset 100$ mm and an inner diameter of $D_i = \emptyset 60$ mm. Additionally, each of the bearing pairs in the front set, are considered as a single support point, therefore their mid points are assumed to be the support locations. In figure, the simplified spindle model is depicted.

Note that the cutting force F_t is actually generated on the workpiece and far away from the spindle shaft, but in the simplified model it is moved on the spindle tip together with a coupled moment M_t , where

$$M_t = bF_t \quad (54)$$

s_1 and s_2 are the distances between the support locations, or bearing spans, that have effect on the static stiffness and deflection of the structure. The bearing spans can be changed to reduce the deflection and increase the stiffness. However there is a design constraint for the allowable maximum length, hence it is aimed that the spindle in total should have a maximum length of 650 mm. By taking into consideration other necessary parts (spacers, locknuts, hydraulic

cylinder adapter, etc.), and keeping overhung distance, a , as small as possible, the constraint in equation (55) is defined for the bearing spans.

$$s_1 + s_2 \leq 445 \text{ mm} \quad (55)$$

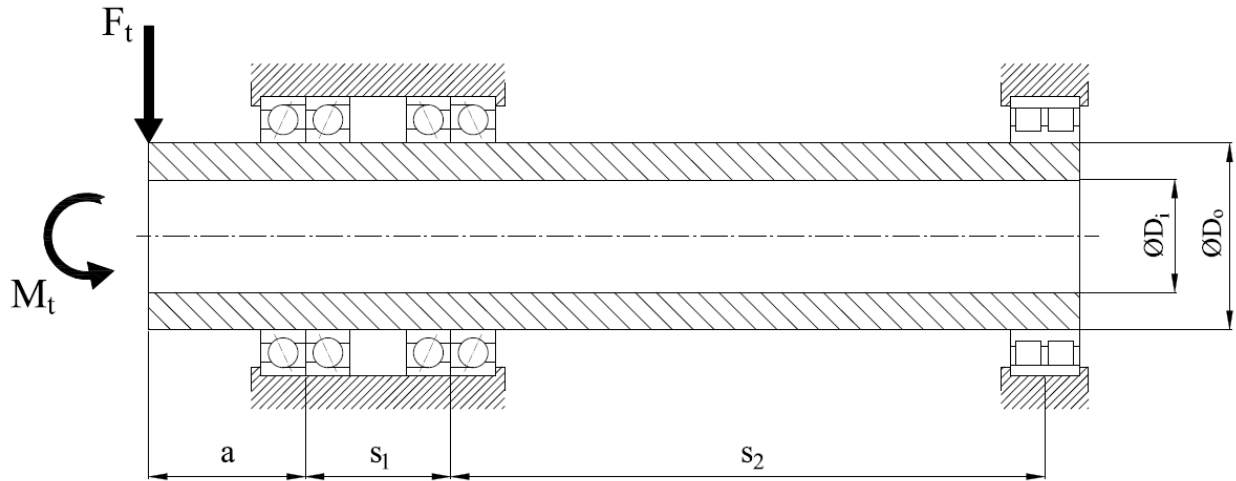


Figure 32. Simplified model of the preliminary spindle design

Additional design considerations and other assembly parts such as rotor, spacers, etc. create more limitations, which result in equations (56) and (57) that s_1 and s_2 cannot be lower than certain values.

$$s_1 \geq 78 \text{ mm} \quad (56)$$

$$s_2 \geq 319 \text{ mm} \quad (57)$$

An optimization analysis will be done for s_1 and s_2 to achieve the best static stiffness and lowest deflection in the spindle under these length constraints. Obtained optimum s_1 and s_2 bearing spans will also be used in the dynamic analysis and final assembly design.

a. Analytic analysis of the spindle

Since superposition method is validated with the test model, it is applied on the spindle model as well. The deflection of the spindle tip and hence static stiffness of the spindle are the main concerns in the static analysis, therefore the shaft is analyzed for the sample worst cutting operation.

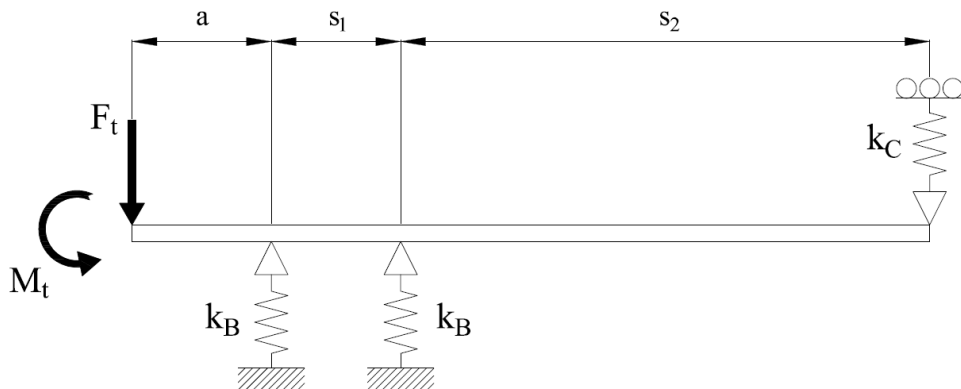


Figure 33. Simplified spindle model representation

Different than the test model, spindle is a statically indeterminate structure with three support points as seen in Figure 33. Angular contact ball bearings in the front constraint the shaft in all

directions, while the rear cylindrical bearings let the shaft move in axial direction and restricts in the radial one. These properties of the bearings are applied in the models as well.

To be able to find the deflection at the tip of spindle, above model is analyzed in two different cases as it was in the test model. Superposition of the spindle is shown in Figure 34.

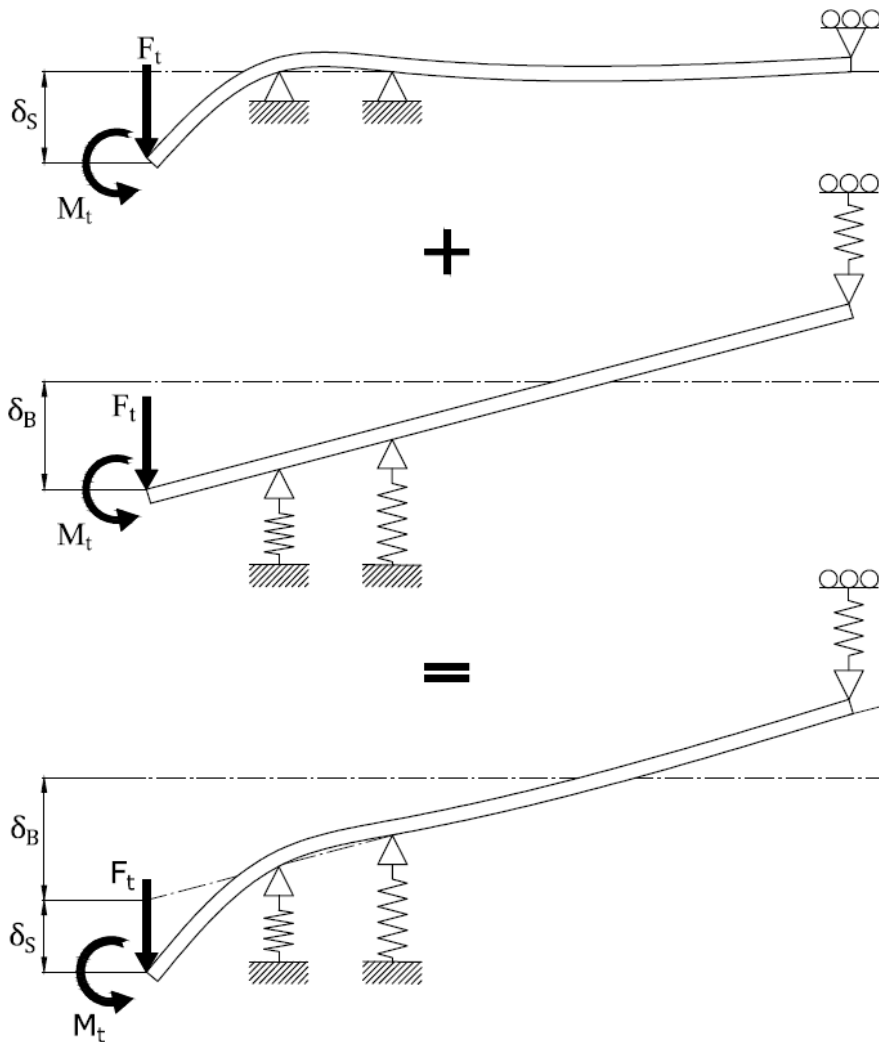


Figure 34. Superposition of the spindle model

The assumptions made for the test model in superposition solution are also valid for the spindle analysis. Additionally, below assumptions are also necessary for the spindle analysis:

1. The spindle experiences only cutting and reaction forces.
2. Cutting force occurs only in tangential –longitudinal- direction. Other components are not of interest in the analysis.
3. The shaft and other circular components assembled on it (rotor, bearings, etc) are perfectly concentric.
4. Parts that have transition or interference fit with the shaft (rotor, rear bearing seat) are assumed to be perfectly bonded with the shaft and considered as parts of the shaft.
5. Each ball bearing pair in the front are assumed to be single supports, and their mid points are the support locations.

6. The bearing housings are assumed to have infinite stiffness, their contributions to the overall deflection are neglected.
7. All the drill holes and similar features on the spindle are ignored.

As shown Figure 34, the total deflection at spindle shaft end, $\delta_{spindle}$, is calculated from the algebraic sum of δ_S , the deflection in elastic beam-rigid support case and δ_B , the deflection in rigid beam-elastic support case.

$$\delta_{spindle} = \delta_S + \delta_B \quad (58)$$

The analysis is performed for each s_1 and s_2 values within the specified range conforming to the spindle length restrictions defined with the equations (55), (56) and (57). The iteration is made in Matlab and optimum s_1 and s_2 values are found for minimum deflection (see Appendix E).

Spindle superposition I

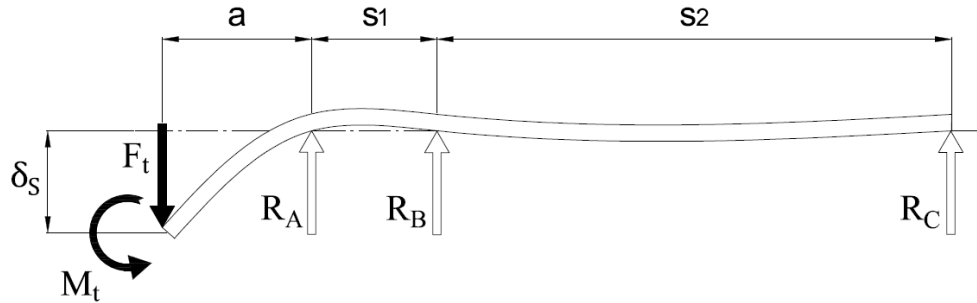


Figure 35. Free body diagram of the superposition I

$$R_A + R_B + R_C = F_t \quad (59)$$

$$R_B s_1 + R_C (s_1 + s_2) + F_t a + M_t = 0 \quad (60)$$

The loading-shaft system shown in the free body diagram, in Figure 35, is statically indeterminate to the first degree, because equilibrium equations (59) and (60) are not enough to solve for the unknown reaction forces, R_A , R_B and R_C . However we can use the deflection equations and boundary conditions to calculate the reaction forces and then the deflection at any point along the shaft.

From equations (59) and (60) R_B and R_C can be expressed in terms of R_A ,

$$R_B = \frac{F_t(s_1 + s_2 + a) - R_A(s_1 + s_2) + M_t}{s_2} \quad (61)$$

$$R_C = -\frac{F_t(s_1 + a) - R_A s_1 + M_t}{s_2} \quad (62)$$

Similar to the method used in the test model, the loading function of the shaft is written using Macaluay and singularity functions. Integrating the loading function four times based on the specific rules of Macaluay and singularity, the deflection function of the shaft can be obtained. The loading function of the shaft can be expressed as,

$$w_s = F_t(x - 0)^{-1} + M_t(x - 0)^{-2} - R_A(x - a)^{-1} - R_B(x - (s_1 + a))^{-1} \quad (63)$$

Then integrating the loading function will yield to the shear function, where $dV_s/dx = -w_s(x)$;

$$V_s = -F_t(x - 0)^0 - M_t(x - 0)^{-1} + R_A(x - a)^0 + R_B(x - (s_1 + a))^0 \quad (64)$$

$dM_s/dx = V_s(x)$, therefore integrating again will yield to moment function of the shaft;

$$M_s = -F_t(x - 0)^1 - M_t(x - 0)^0 + R_A(x - a)^1 + R_B(x - (s_1 + a))^1 \quad (65)$$

$$M_s = -F_t x - M_t + R_A(x - a)^1 + R_B(x - (s_1 + a))^1 \quad (66)$$

Using the moment and deflection relationship,

$$EI \frac{d^2 v_s}{dx^2} = M_s(x) \quad (67)$$

$$EI \frac{d^2 v_s}{dx^2} = -F_t x - M_t + R_A(x - a)^1 + R_B(x - (s_1 + a))^1 \quad (68)$$

Then the slope function of the shaft will be as,

$$EI \frac{dv_s}{dx} = -\frac{F_t x^2}{2} - M_t x + \frac{R_A}{2}(x - a)^2 + \frac{R_B}{2}(x - (s_1 + a))^2 + C_1 \quad (69)$$

Integrating above equation once more will provide the deflection function of the shaft.

$$EI v_s = -\frac{F_t x^3}{6} - \frac{M_t x^2}{2} + \frac{R_A}{6}(x - a)^3 + \frac{R_B}{6}(x - (s_1 + a))^3 + C_1 x + C_2 \quad (70)$$

For the three boundary conditions at the support points, $v_s = 0$ at $x = a$, $v_s = 0$ at $x = (a + s_1)$ and $v_s = 0$ at $x = (a + s_1 + s_2)$, solving the deflection equation will give us C_1 , C_2 and R_A .

$$-\frac{F_t a^3}{6} - \frac{M_t a^2}{2} + C_1 a + C_2 = 0 \quad (71)$$

$$-\frac{F_t(a + s_1)^3}{6} - \frac{M_t(a + s_1)^2}{2} + \frac{R_A}{6}s_1^3 + C_1(a + s_1) + C_2 = 0 \quad (72)$$

$$\begin{aligned} & -\frac{F_t(a + s_1 + s_2)^3}{6} - \frac{M_t(a + s_1 + s_2)^2}{2} + \frac{R_A}{6}(s_1 + s_2)^3 \\ & + \frac{(F_t(s_1 + s_2 + a) - R_A(s_1 + s_2) + M_t)}{6s_2} s_2^3 + C_1(a + s_1 + s_2) \\ & + C_2 = 0 \end{aligned} \quad (73)$$

Above equations can be simplified in the form of $AX = B$ and then solved through $X = A^{-1}B$ in Matlab (see Appendix E).

$$\begin{aligned} & \left[\begin{array}{ccc|c} 0 & a & 1 & R_A \\ \frac{s_1^3}{6} & (a + s_1) & 1 & C_1 \\ \frac{(s_1 + s_2)^3 - (s_1 + s_2)s_2^2}{6} & (a + s_1 + s_2) & 1 & C_2 \end{array} \right] \\ & = \left[\begin{array}{c} \frac{F_t a^3}{6} + \frac{M_t a^2}{2} \\ \frac{F_t(a + s_1)^3}{6} + \frac{M_t(a + s_1)^2}{2} \\ \frac{F_t(a + s_1 + s_2)^3}{6} + \frac{M_t(a + s_1 + s_2)^2}{2} - \frac{F_t(s_1 + s_2 + a)s_2^2}{6} - \frac{M_t s_2^2}{6} \end{array} \right] \end{aligned} \quad (74)$$

After obtaining the unknowns, C_1 , C_2 and R_A , the deflection equation of the shaft $v_s(x)$ can be used to find the deflection at any point along the shaft. In our case, the deflection at the spindle tip is necessary, where $x = 0$, and it eventually yields to,

$$\delta_S = v_s(x = 0) = \frac{C_2}{EI} \quad (75)$$

Spindle superposition II

Bearings are one of the most critical elements defining spindle rigidity. The stiffness of the bearing depends on various factors such as, type, contact angle, ball dimensions. Finding the exact radial and axial stiffness values of the bearings are extremely difficult and the best way is to obtain these values experimentally. However, since there is no chance of getting these coefficients through experiments in this thesis, the stiffness values will be taken from the bearing catalogues of the suppliers. These values are calculated by the supplier for generic applications. For more accurate and reliable bearing stiffness values for specific cases, advanced computer programs supplied by bearing producers can be used.

For the set of four 7020A5-TRS-DB-EL-P3 angular contact ball bearings with DBB arrangement the radial stiffness is given as 860 N/ μm in the product catalogue (NSK, 2011). Because in the design, bearings are placed in pairs on the shaft with a span distance of s_1 , the stiffness of a bearing pair is assumed to be the half of the radial stiffness of the complete set, which is $k_B = 4.3 \times 10^5 \text{ N/mm}$.

For NN3020-TB-KR-CC1-P3 double-row cylindrical roller bearing, the radial stiffness is given as $k_C = 1.96 \times 10^6 \text{ N/mm}$ (with a clearance of 0 μm after preloading) in the product catalogue (NSK, 2011).

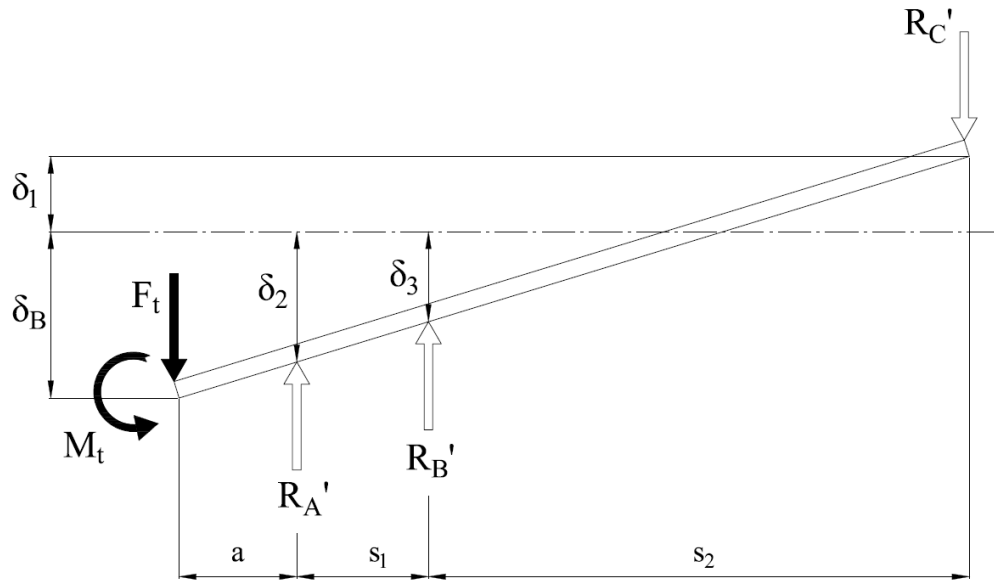


Figure 36. Free body diagram of the superposition II

From the free body diagram of the rigid beam in Figure 36,

$$R'_A + R'_B - R'_C = F_t \quad (76)$$

$$R'_A a + R'_B(a + s_1) - R'_C(a + s_1 + s_2) + M_t = 0 \quad (77)$$

If we write the deflections at locations of R'_A , R'_B and R'_C ,

$$\delta_1 = -\frac{R'_C}{k_C} \quad (78)$$

$$\delta_2 = -\frac{R'_A}{k_B} \quad (79)$$

$$\delta_3 = -\frac{R'_B}{k_B} \quad (80)$$

The negative signs in the deflection equations (78), (79) and (80) are due to the fact that the directions of deflections are opposite to the reaction forces. Since the beam is accepted as rigid, the deflections will be proportional;

$$\frac{\delta_1 + \delta_3}{\delta_1 + \delta_2} = \frac{s_2}{(s_1 + s_2)} \quad (81)$$

If we include the reaction forces in equation (81),

$$\frac{\frac{R'_C}{k_C} + \frac{R'_B}{k_B}}{\frac{R'_C}{k_C} + \frac{R'_A}{k_B}} = \frac{s_2}{(s_1 + s_2)} \quad (82)$$

which then yields to,

$$-R'_A \frac{s_2}{k_B} + R'_B \frac{(s_1 + s_2)}{k_B} + R'_C \frac{s_1}{k_C} = 0 \quad (83)$$

If we re-write the equilibrium and deflection equations in the matrix form as $GR' = H$,

$$\begin{bmatrix} 1 & 1 & -1 \\ a & (a + s_1) & -(a + s_1 + s_2) \\ -\frac{s_2}{k_B} & \frac{(s_1 + s_2)}{k_B} & \frac{s_1}{k_C} \end{bmatrix} \begin{bmatrix} R'_A \\ R'_B \\ R'_C \end{bmatrix} = \begin{bmatrix} F_t \\ -M_t \\ 0 \end{bmatrix} \quad (84)$$

The reaction forces can be obtained by solving equation (84) for $R' = G^{-1}H$ through Matlab (see Appendix E).

Finally, δ_B the deflection at the spindle tip due to the spring behavior of the bearings will be retrieved from the proportional deflections at the tip and R'_A location.

$$\frac{\delta_1 + \delta_3}{\delta_1 + \delta_B} = \frac{s_2}{(a + s_1 + s_2)} \quad (85)$$

$$\frac{-\frac{R'_C}{k_C} - \frac{R'_B}{k_B}}{-\frac{R'_C}{k_C} + \delta_B} = \frac{s_2}{(a + s_1 + s_2)} \quad (86)$$

$$\delta_B = -\frac{(s_1 + a)}{s_2} \left(\frac{R'_B}{k_B} + \frac{R'_C}{k_C} \right) - \frac{R'_B}{k_B} \quad (87)$$

Since we have δ_S and δ_B now, we can calculate $\delta_{spindle}$, the total deformation at the tip of the spindle.

$$\delta_{spindle} = \delta_S + \delta_B \quad (88)$$

If we iterate the resulting $\delta_{spindle}$ for different s_1 and s_2 bearing span distances, we can understand their effects on the rigidity and the deflection of the spindle. The graph in Figure 37 plots the spindle deflection for different s_1 and s_2 values within the ranges defined with the equations (55), (56) and (57).

As can be seen from the plot, the deflection is at minimum, when s_1 is kept as low as possible while s_2 is at maximum. Between the minimum and maximum values of s_1 , the deflection increases 9.4% (when s_2 is kept constant), whereas maximum of s_2 helps a decrease of 5.8% in the total deflection. Therefore, compared to s_2 , s_1 span has more effect on the spindle tip deflection within the specified ranges.

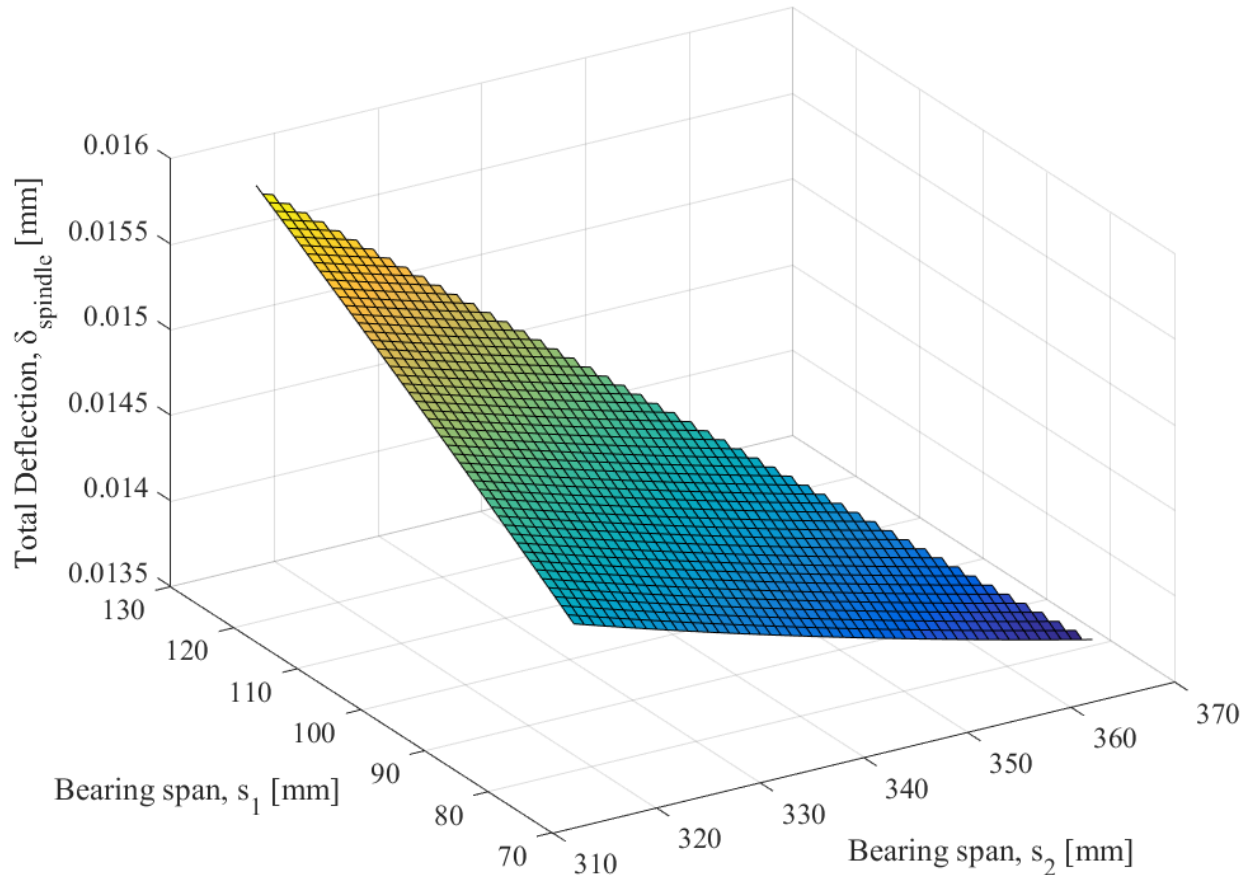


Figure 37. Total deflection vs bearing spans plot

For further analysis, $s_1 = 78$ mm and $s_2 = 367$ mm will be used as the optimum bearing spans in the design, to be able to make the spindle design as rigid as possible given the boundary conditions. In Figure 38 the deflection plots of each superposition case and the combined case for the optimum spans are given. The maximum deflection occurs at the spindle tip as $\delta_{\text{spindle}} = 0.012$ mm, and the spring behavior of the bearings contributes most to the total deformation.

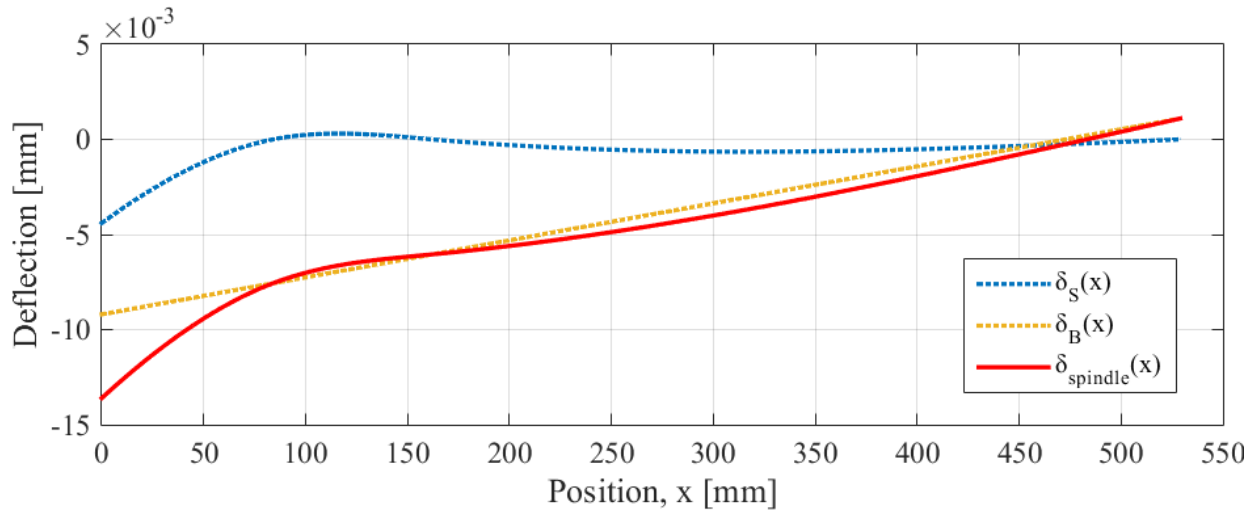


Figure 38. Deflection plot of the spindle for superposition and combined cases

b. FE analysis of the spindle

The same modelling and analysis methods in the test model are used for the spindle as well. The spindle shaft is represented with a line which has an inertia of I and consists of 215 nodes and 107 elements as shown in Figure 39. A very large value is given for the shaft area, so that the beam can act as an Euler-Bernoulli beam. The shaft is built with BEAM188 elements.

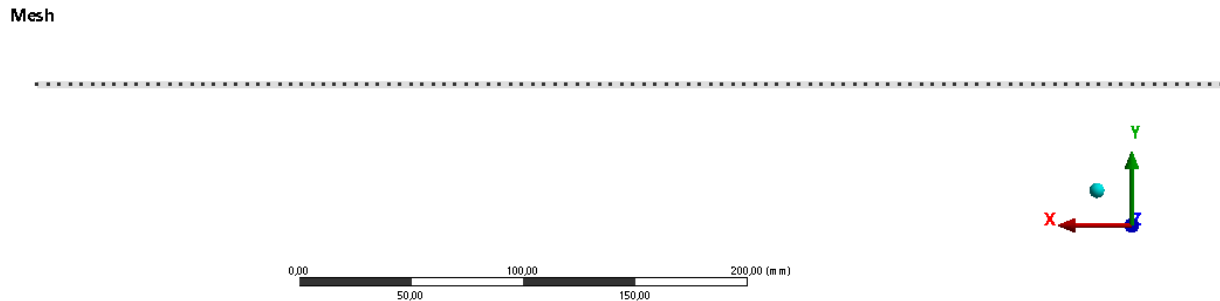


Figure 39. FE mesh model of the spindle

All the bearings on the shaft are modeled with ground-to-body type bearing connection and COMBI214 elements. Damping (C_{11} and C_{22}) and cross-coupling behavior of the bearings (K_{12}, K_{21} and C_{12}, C_{21}) are neglected in the analysis. The vertical load of 3,700 N together with the moment of 4.44×10^5 Nmm is applied to the model as shown in Figure 40.

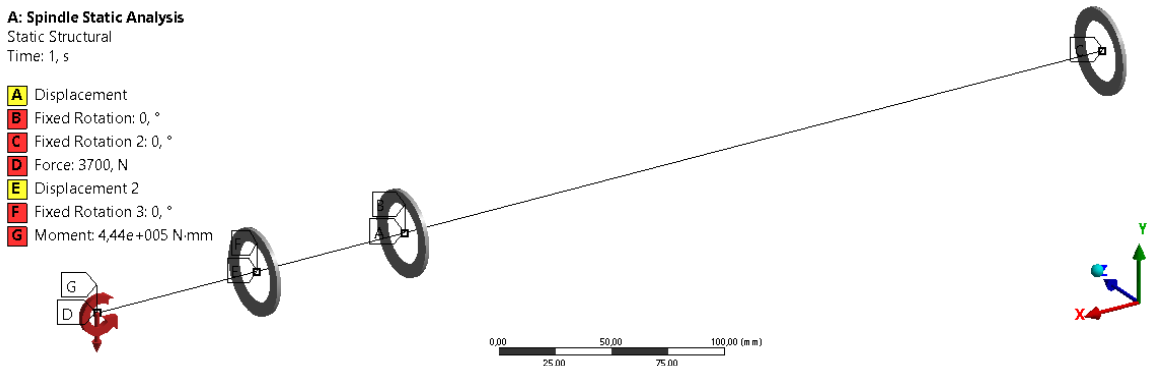


Figure 40. Spindle model in ANSYS

Same as in the test model, spindle shaft is analyzed for three different cases to compare and validate the FEM results with the analytical model. The cases are;

1. Elastic shaft, rigid bearings: Bearings are modelled with a very high stiffness ($k_B = k_C = 1 \times 10^{12}$ N/mm), therefore the bearings deform at negligible amounts and act as rigid supports; only shaft deformation is calculated.
2. Rigid shaft, elastic bearings: The shaft is modelled as rigid with a very high modulus of elasticity ($E = 1 \times 10^{12}$ MPa), therefore the shaft deforms at a negligible amount and act as rigid beam; only bearing deformations are calculated.
3. Combined case: The original case where both the shaft and the bearings act elastically and deform. According to the superposition method, this case is assumed to be the combination of case 1 and case 2.

Figure 41, Figure 42 and Figure 43 shows the FEM results obtained with ANSYS for each of these three cases, respectively.

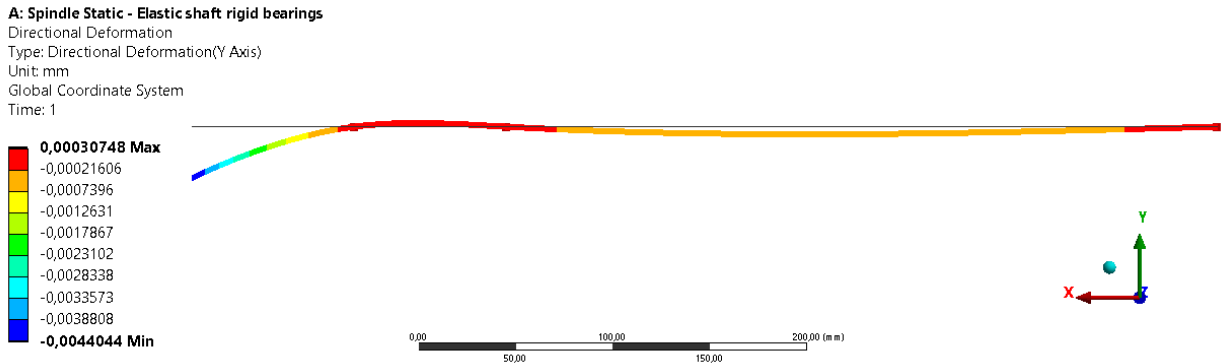


Figure 41. Deflection of the spindle for elastic shaft-rigid bearings case

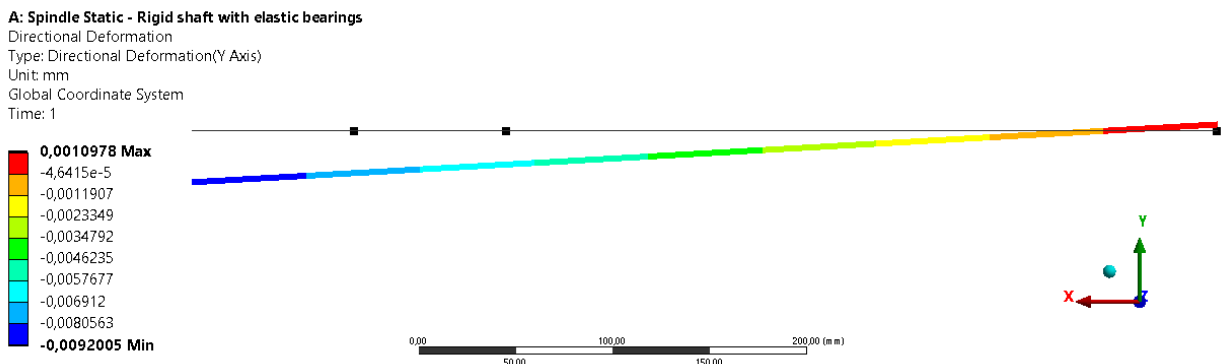


Figure 42. Deflection of the spindle for rigid shaft-elastic bearings case

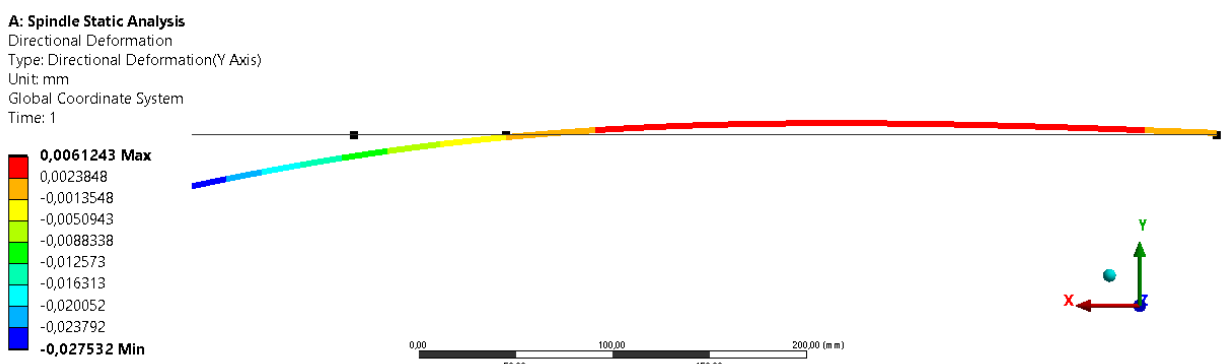


Figure 43. Deflection of the spindle for combined (original) case

The comparison of the reaction forces and deflections obtained through analytic solution and FEM are given in Table 13. As it is clearly seen from the results, although the superposition method was validated with the test model, it does not work well with the spindle. For separate cases of superposition, analytical results perfectly match the FEM results, nevertheless the combined case in FEM analysis gives higher deflection results, as well as different reaction forces, than the analytical model. Please note that the sum of the reaction forces in the analytical model for the combined case is almost twice of the cutting force F .

Table 13. Comparison of the results of the analytic and FEM models for the spindle

	Superposition I: Elastic shaft, rigid bearings		Superposition II: Rigid shaft, elastic bearings		Combined		
	Matlab	ANSYS (Euler- Bernoulli)	Matlab	ANSYS (Euler- Bernoulli)	Matlab	ANSYS (Euler- Bernoulli)	ANSYS (Timo- shenko)
Reaction at first bearing	14,225 N ↑	14,223 N ↑	3,252 N ↑	3,252 N ↑	17,477 N ↑	4,909 N ↑	4,940 N ↑
Reaction at second bearing	10,705 N ↓	10,703 N ↓	2,600 N ↑	2,600 N ↑	8,106 N ↓	591 N ↑	553 N ↑
Reaction at third bearing	180 N ↑	180 N ↑	2,152 N ↓	2,153 N ↓	1,972 N ↓	1,800 N ↓	1,793 N ↓
Spindle tip deflection	0.0044 mm	0.0044 mm	0.0092 mm	0.0092 mm	0.0136 mm	0.0275 mm	0.0297 mm

Even though the analytical model results for the combined case differ than the FEM model, the correlation of superposition I and superposition II results proves that our approach to analyze the spindle is mostly correct. The analytical model is still useful to understand the behavior of spindle rigidity when the design parameters, such as stiffness and bearing span, are changed. Hence, the analytical model is still found useful for the optimization of the bearing spans, and as a result the optimum s_1 and s_2 values obtained through this model are used in the final design of the spindle. However for better estimations of the deflection and rigidity, FEM solution and results should be used.

The FEM analysis of the spindle with the Timoshenko solution is also done in ANSYS as seen in Figure 44 to understand the shear deformation effects of the beam elements (BEAM188) which are actually based on the Timoshenko beam theory. Since the cross section-length ratio of the spindle is not very small as usually expected for Euler-Bernoulli beams, Timoshenko solution gives slightly different results (8% higher deflection) than the ones given in Table 13. Even with the Timoshenko solution, the deflection of the spindle tip seems to be within the limit of 0.03 mm.

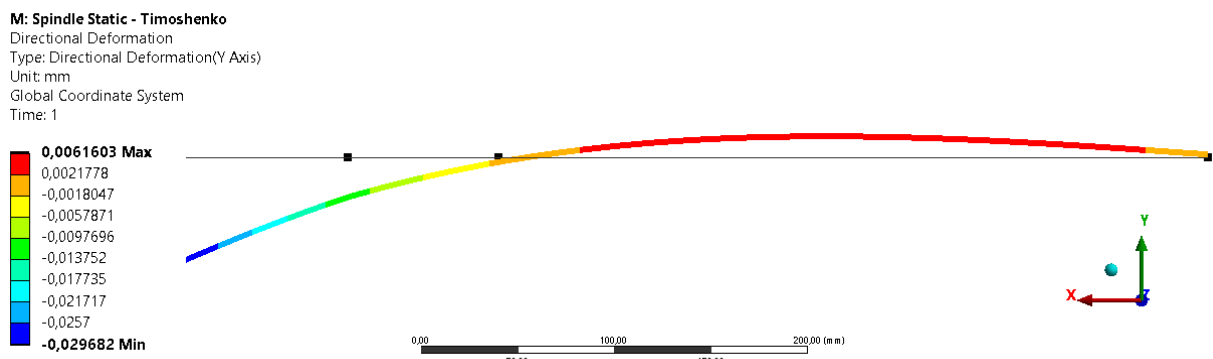


Figure 44. Deflection of the spindle with Timoshenko method

The spindle shaft only experiences elastic deformation under the cutting forces studied. As shown in Figure 45, the maximum von-Mises stresses generated in the shaft are at the bearing locations and have the value of 9,5 MPa, which are fairly below 485 MPa, the yield strength of

Ck45 steel -spindle shaft material. Therefore, the shaft is sufficient to carry the loads without any plastic deformation or failure.

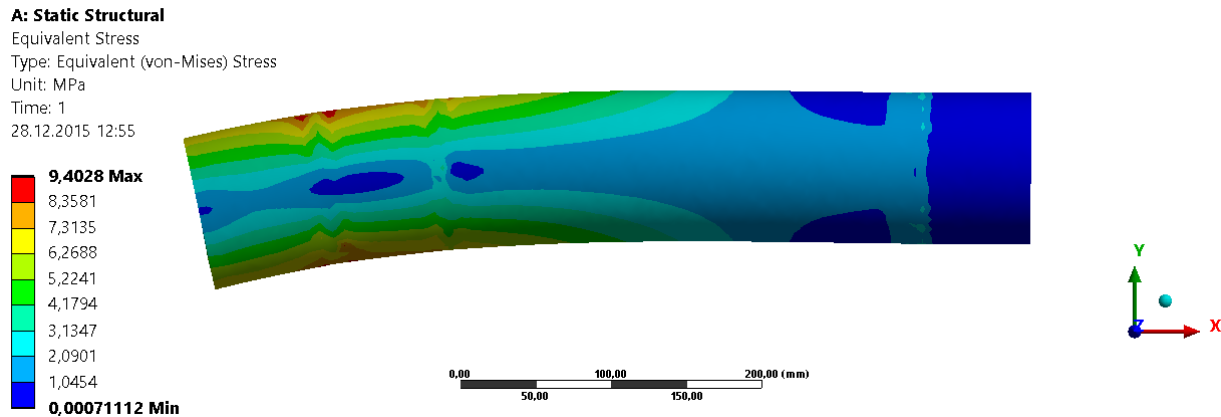


Figure 45. Stresses in the spindle shaft under cutting forces

3.2.2 Dynamic analysis

3.2.2.1 Modal analysis

The dynamic analysis of the preliminary spindle design is also done using ANSYS Workbench 15.0. The analysis is performed with the same simplified spindle model used in the static FEM analyses. The Eigen frequencies of the spindle calculated for the first 6 modes and the results are given in Table 14.

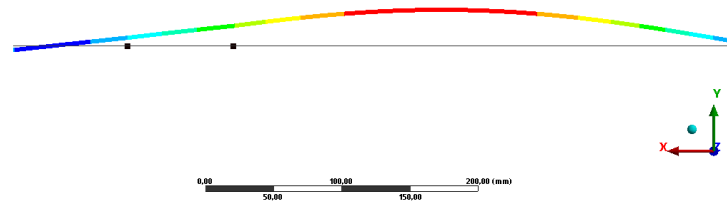
Table 14. The first six modes of the spindle

Mode	Frequency [Hz]
1 st	1,096
2 nd	1,096
3 rd	1,421
4 th	1,421
5 th	2,967
6 th	2,967

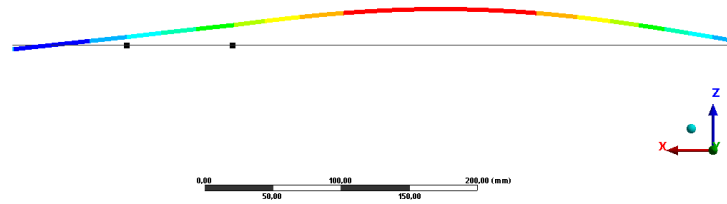
The 1st and 2nd Eigen frequencies of the spindle are same and mutually orthogonal, and can be considered as multiple roots, as shown in Figure 46. 1st natural frequency is the bending mode of the spindle in Y direction, while 2nd is the bending mode in Z direction. Guo, Bai, Zheng and Pan (2013) states that for the sake of guaranteeing machining accuracy and machine tools' security, the maximum rotating speed cannot exceed 75% of its critical speed. The working speed for these first two modes are 65,760 rpm, which is substantially above the working speed range of the spindle, 0-6,000 rpm. This is usually the expected case for lathe spindles due to their higher rigidity and lower working speed ranges compared to the milling spindles. Therefore, the modal analysis prove that the preliminary design of the spindle sufficient to avoid the resonance region within the defined working speed range.

N: Spindle Dynamic Analysis

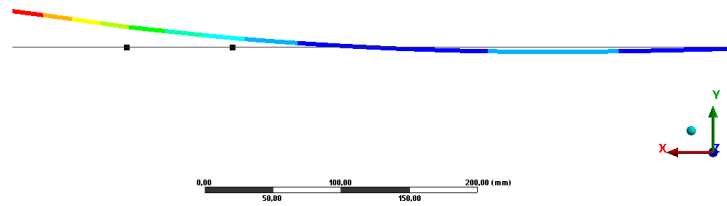
1st Mode
Type: Total Deformation
Frequency: 1096,1 Hz
Unit: mm

**N: Spindle Dynamic Analysis**

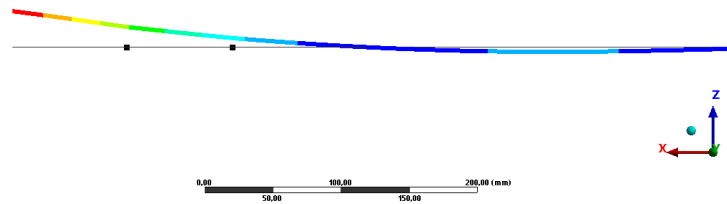
2nd Mode
Type: Total Deformation
Frequency: 1096,1 Hz
Unit: mm

**N: Spindle Dynamic Analysis**

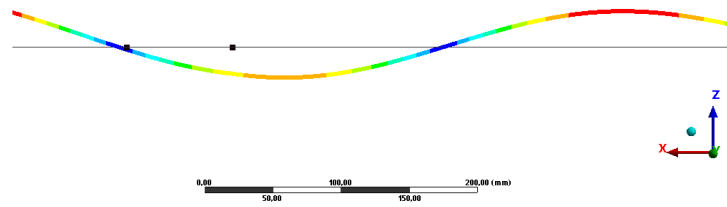
3rd Mode
Type: Total Deformation
Frequency: 1421,4 Hz
Unit: mm

**N: Spindle Dynamic Analysis**

4th Mode
Type: Total Deformation
Frequency: 1421,4 Hz
Unit: mm

**N: Spindle Dynamic Analysis**

5th Mode
Type: Total Deformation
Frequency: 2966,8 Hz
Unit: mm

**N: Spindle Dynamic Analysis**

6th Mode
Type: Total Deformation
Frequency: 2966,8 Hz
Unit: mm

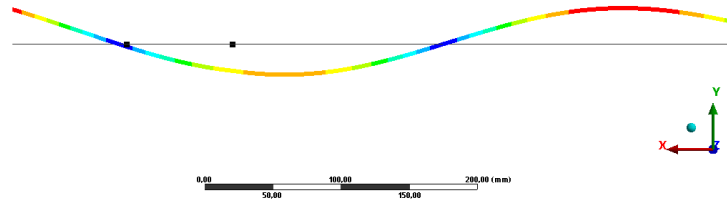


Figure 46. The first six mode shapes of the spindle

3.2.2.2 Critical speeds and Campbell diagram

To investigate further, the dynamic behavior of the spindle with different rotational speed are analyzed. Although the spindle working speed ranges between 0 to 6,000 rpm and it is expected that the critical speeds are much above this range, the analysis is conducted for the speeds between 0 to 100,000 rpm with multiple load steps to only find the critical speeds. With the Campbell diagram it is also possible to obtain the natural frequency of the spindle at any working speed within the speed range analysis conducted.

The critical speeds of the spindle are marked on the Campbell diagram in Figure 47 and listed in Table 15. Critical speeds of the spindle It is found that within the working speed range of the spindle (0-6,000 rpm) the natural frequencies always stays above 1,000 Hz.

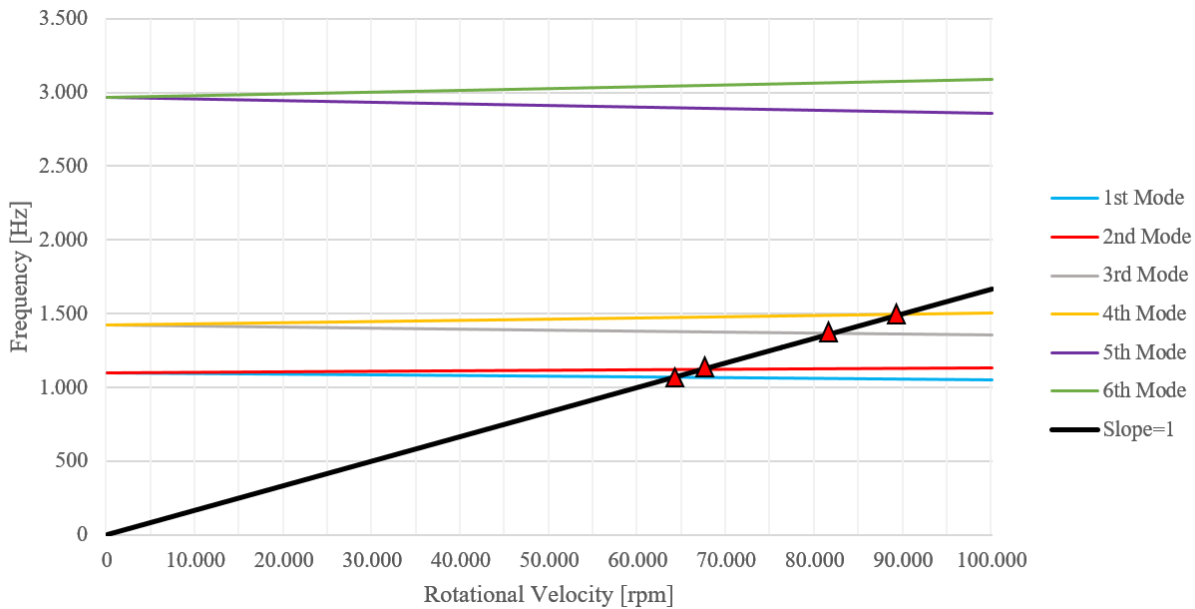


Figure 47. Campbell diagram of the spindle

Table 15. Critical speeds of the spindle

No	Critical Speed	Mode
1	64,203 rpm	1 st
2	67,192 rpm	2 nd
3	81,864 rpm	3 rd
4	89,593 rpm	4 th

3.2.2.3 Harmonic response analysis

Due to the nature of the machining operation, a periodic cutting force is generated on the spindle which produces a continuous cyclic response. As it is depicted in Figure 48, the elastic properties of the tool, material or the spindle causes this harmonic behavior in the cutting force. If the frequency of the exciting cutting force is the same as the spindle inherent frequency then the resonance will occur in the spindle. Resonance leads to chatter and vibrations with extreme amplitudes. It greatly affects the precision of the process and even leads to spindle and bearing failures due to high cyclic loads generated in the structure. Therefore in the cutting operations, the resonance should always be avoided no matter what the source is, spindle, cutting tool, fixture, etc.

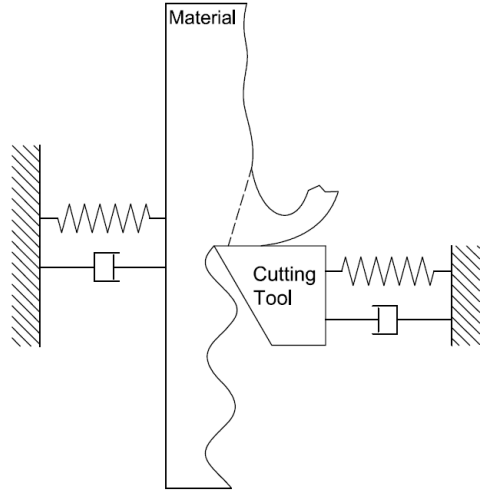


Figure 48. Mechanics of cutting operation

To be able to ensure that the spindle design is away from the resonance regions within its working speed range, harmonic response analysis is carried out. A cyclic excitation force of 200 N is applied, to simulate the cutting force, with the excitation frequency range from 0 to 2,000 Hz with 10 Hz incremental steps. Again the damping effects are neglected in this analysis. The harmonic response plot of the spindle under the cyclic excitation force is given in Figure 49.

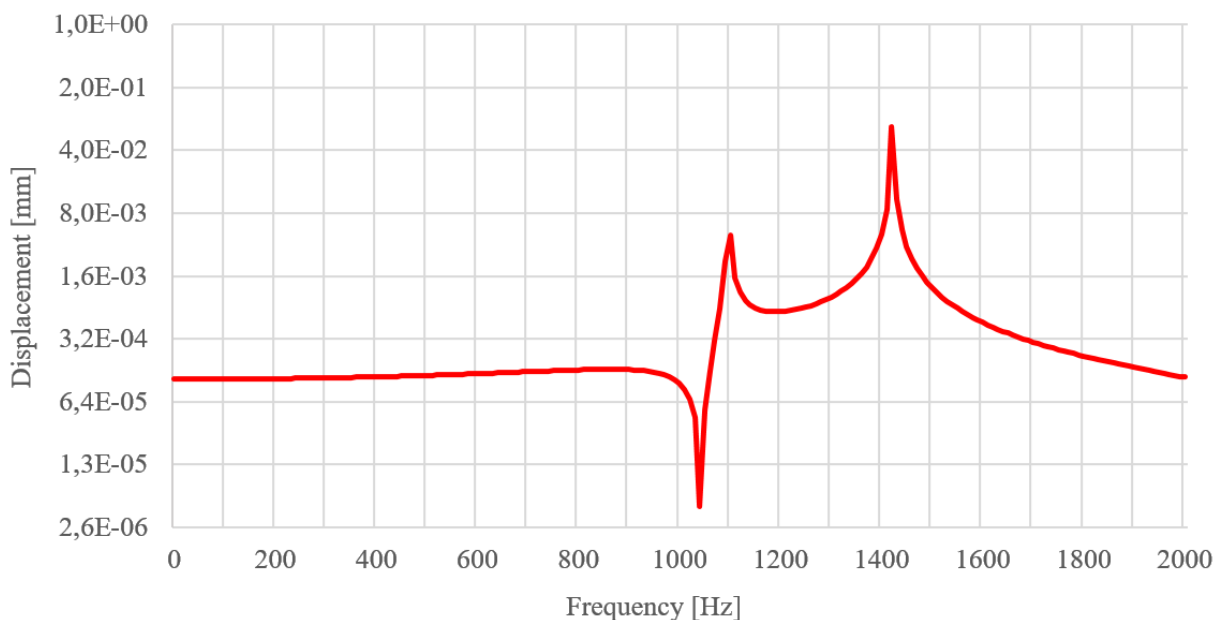


Figure 49. Harmonic response diagram of the spindle under a 200 N load

As can be seen from the plot, the displacement at the spindle tip increases rapidly at 1,100 Hz to 0.0043 mm and at 1,420 Hz excitation frequency it reaches to the maximum, 0.073 mm. Therefore these peaks indicate to the resonance frequencies under cyclic loads, which are also close to the 1st and 2nd natural frequencies (1,096 Hz and 1,421 Hz) of the spindle found in the modal analysis. In the frequencies below 1,100 Hz the spindle deflection will be around 1.2×10^{-4} mm and negligible, hence the design proves to be avoiding resonance under cyclic loads within its working speed range of 0 to 6,000 rpm (=100 Hz).

4 FINAL DESIGN

In this chapter, the final assembly design of the spindle which is made based on the findings in the analyses is presented. The details of the design including the shaft design, sealing, assembly, etc. are explained.

4.1 Assembly Design

Based on the results obtained through the analyses, the detail design of the spindle is finalized. Different than the simplified models used in the analyses, the spindle shaft is a stepped shaft with different diametric sections. The design of the spindle shaft and bearings arrangement are shown in Figure 50. As a result of the optimization, the bearing spans are as $s_1 = 78$ mm and $s_2 = 367$ mm, which are found to provide the highest rigidity in the analysis. The span distance between the angular contact ball bearing pairs is maintained with spacers. The ball bearings in the front and the roller bearing at the rear are all secured at their positions on the shaft and preloaded by standard locknuts, M95x2 and M100x2 respectively.

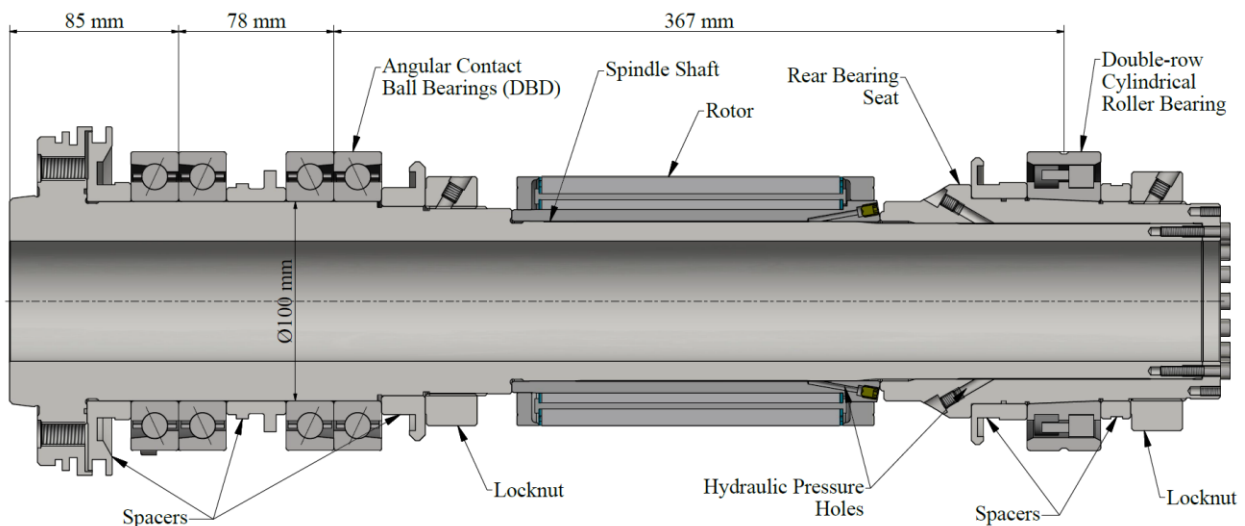


Figure 50. Final spindle shaft assembly

The rotor is assembled and fixed on the spindle shaft with interference fit, therefore the rotor must be heated and then assembled on the shaft. Similarly, the rear bearing seat has also interference fit with the spindle shaft, and additionally fixed with standard M5 DIN912 screws. Since the rotor and the rear bearing seat have interference fit, hydraulic pressure holes are added to be able disassemble them in case of maintenance. The disassembly procedure is to fill the small gaps between the shaft and the rotor/bearing seat with high pressure oil, so the parts can expand enough to be saved from the shaft.

The cross-section of the complete design and assembly is given in Figure 51. The spindle is designed to be a complete unit which was defined as “the cartridge type” and one of the design requirements of the thesis. All the necessary parts are assembled into a single housing as can be seen in Figure 51. Stator of the motor is directly press fitted into the housing with a clearance fit and secured against rotation and longitudinal motion with M8 DIN912 screws. Both the front and the rear bearing housings are also assembled into the stator housing, which becomes the ultimate shell for the whole unit.

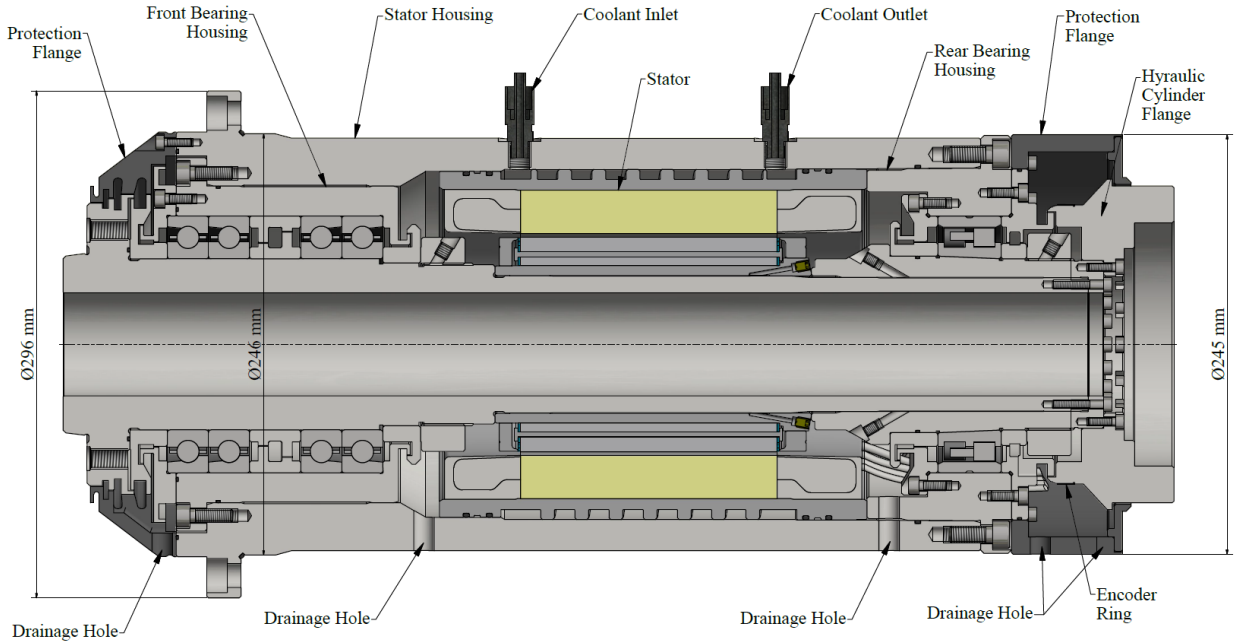


Figure 51. Section view of the final spindle assembly design

The maximum outer diameter of the spindle housing, which is vital, is designed to be Ø246 mm, below the predefined limit of Ø250 mm. However together with the fixing flange of the housing, the diameter of the spindle goes up to Ø296 mm, which has negligible effects on the dimensions of the spindle housing and the machine.

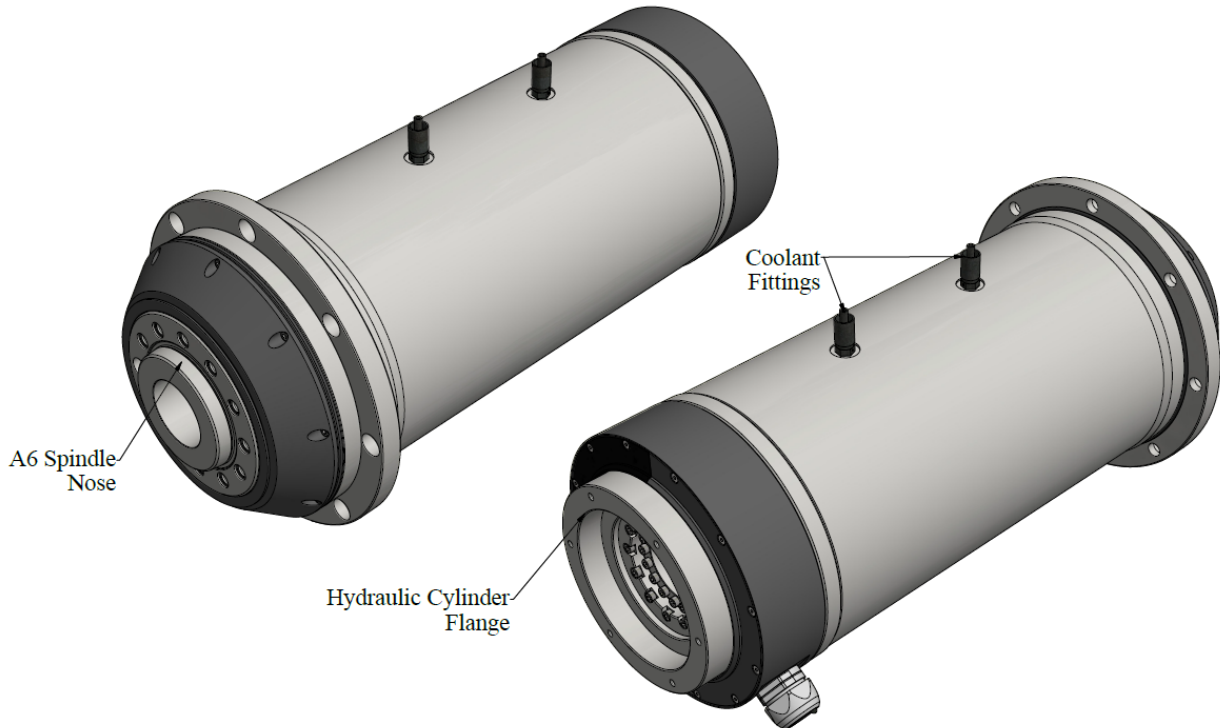


Figure 52. Isometric view of the complete spindle assembly

The stator housing possesses inlet and outlet holes, as shown in Figure 52, necessary for the coolant circulation to cool down the stator during operation. The coolant goes into the housing from the inlet and circulates around the stator inside the coil groove and then leaves through the outlet. The inlet and outlet holes have 1/4" pipe threads for the hose fittings.

4.1.1 Overcoming the thermal expansion

The temperature increase and its significant effects are discussed in detail in previous sections. The thermal expansion in the spindle occurs in every direction. However the effects in axial direction matters more because longitudinal expansion is more than the radial one and as a result axial elongation in the shaft puts much more preload on the bearings. Also any thermal deformation in the spindle causes an instability in the accuracy and precision of the spindle.

Controlling the thermal deformation in longitudinal direction is important and can be solved with design tricks. To overcome the expansion, in the design cylindrical roller bearings with tapered bore are used. As discussed before, these bearings have free outer rings which do not constrain the rollers in axial direction at all. As it is depicted in Figure 53, in case of a temperature increase, the shaft will tend to expand towards the rear side since it is fixed by the angular contact ball bearings in the front. The cylindrical roller bearing will slide in its outer ring, therefore any undesired stresses and bearing preload will be prevented.

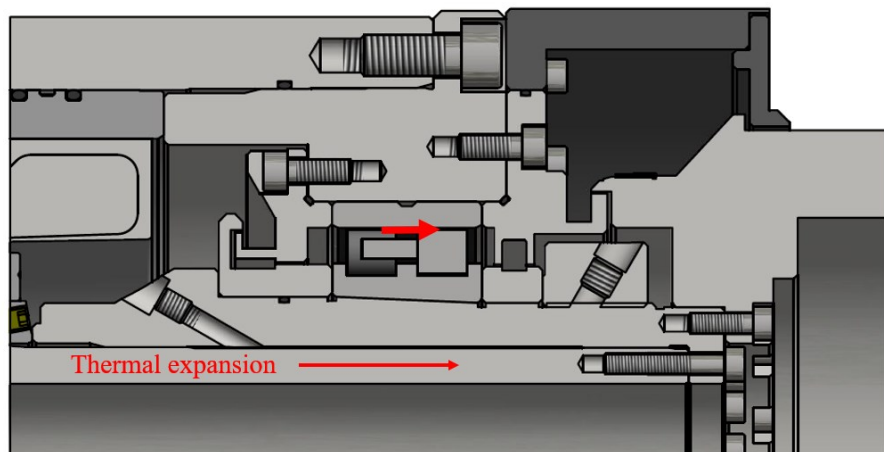


Figure 53. Cylindrical roller bearing lets the shaft expand freely in axial direction.

4.1.2 Sealing design

Lubrication is vital for spindle bearings to function and avoid failure. Protection of the grease/oil and bearings from any contamination, cutting fluid or the motor coolant should be ensured to prevent bearing failures and as a result spindle failures. Cutting fluid, used to dissipate the heat generated at the cutting zone, can follow incredible paths to reach bearings due to high pressure and centrifugal forces. Many o-rings and a unique labyrinth design are used for the sealing of the spindle.

Although many parts seem to have perfectly mating surfaces with the ones they are assembled to, water can easily penetrate between these surfaces. Therefore almost at every point where a leakage might occur, o-rings are used. In the front side of the spindle as shown in Figure 54, many o-rings are placed between the parts to ensure water-tightness of the system.

O-rings are the sealing elements usually preferred in between stationary parts. On the functioning and moving surfaces with high speeds, o-rings cannot provide efficient sealing due to the heat and deformation generated by friction. There are other sealing elements that can provide protection at high speeds and high temperatures. However, any extra heat source like these sealing elements should always be avoided in the spindle. Therefore instead of using sealing elements between the rotating parts, a labyrinth system is designed to drain away the leaking cutting fluid, or the coolant from the stator, before it can reach the bearings.

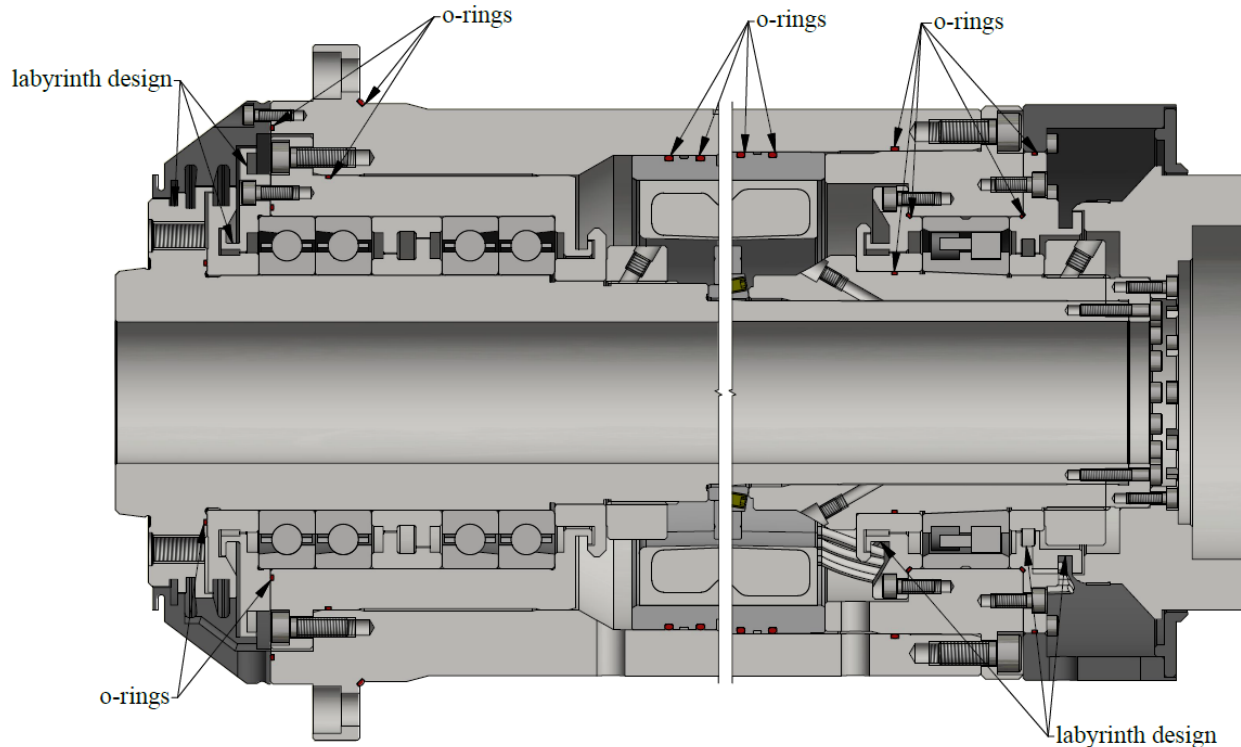


Figure 54. Sealing design of the spindle

As illustrated in Figure 55, the main purpose of the labyrinth design in the parts is to collect the leaking fluid in certain grooves and then dispose it through the holes at the bottom side of the spindle (Fritz, Haas and Müller, 1991). A several step protection and drain design is used in the front side where the leakage occurs most. Figure 55 shows the possible paths that the cutting fluid can follow and the points it can be drained away from the spindle. Similar design principles are used at every point in the spindle where a leakage might occur.

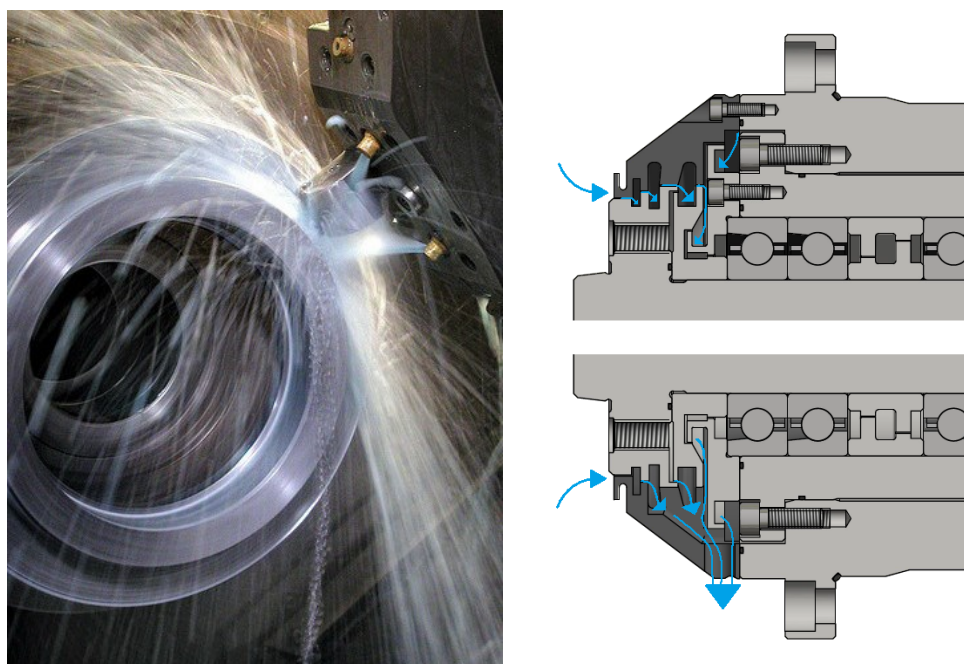


Figure 55. Cutting fluid used during machining can easily leak into the spindle. (Left image: F&M Engineering, 2015)

4.1.3 Encoder

The synchronous built-in motor alone cannot provide any speed or position data during operation, therefore to be able to measure the rotational speed and position of the spindle correctly an encoder is required in the spindle. Especially precise measurement of the angular position helps to obtain accurate machining results in C-axis operations. In this spindle, an incremental rotary encoder which consists of a measuring head and a ring, and produced by AMO GmbH, is used. The encoder works based on the inductive principles; the mutual inductance in the windings of the measuring head changes due to the relative position of the ring which has highly precise graduations as illustrated in Figure 56.

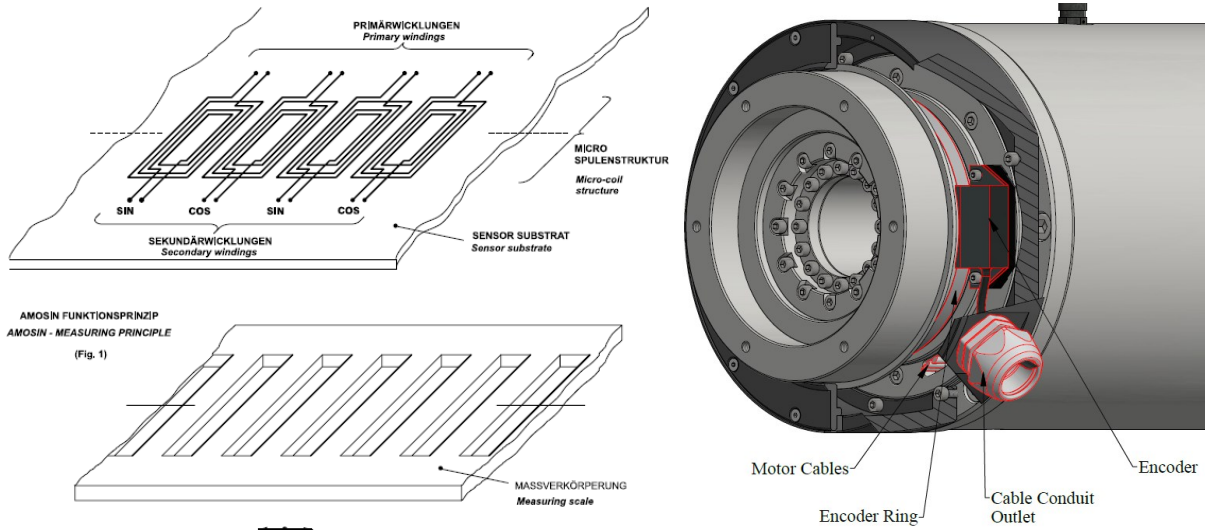


Figure 56. Speed and position measurements of the spindle are made with rotary encoder. (Left image: AMOSIN, 2011)

The encoder cable and motor cable paths are also taken into account and designed. They are collected together inside the protection flange at the back of spindle and exits through the cable conduit outlet.

4.2 Assembly to the machine

The spindle is assembled into a sample spindle housing as depicted in Figure 57. The spindle is fitted in the housing through the Ø246 mm diameter in the front with a small clearance fit and fixed with M12 DIN912 screws. The housing should also have the necessary holes for the coolant hoses as shown.

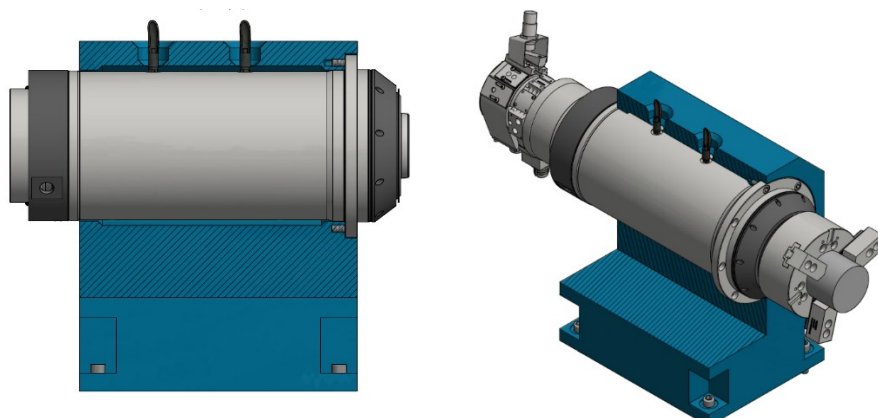


Figure 57. Cartridge spindle assembled into a spindle housing

An example of a simple lathe, which uses the cartridge spindle designed, is illustrated in Figure 58.

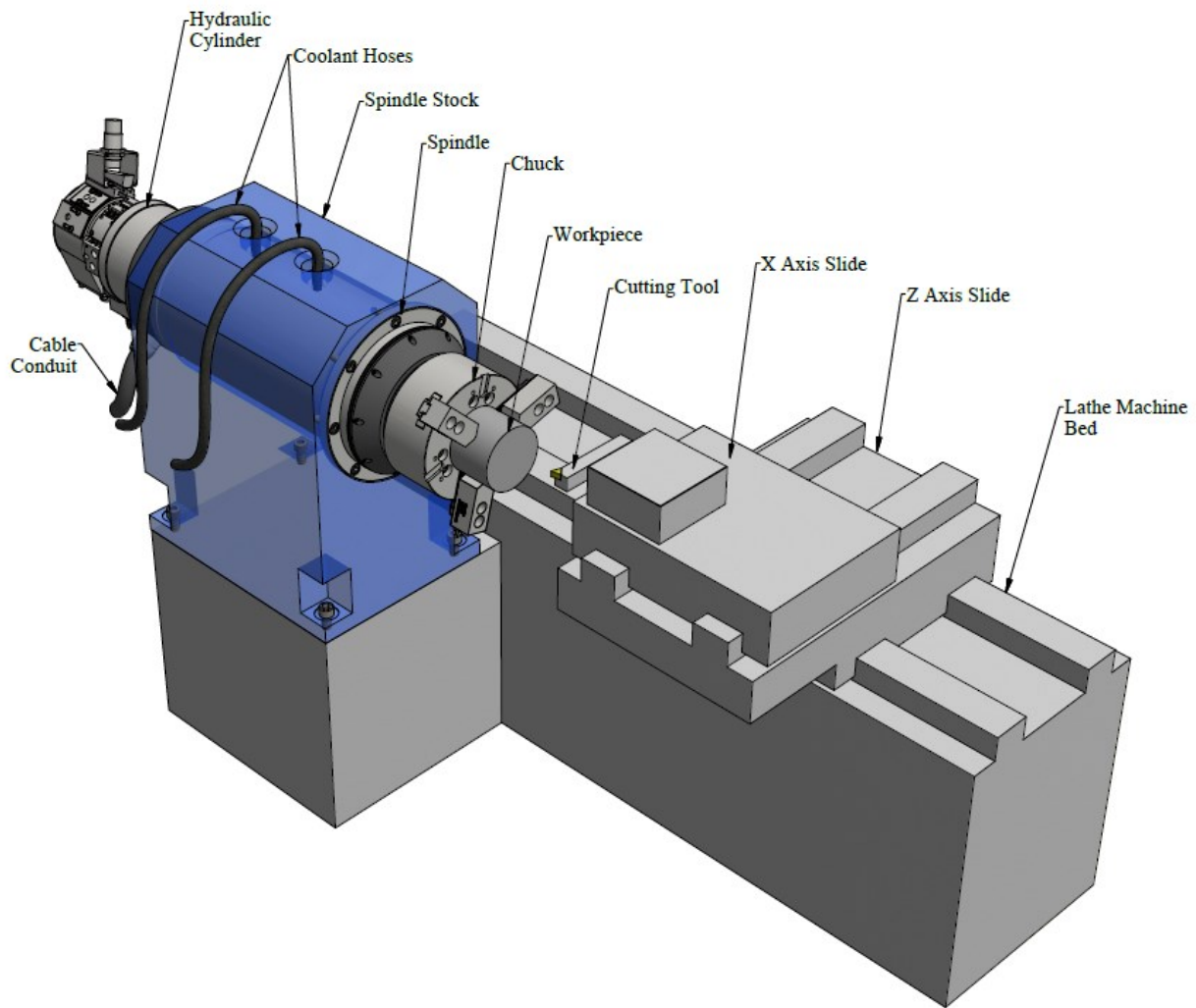


Figure 58. Example of a simple lathe with the cartridge spindle designed

4.3 Spindle BOM

The parts designed and components used in the spindle are shown in Figure 59 and listed in the BOM in Table 16 together with the quantities and the possible materials.

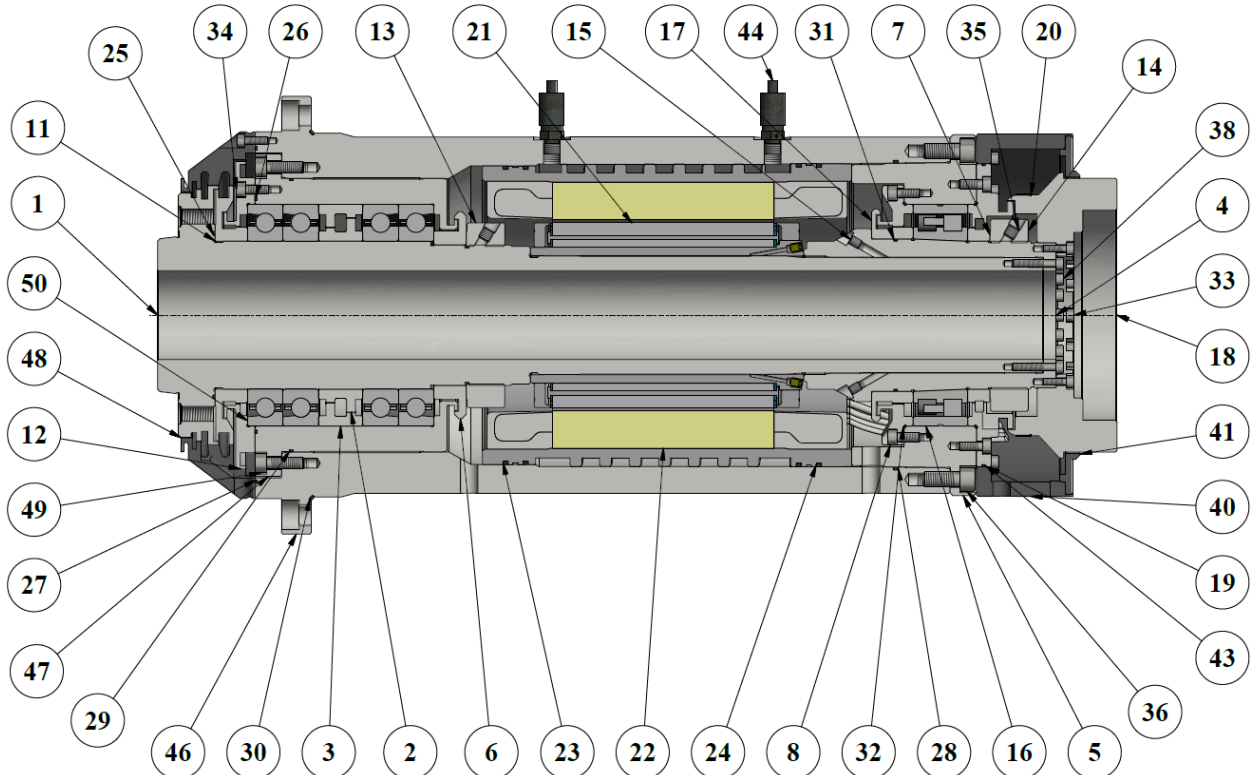


Figure 59. Spindle assembly

Table 16. BOM of the spindle

ITEM	QTY	PART DESCRIPTION	MATERIAL
1	1	Spindle Shaft	Steel Ck45
2	1	Front Inner Spacer	Steel st52
3	1	Front Outer Spacer	Steel st52
4	1	Rear Bearing Seat	Steel 16MnCr5
5	1	Rear Bearing Housing	Steel st52
6	1	Front Preload Spacer	Steel st52
7	1	Rear Preload Spacer	Steel st52
8	1	Rear Bearing Flange	Steel st52
9	1	Encoder Plate	Steel st37
10	1	Encoder AMO WMK201.30.512	
11	1	Front Inner Labyrinth	Steel st52
12	1	Front Outer Labyrinth	Steel st52
13	1	Locknut M95x2	
14	1	Locknut M100x2	
15	2	M6 x 8 DIN 913	
16	1	Bearing NN3020-TB-KR-CC1	
17	1	Rear spacer	Steel st52
18	1	Cylinder Flange	Steel st52
19	1	Rear Preload Flange	Steel st52
20	1	Encoder Ring AMO WMR100.512	
21	1	Rotor 1FE1093-6WV11-1BC0	
22	1	Stator 1FE1093-6WV11-1BC0	
23	2	O-ring 01	Rubber NBR70

24	2	O-ring 02	Rubber NBR70
25	1	O-ring 03	Rubber NBR70
26	1	O-ring 04	Rubber NBR70
27	1	O-ring 05	Rubber NBR70
28	1	O-ring 06	Rubber NBR70
29	1	O-ring 07	Rubber NBR70
30	1	O-ring 08	Rubber NBR70
31	1	O-ring 09	Rubber NBR70
32	2	O-ring 10	Rubber NBR70
33	34	M5 x 16 DIN 912	
34	25	M6 x 16 DIN 912	
35	6	M8 x 8 DIN 913	
36	12	M10 x 25 DIN 912	
37	6	M6 x 55 DIN 912	
38	16	M5 x 30 DIN 912	
39	2	M4 x 8 DIN 912	
40	1	Protection Flange	Steel st37
41	2	Protection Plate	Steel st37
42	12	M4x10 DIN 7991	
43	1	O-ring 11	Rubber NBR70
44	2	Fitting Male Straight Thread 1/4"	
45	1	Conduit Fitting VG.M25-K	
46	1	Stator Housing	Steel st52
47	1	Front Bearing Housing	Steel st52
48	1	Front Protection Flange	Steel st37
49	8	M8 x 25 DIN 912	
50	4	Bearing 7020A5-TRS-DB-EL	

5 DISCUSSION AND CONCLUSIONS

A discussion on the design methodology, analyses and spindle design are presented in this chapter together with the conclusions draw.

5.1 Discussion

Designing a spindle requires not only the knowledge of machining and physical laws, but also an extensive experience in the area. From identifying the specifications tilll making the final detail design, what possible situations or problems would be encountered during the use of spindle in real life must be considered.

To specify the machining capabilities of the spindle (or power and speed in this case) possible customer needs are taken as the basis in this thesis, and the worst case machining parameters are the reference point of the basis. However in most cases, such cutting operations take less place within the lifetime of spindles, thus bearings and spindle experience such loads less than expected. Accordingly, the calculations for the fatigue life and load rating of the bearings are found to be unnecessary, because, as it is given in Table 7, even for a single bearing, the load ratings are much higher than the cutting forces calculated for the worst case. Therefore, bearings are assumed to have sufficient load ratings and fatigue life, no further analysis is made.

Literature survey for the spindle design showed that in many cases spindle analyses are made by assuming the spindle as a beam with two simple supports regardless of the number of the bearings, which is the case in the test model in this thesis. However, in reality especially lathe spindles consist of many bearings and support points, which makes the spindle an indeterminate beam. Simplifying the spindle by reducing the number of supports by combining a few, might result in different static and dynamic stiffness values than actual.

In the static and dynamic analyses, the spindle shaft is assumed to be a straight shaft with a single diameter, together with the parts assembled on it. However in reality the shaft is a stepped design with different sections, and has many different parts assembled on with different shapes and diameters. To be able to obtain more precise results, the complex geometry should be included in the analysis. Especially for the dynamic analysis, the results are expected to be different. Still though, it can be foreseen to have the design sufficient dynamically since the Eigen frequencies and critical speeds found are much above the working speed range of the spindle.

Although the analytical solution method is validated with the test model in the analyses, the FEM analysis results for the spindle shows the opposite. In separate cases, FEM results matches the analytical model results, but for the superposition case FEM analysis gives unexpectedly higher results. As given in Table 13, the reaction forces found with the analytical solution are relatively high while the total deflection is much smaller than in the FE model. Also the sum of the reaction forces for the combined case is not equal to the external load in the analytical model. This might be explained by the simplifications and the assumptions made for the superposition method. Better and more realistic assumptions should be made to be able to get more accurate results. However, the analytical model still provides important and sufficient results regarding the relationship between the bearings span and spindle deflection.

Spindle deflection under the cutting forces primarily affects the accuracy and the life rating of the spindle. Especially for the case in this thesis, where the stresses generated in the shaft and

bearings are far below the maximum limits, accuracy and precision matter more while defining the deflection limits. In such cases, allowable deflection limit of the spindle tip is usually determined by the producer based on the machine specifications regarding precision. Maximum deflection of 0.03 mm for the worst case loading in this spindle is found to be an adequate limit. Moreover, lower deflection and higher precision are usually demanded in finishing cuts, which have lower chip thicknesses and higher speeds, and lower cutting forces as result.

The final detail design of the spindle is constructed around the shaft and bearings of which the design inputs are analyzed and optimized. The final assembly consisting of all the necessary parts can be designed in many different ways based on the manufacturability and assemblability. It is hard to create a spindle with “the best design”, because the final design does not only depend on the calculations, analyses, but also other factors such as the machine to be used, operating conditions, assembling capabilities of the facility etc.

The complete design requires a vast experience about the spindle assembly, because the assembly order and methods for the parts significantly affects the design. Some parts require to be assembled and disassembled for measurements, preloading and adjustments, and some parts require to be heated and fitted onto the shaft due to interference fits. Therefore it is vital to have and use these information during the design.

As illustrated in Figure 54, many sealing elements and design methods are used in the design. Running of the cooling liquid or the coolant circulating around the stator into the bearings, then spoiling the grease, which ultimately causes the spindle to fail is a very common case in the manufacturing industry. To prevent it from happening serious design precautions has to be taken care of on the spindle. With the help of o-rings, sealing of stationary parts are relatively easy than rotating parts. For the rotating parts, providing the sealing with the design of a labyrinth and drainage system is easier and cost effective than using sealing elements.

5.2 Conclusions

As the result of this thesis, a spindle is designed with the following specifications:

1. It can cut 200HB AISI 4340 material with a diameter of Ø110 mm and 50 mm length, with a feed rate of 0.35 mm/rev and 6 mm depth of cut at the speed of 600 rpm.
2. It has the motor power of 16.8 kW and 6,000 rpm rotational speed, more than the lower limit set, 15 kW.
3. It is designed to run with a built-in synchronous spindle motor, which is cooled with a circulating coolant system.
4. It is a cartridge type spindle, designed to be a complete single unit with a shell housing of Ø246 mm fitting diameter, which is within the desired limits. It has the total length of 649.5 mm.
5. The spindle tip deflection in the worst case loading is 0.297 mm, which is at the maximum allowable limit of 0.03 mm.
6. The stresses generated in the spindle shaft for the worst case loading are much lower than the yield limit 485 MPa of the shaft material, Ck45. Therefore, no plastic deformation is expected during cutting operations.
7. Its first mode frequency is 1,096 Hz which is far above the working speed range, 0-6000 rpm (100 Hz). Additionally its lowest resonance frequency of 1,100 Hz and critical speed of 64,203 rpm proves that the spindle avoids any resonance during cutting. Note that only spindle is of issue, other possible vibration sources such as cutting tool, material, etc. are not considered.

8. Its static stiffness is optimized as much as the space limits allow. The span distance between the front bearing pairs has more effect on the stiffness than the distance between the rear bearing and front pair. Both the dynamic and static properties are found to be sufficient to operate within the specified speed and load conditions.
9. It has four angular contact ball bearings with DBB arrangement in the front, and a double row cylindrical roller bearing with a tapered bore at the rear.
10. It has a sealing and labyrinth system to prevent leakage into the spindle, and if happens to drain it away without reaching the bearings.

6 RECOMMENDATIONS AND FUTURE WORK

In this chapter, recommendations on more detailed solutions and/or future work in this field are presented.

6.1 Recommendations

Since spindle design task itself involves many steps and parameters to take into account, it might be difficult to cover and handle in detail each of them. Following recommendations can be made to the one with such task regarding spindle design:

- Bearings might be checked to ensure that their load ratings and fatigue life are sufficient for the design.
- For the static analysis, a better analytical solution might be worked on to understand the actual shaft behavior and FEM solution.
- The complex geometry of the spindle shaft should be included in the calculations to get more accurate results.
- The workpiece holder, hydraulic cylinder and the workpiece can be included in the analysis and calculations to investigate their effects.
- Thermal behavior of the spindle due to temperature increase in the motor, and its effects on the accuracy can be evaluated.
- The stiffness of the stator and bearing housings can be checked to ensure the precision of the final assembly.
- Although almost all rotating parts are designed symmetrical to prevent any undesired vibration, it is inevitable to have balance problems in the spindle due to the inhomogeneity in materials and parts. Therefore a simple system can be designed to make the spindle balanced.
- More measurement systems can be adapted to the spindle to improve the performance. Sensors to measure the bearing temperature helps to prevent any failure due to significant temperature and preload increase. Vibration sensors can help to measure the spindle frequency during operation and hence to avoid the unstable chatter zones through the feedback sent to controller.

6.2 Future work

The following are the possible ideas for future work:

- Spindle bearing stiffness coefficients has substantial effects on the spindle static and dynamic behavior. To be able to get more accurate results and predict the spindle behavior, the stiffness values of the bearings can be found experimentally and included in the analysis.
- Manufacturing drawings can be made for future prototype testing.
- Prototype manufacturing and testing of the spindle can be made.

- Bearings with different properties or precision levels and their effects on the rigidity and accuracy can be investigated.
- Tolerance stack up in the assembly and its effects on the rigidity and accuracy can be investigated.

7 REFERENCES

- Wikipedia, “*Machine Tool*”, https://en.wikipedia.org/wiki/Machine_tool, accessed 2015-05-29, 2003.
- DMG Mori Co., Ltd., <http://en.dmgmori.com/products>, accessed 2015-12-29, 2015
- Seco Tools AB, “*Multi Directional Turning*”, <http://www.secotools.com/mdt>, accessed 2015-12-29, 2015.
- Goodway Machine Corp., “*Enhanced Automations: Bar feeders*”, http://www.goodwaycnc.com/exhtml_goodway_en/automation/turning/bar_feeders, accessed 2015-07-02, 2015.
- Ima Techno S.R.L., “*Turning Spindles: CODE 11011A150*”, <http://www.imatecno.com/index.php/en/products/electrospindles/turning/item/238-code-11011a150-idrostatic.html>, accessed 2015-12-29, 2015.
- Hyundai WIA Machine Tools, “*Multi-axis T/C: LM1800 Series*”, http://www.hyundai-wiamachine.com/home/products/multitasking_machines/lm1800-series.html, accessed 2015-12-29, 2015.
- Dynomax, Inc., “*Book of Spindles, Part I: Spindle Facts*”, 2011.
- Hurco Companies, Inc., “*CNC Lathe Considerations: bed design*”, <http://blog.hurco.com/blog/bid/374362/CNC-Lathe-Considerations-bed-design>, accessed 2015-12-29, 2014.
- Abele, E., Altintas Y., and Brecher C., “*Machine Tool Spindle Units*”, CIRP Annals - Manufacturing Technology, Vol. 59, Issue 2, 2010, pp 781-802.
- Altintas Y. and Cao Y., “*Virtual Design and Optimization of Machine Tool Spindles*”, CIRP Annals - Manufacturing Technology, Vol. 54, Issue 1, 2005, pp 379-382.
- Maeda O., Cao Y., and Altintas Y., “*Expert spindle design system*”, International Journal of Machine Tools and Manufacture, Vol. 45, Issue 4-5, 2005, pp 537-548.
- Sawamoto T. and Konishi K., “*Development of machine tool spindles with higher rotational speeds*”, Tribology International, Vol. 15, Issue 4, 1982, pp 199-207.
- Soshi M., Yu S., Ishii S. and Yamazaki K., “*Development of a high torque-high power spindle system equipped with a synchronous motor for high performance cutting*”, CIRP Annals - Manufacturing Technology, Vol. 60, Issue 1, 2011, pp 399-402.
- Xin-yun Z., Min W., Tao Z. and Jian-zhong H., “*The Static and Dynamic Analysis of High-speed Electric Spindle Based on ANSYS*”, Second International Conference on Digital Manufacturing and Automation (ICDMA) Proceedings, 2011, pp 1332-1335.
- Lin C., “*Optimization of Bearing Locations for Maximizing First Mode Natural Frequency of Motorized Spindle-Bearing Systems Using a Genetic Algorithm*”, Applied Mathematics, Vol. 5, No. 14, 2014, pp 2137-2152.
- Zhu L., Zhu C., Yu T., Shi J. and Wang W., “*Dynamic Analysis and Design of the Spindle-Bearing System in Turn-milling Centre*”, IEEE International Conference on Automation and Logistics Proceedings, 2007, pp 2394-2398.
- Altintas Y. and Budak E., “*Analytical Prediction of Stability Lobes in Milling*”, CIRP Annals - Manufacturing Technology, Vol. 44, Issue 1, 1995, pp 357-362.

Gagnol V., Bouzgarrou B.C., Ray P. and Barra C., “*Stability-Based Spindle Design Optimization*”, *Journal of Manufacturing Science and Engineering*, Vol. 129, Issue2, 2006, pp 407-415.

Akkurt M., “*Talaş Kaldırma Yöntemleri ve Takım Tezgahları*”, Birsen Yayınevi, İstanbul, 2000.

Altintas Y., “*Manufacturing Automation: Metal Cutting Mechanics, Machine Tool Vibrations, and CNC Design*”, Cambridge University Press, 2012.

Budak E. and Ozlu E., “*Modelling of Machining Operations: Turning and Milling*”, *Training Material*, Sabancı University, 2014.

Siemens AG, “*SINAMICS S120 Synchronous Built-in Motors IFE1 Configuration Manual*”, 2010.

Weck M., “*Machine Tools: Construction and Mathematical Analysis, Vol. 2*”, Wiley, Chichester 1984.

Stephenson D.A., Agapiou J.S., “*Metal Cutting Theory and Practice*”, CRC Press, Boca Raton, 1997.

Kaydon Bearings, “*Bearing load scenarios*”, <http://www.kaydonbearings.com/typesACX.htm>, accessed 2015-12-31, 2015

NSK Bearings, “*Machine Tool Spindle Bearing Selection & Mounting Guide*”, 2009.

NSK Bearings, “*Super Precision Bearings*”, 2011.

FAG Bearings, Schaeffler Group, “*Super Precision Bearings*”, 2010.

Matweb, Material Property Data, “*AISI 1045 Steel, as cold drawn, 50-75 mm (2-3 in) round*”, <http://www.matweb.com/search/DataSheet.aspx?MatGUID=3135b629bdee490aa25f94230424c08a&ckck=1>, accessed 2015-09-03, 2015.

ANSYS, Inc., “*ANSYS Mechanical APDL Element Reference*”, 2013.

Guo C., Bai L., Zheng B. and Pan Y., “*Spindle Static and Dynamic Characteristics Analysis of Precision CNC Turning Center*”, *Advanced Materials Research*, Vol. 619, pp 47-50.

F&M Engineering, Ltd., “*Our Services*”, <http://fandmengineering.co.uk/our-services/>, accessed 2015-12-30, 2015.

Fritz E., Haas W. and Müller K., “*Berührungsreie Spindelabdichtung im Werkzeugmaschinenbau: Konstruktions-Richtlinien- und Lösungskatalog*”, Institute of Machine Components, University of Stuttgart, Stuttgart, 1991.

AMO GmbH, “*Incremental Angle Measuring Systems based on the AMOSIN – Inductive Measuring Principle*”, 2011.

DMG MORI Corporation, Ltd., “*NZX 1500 / NZX 2000 Product Documentation*”, 2014.

Yamazaki Mazak Corporation, “*Quick Turn Nexus II Series Product Documentation*”, 2013.

Doosan Infracore Machine Tools, “*Lynx 220 Y Series Product Documentation*”, 2013.

SKF Bearings, “*Super-precision bearings*”, 2013.

Joshi P.H., “*Machine Tools Handbook*”, Tata McGraw-Hill Publishing Co, Ltd., New Delhi, 2007.

Hibbeler R.C., “*Mechanics of Materials*”, Pearson Prentice Hall, New Jersey, 2005.

Srikrishnanivas, D., “*Rotor Dynamic Analysis of RM12 Jet Engine Rotor using ANSYS*”, Blekinge Institute of Technology, Karlskrona, 2012.

Freudenberg Sealing Technologies GmbH & Co. KG, “*O-rings and Static Seals Technical Manual*”, 2015.

Yinsh Precision Industrial Co., Ltd., “*Precision Locknuts for Bearings, YS Series*”, 2015.

APPENDIX A: SPECS OF SIMILAR SPINDLES ON THE MARKET

The spindle specifications of DMG MORI NZX 1500, Mazak Quick Turn Smart 100-II Series and Doosan Lynx 220 YA Series are listed in below tables. The spindles are selected based on their bar working capacities that are similar to the design requirement (52 mm) in this thesis.

DMG MORI
NZX 1500

Spindle

	NZX 1500	NZX 2000
Chuck size	6-inch	8-inch
Bar work capacity	φ 52 mm (ϕ2.0 in.)	φ 65 mm (ϕ2.5 in.)
Max. spindle speed	6,000 min ⁻¹	5,000 min ⁻¹
Spindle drive motor	22/18.5 kW (30/24.7 HP) (30 min./cont) 25/22 kW (33.3/30 HP) (30 min./cont) OP	25/22 kW (33.3/30 HP) (30 min./cont)

	NZX 1500		NZX 2000	
Chuck size	6-inch (Spindle 1)	6-inch (Spindle 2)	8-inch (Spindle 1)	8-inch (Spindle 2)
Spindle acceleration time	3.58 sec. (0→6,000 min ⁻¹)	3.65 sec. (0→6,000 min ⁻¹)	3.26 sec. (0→5,000 min ⁻¹)	3.18 sec. (0→5,000 min ⁻¹)
Spindle deceleration time	3.10 sec. (6,000→0 min ⁻¹)	3.10 sec. (6,000→0 min ⁻¹)	2.67 sec. (5,000→0 min ⁻¹)	2.65 sec. (5,000→0 min ⁻¹)

• Measurements are with a chuck fitted.

(DMG Mori, 2014)

QUICK TURN NEXUS II SERIES

Standard Machine Specifications			
QUICK TURN NEXUS			
	100-II	100-II M	100-II MS
Capacity	Max. swing	φ550 mm	φ550 mm
	Swing over carriage	φ280 mm	φ280 mm
	Max. machining Dia.	φ280 mm	φ280 mm
	Max. machining length ^{a1}	309 mm	334 mm
	Distance between jaw faces (both spindles)	-	455 mm
Travel	Bar work capacity ^{a2}	φ51 mm	φ51 mm
	X-axis travel	190 mm	185 mm
	Y-axis travel	-	-
Main spindle	Z-axis travel	330 mm	385 mm
	Chuck size	6"	6"
	Spindle speed ^{a3}	6000 rpm	6000 rpm
	Number of spindle speed ranges	1-Stepless	1-Stepless
	Spindle nose	A2-5	A2-5
Second spindle	Spindle bore	φ61 mm	φ61 mm
	Chuck size	-	5"
	Spindle speed	-	6000 rpm
	Second headstock stroke (W-axis)	-	460 mm
Turret	Second headstock stroke positioning speed	-	30000 mm/min
	Turret type	12 position drum turret (Bolt-on)	12 position drum turret (VDI type)
	Number of tools	12 tools	12 tools
	Turning tool shank	20 mm	20 mm
Rotary tool spindle	Boring bar shank diameter	φ32 mm	φ32 mm
	Turret indexing time	0.18 sec. / 1 step	0.18 sec. / 1 step
	Spindle speed	-	4500 rpm
	Milling capacity	-	Drill : φ16 mm, Endmill : φ16 mm, Tap : M16×2.0 Endmill : φ16 mm, Tap : M16×2.0
Feedrate	Rapid traverse rate:X-axis	30000 mm/min	30000 mm/min
	Rapid traverse rate:Y-axis	-	-
	Rapid traverse rate:Z-axis	33000 mm/min	33000 mm/min
Tailstock	Rapid traverse rate:C-axis	-	555 rpm
	Tailstock stroke	350 mm	350 mm
	Taper	MT 4 (Dead center)	MT 4 (Dead center)
Motors	Main Spindle (30 min. rating)	11 kW (15 HP)	11 kW (15 HP)
	Main Spindle (Cont. rating)	7.5 kW (10 HP)	7.5 kW (10 HP)
	Second spindle (25%ED)	-	11 kW (15 HP)
Power requirements	Rotary tool spindle motor (5 min. rating)	-	5.5 kW (7.5 HP)
	Coolant pump motor	0.18 kW	0.18 kW
	Required power capacity(Cont. rating)	17.2 kVA	17.5 kVA
Coolant	Air source pressure	0.5 MPa [5 kgf/cm ²] 100 L/min (ANR)	0.5 MPa [5 kgf/cm ²] 150 L/min (ANR)
	Tank capacity	130 L	160 L
Machine size	Height	1800 mm	1800 mm
	Floor space requirement	1790 mm X 1630 mm	2090 mm X 1630 mm
	Machine weight	3400 kg	3800 kg

(Mazak, 2013)



Lynx 220 Y series

Machine Specifications

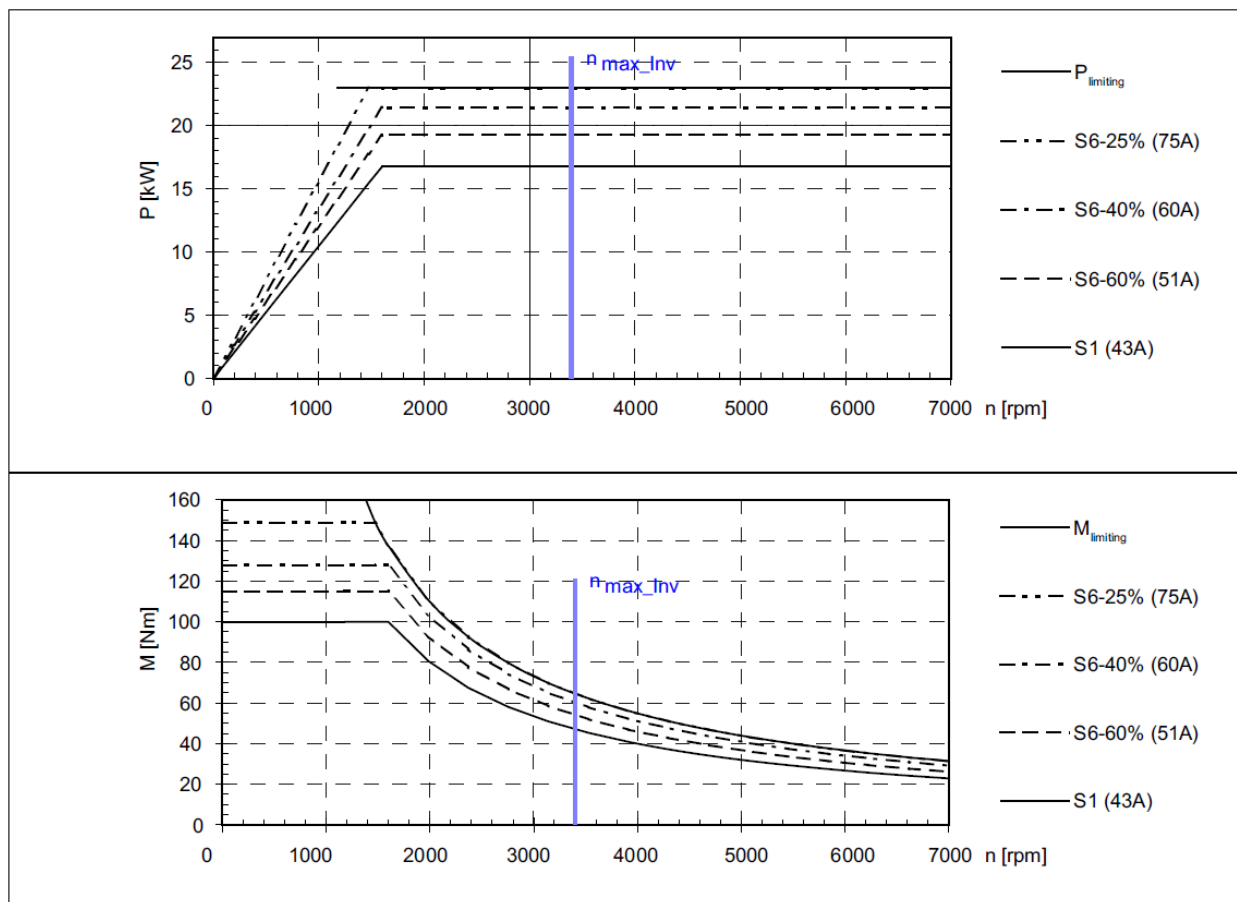
	Description	Unit	Lynx 220YA	Lynx 220YC	Lynx 220LYA	Lynx 220LYC	Lynx 220LSYA	Lynx 220LSYC
Capacity	Swing over bed	mm (inch)			600 (23.6)			
	Swing over saddle	mm (inch)			400 (15.7)			
	Recom. Turning diameter	mm (inch)	170 (6.7)	210 (8.3)	170 (6.7)	210 (8.3)	170 (6.7)	210 (8.3)
	Max. Turning diameter	mm (inch)			300 (11.8)		300 (11.8)	
	Max. Turning length	mm (inch)					510 (20.1)	
	Chuck size	inch	6	8	6	8	6	8
Travels	Bar working diameter	mm (inch)	51 (2.0)	65 (2.6)	51 (2.0)	65 (2.6)	51 (2.0)	65 (2.6)
	Travel distance	X-axis mm (inch)				205 (8.1)		
	Z-axis mm (inch)		350 (13.8)			560 (22.0)		
	Y-axis mm (inch)				105 (± 5.2) (4.1 (± 2.1))			
Feedrate	C1, C2-axis mm (inch)				360 (in 0.001) (14.2)			
	Rapid Traverse Rate	X-axis m/min (ipm)			30 (1181.1)			
	Z-axis m/min (ipm)				10(393.7)			
	Y-axis m/min (ipm)				36 (1417.3)			
Main spindle	C-axis m/min (ipm)				200 (7874.0)			
	Max. Spindle speed	r/min	6000	4500	6000	4500	6000	4500
	Spindle nose	ASA	A2-5	A2-6	A2-5	A2-6	A2-5	A2-6
	Spindle bearing diameter (Front)	mm (inch)	90 (3.5)	110 (4.3)	90 (3.5)	110 (4.3)	90 (3.5)	110 (4.3)
	Spindle through hole	mm (inch)	61 (2.4)	76 (3.0)	61 (2.4)	76 (3.0)	61 (2.4)	76 (3.0)
	Min. spindle Indexing angle(C-axis)	deg			0.001			
Turret	No. of tool stations	ea			12 (24 Position Index)			
	OD tool size	mm (inch)			20×20 (0.8×0.8)			
	Max. boring bar size	mm (inch)			32 / 20 (1.3 / 0.8)			
	Turret Indexing time (1 station swivel)	s			0.15			
Tail Stock	Max. Rotary tool speed	r/min			6000			
	Quill diameter	mm (inch)	-	-	65 (2.6)	-	-	-
	Quill bore taper	MT	-	-	#4	-	-	-
Sub spindle	Quill travel	mm (inch)	-	-	80 (3.1)	-	-	-
	Spindle speed	r/min	-	-	-	-	6000	
	Spindle nose	FLAT	-	-	-	-	Ø110	
	Spindle bearing diameter (Front)	mm (inch)	-	-	-	-	70 (2.8)	
	Spindle through hole	mm (inch)	-	-	-	-	43 (1.7)	
Motors	Min. spindle Indexing angle(C-axis)	deg	-	-	-	-	0.001	
	Main spindle motor power (30min/ cont.)	kW (Hp)			15 / 11 (20.1 / 14.8)			
	Sub spindle motor power	kW (Hp)	-	-	-	-	5.5 / 3.7 (7.4 / 5.0)	
	Rotary tool motor power	kW (Hp)			3.7 (5.0)			
Power source	Coolant pump motor power	kW (Hp)			0.4 (0.5)			
	Electric power supply (rated capacity)	kVA			27.8		33.7	
Machine Dimensions	Height	mm (inch)			1920 (75.6)			
	Width	mm (inch)			1710 (67.3)			
	Depth	mm (inch)	2425 (95.5)	2455 (96.7)	2850 (112.2)	2880 (113.4)	2850 (112.2)	2880 (113.4)
	Weight	kg (lb)	3400 (7495.6)	3500 (7716.1)	3900 (8597.9)	4000 (8818.4)	3900 (8597.9)	4000 (8818.4)
NC CONTROL					DOOSAN Fanuc i series			

(Doosan, 2013)

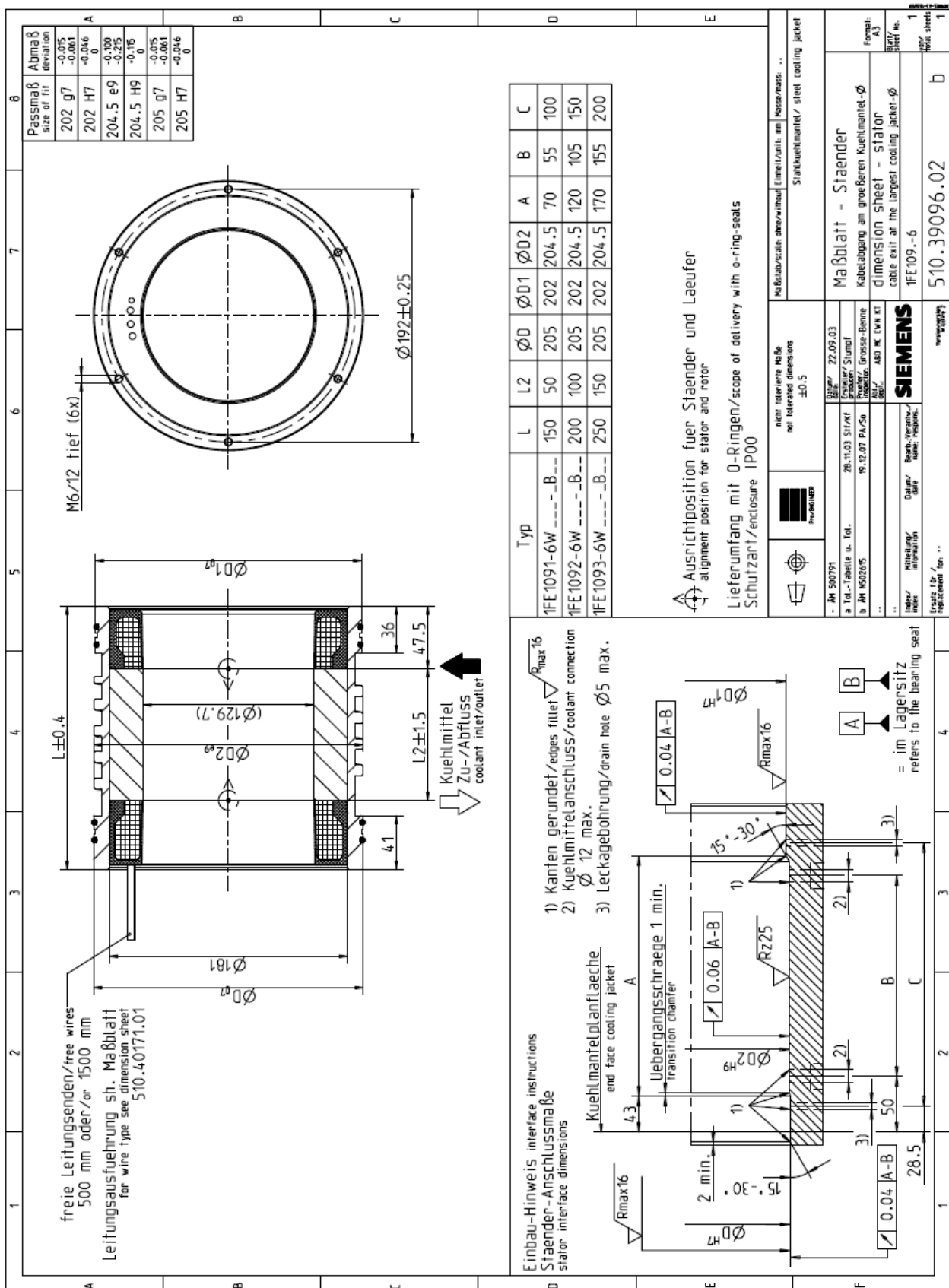
APPENDIX B: SIEMENS 1FE1093 MOTOR SPECS

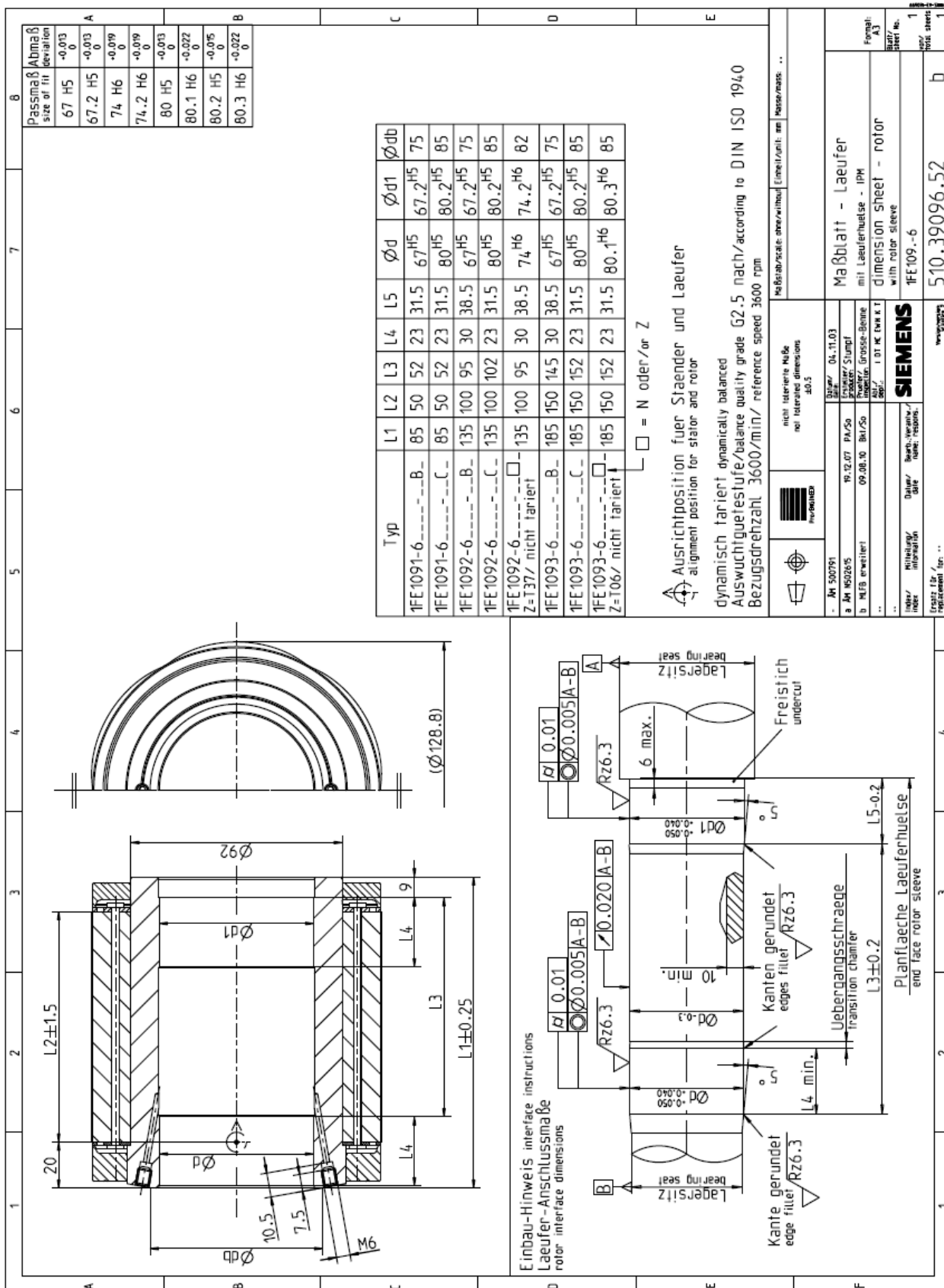
The specifications of the Siemens 1FE1093-6WV*I synchronous built-in motor are given below. Necessary dimensions for spindle assembly and design are also given in the motor drawings. (Siemens, 2010)

Rated power	P_N	kW	16.8
Rated speed	n_N	rpm	1,600
Rated torque	M_N	Nm	100
Rated current	I_N	A	43
Maximum current	I_{msx}	A	86
Maximum speed	n_{max}	rpm	7,000
Maximum torque	M_{max}	Nm	165
Moment of inertia	J_{rot}	kg m^2	0.02317
Voltage constant	k_E	V/1000 rpm	168
Thermal time constant	T_{therm}	min	3
Stator weight with cooling jacket	m_{st}	kg	28
Rotor weight	m_{rot}	kg	9.8



The data for duty type S6 are valid for a 2 min. duty cycle.





APPENDIX C: MACALUAY AND SINGULARITY FUNCTIONS

Macaluay and singularity functions helps to define the deflection function of a beam in the form of x , position variable along the beam. The use of Macaluay and singularity functions are explained below.

The Macaulay functions are in the form of,

$$\langle x - p \rangle^n = \begin{cases} 0 & \text{for } x < p \\ (x - p)^n & \text{for } x \geq p \end{cases}$$

where $n \geq 0$. In these functions, x represents the coordinate of the point of interest along the shaft and p represents the locations where a discontinuity occurs. Integration of Macaulay functions subject to ordinary integration rules.

$$\int \langle x - p \rangle^n dx = \frac{\langle x - p \rangle^{n+1}}{n + 1} + C$$

Similarly, singularity functions are described to express only the point loads and moments acting along the shaft. A point load F , can be defined as below in the form of singularity function.

$$w = F \langle x - p \rangle^{-1} = \begin{cases} 0 & \text{for } x \neq p \\ P & \text{for } x = p \end{cases}$$

Additionally, a point moment M_0 can be expressed as,

$$w = M_0 \langle x - p \rangle^{-2} = \begin{cases} 0 & \text{for } x \neq p \\ M_0 & \text{for } x = p \end{cases}$$

Integration of the singularity functions are different than Macaulay functions and follows different rules. The exponent of the function n , increases with the level of integration but the constants of integration is not associated. The integration of singularity functions can be described as,

$$\int \langle x - p \rangle^n dx = \langle x - p \rangle^{n+1}, n = -1, -2$$

APPENDIX D: MATLAB SOLUTION FOR TEST MODEL

```
% Master Thesis
% Design and development of spindle
% Asim Kutlu, KTH Machine Design, 2012-03-08

%% Clean up and reset workspace
clear all % Clear workspace memory
close all % Close all figures
clc % Clear command window

%% TEST MODEL DEFLECTION
% Test Model parameters

Ftest = 1000;      % Load in the test model [N]
Dtest = 50;        % Outer diameter shaft in the test model [mm]
Ep = 200e3;        % Young's modulus for generic steel [MPa]
Ip = pi*(Dtest^4)/64;    % Area moment of inertia [mm^4]

Ltest = 600;        % Length of the shaft in the test model [mm]
atest = 240;        % Overhung distance in the test model [mm]
stest = 360;        % Bearing span in the test model [mm]

ktest = 5e5;        % Rigidity of the bearing in the test model [N/mm]

%% Reaction Forces

R1 = Ftest*Ltest/stest; % Reaction force 1 [N]
R2 = Ftest*atest/stest; % Reaction force 2 [N]

%% Finding c1 and c2 constants in the def.eq. through boundary conditions

Q = [atest 1;
      Ltest 1];

S = [(Ftest*atest^3)/6;
      (Ftest*Ltest^3)/6-(R1/6)*(Ltest-atest)^3];

c = Q\S;           % Matrix solution for c1 and c2

%% Preallocating deflection and position matrices

sigmaStest = zeros(1,Ltest+1); % creating sigmaStest matrix
sigmaBtest = zeros(1,Ltest+1); % creating sigmaBtest matrix
x = 0:1:Ltest;          % x position matrix

%% Superposition I

for i = 1:(Ltest+1)      % Deflection sigmaStest vs x position

    if x(i)<=atest
        sing=0;            % Singularity part in the deflection equation
    else
        sing=(R1/6*(x(i)-atest)^3);
    end
    sigmaStest(i) = 1/(Ep*Ip)*(-(Ftest/6*x(i)^3)+sing+c(1)*x(i)+c(2));
end
```

```

%% Superposition II

sigma1p = -R1/ktest;      % Deflection at reaction point 1
sigma2p = -R2/ktest;      % Deflection at reaction point 2

sigmaBtest(1) = (sigma1p*Ltest+sigma2p*atest)/stest;    % max deflection
slope = (sigmaBtest(1)+sigma2p)/Ltest; % Slope of the rigid beam

for i=1:(Ltest+1)          % Deflection sigmaBtest vs x position

    sigmaBtest(i) = ((Ltest-x(i))*slope)-sigma2p;

end

%% Total deflection and plots

SigmaTest = sigmaStest(1)+sigmaBtest;    % Total deflection at the tip [mm]

plot (x, sigmaStest)                  % Position vs beam deflection
hold on
plot (x, sigmaBtest)                  % Position vs bearing deflection
hold on
plot (x, (sigmaStest+sigmaBtest))    % Position vs total deflection

```

APPENDIX E: MATLAB SOLUTION FOR SPINDLE

```
% Master Thesis
% Design and development of spindle
% Asim Kutlu, KTH Machine Design, 2012-03-08

%% Clean up and reset workspace
clear all % Clear workspace memory
close all % Close all figures
clc % Clear command window

%% SPINDLE STATIC ANALYSIS
% Model parameters

Ft = 3700;           % Cutting force in tangential direction [N]
b = 120;             % Distance of cutting point to the spindle tip [mm]
Mt = Ft*b;           % Moment generated at the tip due to the force [N.mm]
OD = 100;             % Outer diameter of the simplified shaft [mm]
ID = 60;              % Outer diameter of the simplified shaft [mm]
I = pi*(OD^4-ID^4)/64;    % Area moment of inertia [mm^4]
E = 206e3;            % Young's modulus for Ck45 steel [MPa]

a = 85;               % Overhung distance [mm]
s1min = 78;            % Bearing span 1 min [mm]
s2min = 317;            % Bearing span 2 min [mm]
sTmax = 445;            % Max of s1+s2 [mm]
s1max = sTmax-s2min;    % Bearing span 1 max [mm]
s2max = sTmax-s1min;    % Bearing span 2 max [mm]

kB = 430e3;            % Stiffness of 7020A5 bearing pair [N/mm]
kC = 1960e3;           % Stiffness of NN2010 bearing [N/mm]

%% Preallocating the necessary matrices

Span1 = NaN(1,s1max-s1min+1);          % s1 matrix
Span2 = NaN(1,s2max-s2min+1);          % s2 matrix
DeltaS = NaN((s1max-s1min+1), (s2max-s2min+1)); % Shaft def. matrix
RA = NaN((s1max-s1min+1), (s2max-s2min+1)); % R.force matrix for case1
RB = NaN((s1max-s1min+1), (s2max-s2min+1)); % R.force matrix for case1
RC = NaN((s1max-s1min+1), (s2max-s2min+1)); % R.force matrix for case1
DeltaB = NaN((s1max-s1min+1), (s2max-s2min+1)); % Bearing def. matrix
Sigma = NaN((s1max-s1min+1), (s2max-s2min+1)); % Total def. matrix
C1 = NaN((s1max-s1min+1), (s2max-s2min+1)); % Def.eq.constant matrix
C2 = NaN((s1max-s1min+1), (s2max-s2min+1)); % Def.eq.constant matrix
RAP = NaN((s1max-s1min+1), (s2max-s2min+1)); % R.force matrix for case2
RBp = NaN((s1max-s1min+1), (s2max-s2min+1)); % R.force matrix for case2
RCp = NaN((s1max-s1min+1), (s2max-s2min+1)); % R.force matrix for case2

%% Finding total deflection at the spindle and for different s1 and s2

i=1;
for s1 = s1min:s1max      % Looping for s1

    j=1;
    for s2 = s2min:(sTmax-s1)    % Looping for s2
        %% Superposition I

        % Finding RA, RB, RC reaction forces and C1, C2 constants

        A = [
```

```

0 a 1;
(s1^3)/6 (a+s1) 1;
((s1+s2)^3-(s1+s2)*s2^2)/6 (a+s1+s2) 1];

B = [
((Ft*a^3)/6+(Mt*a^2)/2);
((Ft*(a+s1)^3)/6+(Mt*(a+s1)^2)/2);
((Ft*(a+s1+s2)^3)/6+(Mt*(a+s1+s2)^2)/2-(Ft*(s1+s2+a)*s2^2)/6-...
(Mt*s2^2)/6) ];

X = A\B;

C1(i,j) = X(2);
C2(i,j) = X(3);
RA(i,j) = X(1);
RB(i,j) = (Ft*(s1+s2+a)-RA(i,j)*(s1+s2)+Mt)/s2;
RC(i,j) = Ft-RA(i,j)-RB(i,j);

% Deflection at the spindle tip where x=0 for each s1, s2

DeltaS(i,j) = C2(i,j)/(E*I);

%% Superposition II

% Finding RAp, RBp, RCp reaction forces

F = [
1 1 -1;
a (a+s1) -(s1+s2+a);
-s2/kB (s1+s2)/kB s1/kC];

G = [ Ft; -Mt; 0 ];

Y = F\G;

RAp(i,j) = Y(1);
RBp(i,j) = Y(2);
RCp(i,j) = Y(3);

% Deflection at the spindle tip due to bearings for each s1, s2

DeltaB(i,j) = -(s1+a)/s2*(RBp(i,j)/kB+RCp(i,j)/kC)-RBp(i,j)/kB;

%% Total deflection at the spindle tip

Sigma(i,j)= DeltaS(i,j)+DeltaB(i,j);

Span2 (j) = s2;
j=j+1;

end

Span1 (i) = s1;
i=i+1;

end

% Deflection vs bearing span plot
figure(1)
title('Total Deflection vs Bearing Spans s_1 and s_2')

```

```

surf (Span2, Span1, abs(Sigma))

%% Solving for optimum bearing spans, s1=78 & s2=367mm

s1=78;
s2=367;

x = 0:1:(a+s1+s2); % x position matrix for the shaft
DefeqS = NaN(1,(a+s1+s2)+1);% Defl. matrix for each x position in case1
DefeqB = NaN(1,(a+s1+s2)+1);% Defl. matrix for each x position in case2

% Superposition I
for k=1:((a+s1+s2)+1) % Looping for the deflections at each x position

    if x(k)<=a % If statement for the Macaluay funtions in defl.eq.
        sing=0;
    elseif x(k)<=(s1+a)
        sing=RA(1,51)/6*(x(k)-a)^3;
    else
        sing=RA(1,51)/6*(x(k)-a)^3+RB(1,51)/6*(x(k)-(s1+a))^3;
    end

    DefeqS(k) = 1/(E*I)*(-Ft/6*x(k)^3-Mt/2*x(k)^2+sing+...
        C1(1,51)*x(k)+C2(1,51));

end

% Superposition II
slope = (DeltaB(1,51)-RCp(1,51)/kC)/(a+s1+s2); % Rigid beam slope

for k=1:((a+s1+s2)+1) % Looping for the deflections at each x position

    DefeqB(k) = ((a+s1+s2-x(k))*slope)-(-RCp(1,51)/kC);

end

% Deflection plots for optimum bearing spans
figure(2)
title('Displacement vs x')
plot(x, DefeqS) % Position vs shaft deflection
hold on
plot(x, DefeqB) % Position vs bearing deflection
hold on
plot(x, DefeqS+DefeqB) % Position vs total deflection

```